University of California
Santa Barbara

Emergent Phases of Quantum Matter In Strongly Correlated Mott Insulators

A dissertation submitted in partial satisfaction
of the requirements for the degree

Doctor of Philosophy
in
Physics

by

Jason John Iaconis

Committee in charge:

Professor Leon Balents, Chair
Professor Cenke Xu
Professor Andrea Young

June 2018

The Dissertation of Jason John Iaconis is approved.

Professor Cenke Xu

Professor Andrea Young

Professor Leon Balents, Committee Chair

June 2018

Emergent Phases of Quantum Matter In Strongly Correlated Mott Insulators

by

Jason John Iaconis

To my parents, John and Silvana.

Acknowledgements

First and foremost, I would like to thank my advisor Leon Balents. His constant support during my time in Santa Barbara really has meant a lot to me. Leon has always shown great patience and a genuine investment in my development as a physicist. He has never been too busy to offer some advice in both physics and in life. I have also always admired how seriously he takes his role as a mentor to younger scientists. And of course, Leon is a great physicist. I have learnt so much under his guidance. I am constantly amazed at his ability to so clearly and simply articulate complicated ideas. The depth and breadth of his knowledge of such widespread areas of physics is an inspiration to me. I feel very lucky to have had the opportunity to work under Leon and I surely owe him a very large debt of gratitude.

I would also like to thank the many members of the condensed matter group at UCSB. Especially my current and former fellow graduate students, Teddy Parker, Chunxiao Liu, Lucile Savary, Ru Chen, Ryan Mishmash, Jim Garrison, Eugeniu Plamadeala, Katie Hyatt, Alex Rasmussen, Dominic Else, Zhen Bi, Kelly Pawlak, Chaitanya Murthy, and Christina Knapp. I am very grateful to have spent so much time with such a talented group of people. Your dedication and hard work has always inspired me and pushed me to be better. I also learnt quite a bit from the resident KITP post-docs, and am especially grateful to Gábor Halász and Hiro Ishizuka.

I would like to thank Professor Donna Sheng for her help and collaboration in the project which resulted in Chapter 3 of this dissertation. I am also very grateful to Professors Cenke Xu and Andrea Young for sitting on my thesis defense committee.

I spent two summers of grad school at the Boulder Summer School for condensed matter physics. These experiences led to a lot of personal growth for me. The connections I made there were invaluable and I would like to thank the organizers

of these programs for the opportunities they provided me. My time there must have made quite the impression as I am moving to Boulder full time for my post-doc.

I started in the field of condensed matter physics at the University of Waterloo working for Professor Roger Melko. My time working for Roger was an amazing experience. I always look forward to our reunions and to this day still turn to him for advice and for that I am very thankful.

My time in graduate school would not have been what it was without my very close friends. To my roommates Andrew Dunsworth, Nick Noll, Kenny Lee, Kurt Fujiwara and Scott Haselschwardt, I could not imagine a better group of people to have lived with throughout grad school. Andrew, Nick, and Scott, our frequent road trips and climbing adventures will remain as some of my fondest memories. I am also thankful for my good friends Eric Mefford and Naomi DeCelles and our many get-togethers over good food and good drinks. Eric, Scott and Andrew, our early morning surf sessions always served as a great reminder of how lucky I was to live in such a beautiful place.

Finally, I would like to thank my family. My brother Lou and sister Sarah, you have always understood me and the path I was on. Your constant support has meant a lot. It has been difficult living so far from home, but we always seem to pick up right where we left off when we are together. Of course, I would not be where I am today without the constant love and support of my parents. They instilled upon me the importance of family and hard work. My mom has always shown such pride in my accomplishments. She has constantly pushed me to be my best throughout my whole life. My dad has always been my role model. He was the original inspiration for my interest in science. I love you both and truly owe everything I am to the both of you.

Curriculum Vitæ

Jason John Iaconis

Education

2018	Ph.D. in Physics (Expected), University of California, Santa Barbara.
2015	M.A. in Physics, University of California, Santa Barbara.
2012	M.S. in Physics, University of Waterloo
2011	B.S. in Mathematical Physics, University of Waterloo

Publications

Jason Iaconis, Chunxiao Liu, Gábor B. Halász, Leon Balents: *Spin Liquid versus Spin Orbit Coupling on the Triangular Lattice* SciPost Phys. **4**, 003, (2018)

Jason Iaconis, Hiroaki Ishizuka, D.N. Sheng, Leon Balents: *Kinetic Magnetism at the Interface Between Mott and Band Insulators* Phys. Rev. B **93**, 155144, (2016)

Jason Iaconis, Leon Balents: *Many-Body Effects in Topological Kondo Insulators* Phys. Rev. B **91**, 245127, (2015)

Jason Iaconis, Stephen Inglis, Ann B. Kallin, and Roger Melko: *Detecting Classical Phase Transitions with Renyi Mutual Information* Phys Rev. B **87**, 195134, (2013)

J. Iaconis, R. G. Melko, and A. A. Burkov: *Continuous thermal melting of a two-dimensional Abrikosov vortex solid* Phys. Rev. B (Rapid Comm.) **82**, 180504(R), (2010).

Abstract

Emergent Phases of Quantum Matter In Strongly Correlated Mott Insulators

by

Jason John Iaconis

Strongly correlated electron systems have the potential to host very exotic phases of matter. In order to have relevance to real materials, this exotic physics often must *emerge* from relatively simple models. The quantum wavefunctions which describe such phases may bear little resemblance to the original microscopic models. In these cases a variety of complex analytic tools often must be supplemented with controlled numerical calculations to fully understand the essential behavior of these models. In this dissertation, we study such quantum phases of matter and their relationship to real materials.

We focus on three main problems. First, we explore the relationship between strong spin-orbit coupling and spin liquid physics by studying a very general model on the triangular lattice where spin-orbit coupling leads to the presence of highly anisotropic interactions. We use variational Monte Carlo to study both $U(1)$ quantum spin liquid states and ordered ones, via the Gutzwiller projected fermion construction. We thereby obtain the ground state phase diagram in this phase space. We furthermore consider effects beyond the Gutzwiller wavefunctions for the spinon Fermi surface quantum spin liquid, which are of particular importance when spin-orbit coupling is present.

Second we show that the interplay between a high density two-dimensional electron gas and localized electrons in a neighboring Mott insulator leads to kinetic mag-

netism unique to the Mott/band insulator interface. Our study is based upon a bilayer Hubbard model at $U = \infty$ with a potential difference between the two layers. We combine analytic results with DMRG simulations to show that magnetism, and especially kinetic ferromagnetism, is greatly enhanced relative by the proximity of the two subsystems.

Third we study the effect of interactions on the properties of a model 2D topological Kondo insulator phase. We introduce a model Hamiltonian which we believe captures the essential physics of the different competing phases. Perhaps the most dramatic example of many-body physics in symmetry protected topological phases is the existence of exotic gapless edge states. We comment on the potentially dramatic effects that interactions can have on such edge states.

Contents

0.1 Permissions and Attributions

1. The content of chapter 2 is the result of a collaboration with Chunxiao Liu, Gàbor Halàsz, and Leon Balents. It has previously appeared in the journal Scipost Physics [1]. It is reproduced here with the permission of the publisher under the Creative Commons Attribution 4.0 International (CC BY 4.0) License.

2. The content of chapter 3 is the result of a collaboration with Hiroaki Ishizuka, Donna N. Sheng, and Leon Balents. It has previously appeared in the journal Physical Review B [2]. It is reproduced here with the permision of the publisher, the American Physical Society: `http://journals.aps.org/copyrightFAQ.html#thesis`. See `http://publish.aps.org/info/terms.html` for the official copyright transfer agreement.

3. The content of chapter 3 is the result of a collaboration with Leon Balents. It has previously appeared in the journal Physical Review B [3]. It is reproduced here with the permision of the publisher, the American Physical Society: `http://journals.aps.org/copyrightFAQ.html#thesis`.

Chapter 1

Introduction

1.1 Overview: Quantum Phenomena in Interacting Many-Body Systems

In condensed matter physics, we the study the collective behavior of quantum many-body systems, with the ultimate goal of understanding the matter that makes up our world. The fundamental particles of these many-body systems, atoms and electrons, are fully quantum mechanical objects; yet most phases of matter we see can be explained either with classical statistical mechanics or single particle physics. From a modern perspective then, the most interesting phases are those which diverge from this convention and demonstrate collective quantum effects on a macroscopic scale. An immense amount of progress has been made by theorists in developing a host of complex models which exhibit exotic behavior. The connection of these models to real materials, however, is occasionally somewhat tenuous. One of the major goals of the field is therefore to find relatively simple models which can be related to experimental systems and which display large scale quantum behavior.

In this dissertation, the approach we take to this problem is a practical one. We attempt to relate the phenomenology of real materials to the vast theory which has been developed in the field. As a matter of course, we first search for materials which *a priori* show signs of interesting or exotic behavior. Keeping an eye on our practical approach, we define exotic behavior as any effects which deviate dramatically from expectations based on classical or weakly interacting physics. We then identify the fundamental parameters and degrees of freedom which are necessary to accurately describe the microscopic or high energy physics. Using a number of different analytic and numerical tools, and pulling inspiration from different sources, we develop an effective description of the physics. For strongly interacting systems, the complexity of the quantum Hilbert space implies that numerical approaches are often necessary to gain a full understanding of the ground state wavefunction.

In most cases, the Hamiltonian describing the electronic properties of physical systems takes a relatively simple form. The relevant electron degrees of freedom can be determined from the chemistry of partially filled outer orbitals in single ion states, while the nuclear degrees of freedom are generally integrated out. These electrons move throughout the lattice in a way which is determined by the hopping overlap integral between two sites, and interact with each other through a short ranged density-density interaction. With this in mind, most systems of electrons can be modeled by specifying only a few parameters: such as the strength of the interaction, the symmetry of the electron orbitals and the geometry of the lattice. And yet, as we will see, from even the simplest electron models, an amazing array of phenomena can be seen. Often, the collective behavior of the electrons is far too complicated to be described exactly while keeping all the original degrees of freedom. Instead, we attempt only to describe the essential physics which occurs at the lowest

energies and longest wavelengths. This idea of describing a complicated system in terms of a relatively simply theory at a different energy and length scale with new degrees of freedom is a concept known as *emergence*.

Let us first review some historical developments in the field of correlated electron systems. If the interactions in a material are small, we can often treat the electrons as if they are noninteracting, speaking to each other only through their fermion statistics and their combined motion in the periodic potential of the lattice. Nearly free electrons organize themselves into energy bands in momentum space. An even number of electrons per unit cell implies fully filled bands and electronic insulators. An odd number of electrons per unit cell implies partially filled energy bands and the existence of a gapless Fermi surface separating the occupied and empty momentum states. The gaplessness in this case is protected not by any symmetry, but by the fermion statistics themselves. In a groundbreaking work by Landau, it was realized that even strongly interacting electron systems can often be understood as a gas of nearly free electrons. In this case, however, the 'electrons' are really quasiparticles, which are in a one-to-one correspondence with the physical electrons of the system. This framework, known as Landau's Fermi liquid theory, is one of the first examples of an effective field theory. This is the idea that the *universal* properties of a system can be explained using only the collective degrees of freedom that exist at the lowest energies and longest length scales. In Fermi liquid theory, these 'quasiparticle' degrees of freedom have the same form as the physical electrons, but in principle this need not be the case.

At some point, if one tunes the electron interactions up high enough, the above Fermi liquid picture will stop being valid. In these situations, the effects of interactions must be included from the beginning. If there exists an odd number of electrons per

unit cell, band theory predicts that the system should be a metal. However, the Coulomb repulsion between electrons means that an energy cost must be payed to have two electrons occupy the same site. If this repulsion is strong enough, it may be favorable for the electrons to become completely localized on a single site. In this case, we say that the system behaves like a *Mott insulator*. This situation occurs especially often in systems with partially filled d or f electron orbitals, where the hopping band is relatively flat and so the kinetic energy gained by having delocalized electrons is effectively reduced. While the charge degrees of freedom in a Mott insulator are effectively frozen, the spin and angular momentum degrees of freedom are still very much active.

The phenomenology of the metal and Mott insulator phases can be captured effectively by considering the famous single band Hubbard model

$$H_{hub} = -t \sum_{\langle ij \rangle, \sigma} c^{\dagger}_{i\sigma} c_{j\sigma} + U \sum_{i} n_{i\uparrow}(n_{i\downarrow} - 1) \tag{1.1}$$

where $c^{\dagger}_{i\sigma}/c_{i\sigma}$ creates/destroys an electron with spin $\sigma = \uparrow / \downarrow$ at site i. With one electron per site, when U is small, Fermi liquid theory can be justified more rigorously using perturbative renormalization group arguments [1]. The upshot is that as one moves to lower and lower energies, only a small fraction of electrons take part in any scattering processes and the interactions become less and less important. The existence of marginal interactions at special points in momentum space have the effect of modifying the single particle Green's function from its noninteracting value, but otherwise leaves the single particle theory for the ground state largely intact. Ignoring possible instabilities to a superconducting state the interaction U only has the effect

[1] The details can be found in many places. Two particularly good examples are a review by Shankar [4] and a beautiful article by Polchinski [5].

of 'dressing' the bare electrons.

When $U = \infty$, the exact eigenstates of the system are the degenerate set of states where exactly one electron is localized on each site

$$|\{S_i^z\}\rangle = \prod_i (c_{i\uparrow}^\dagger)^{\zeta_i} (c_{i\downarrow}^\dagger)^{1-\zeta_i} |0\rangle \,, \tag{1.2}$$

with $\zeta_i \in \{0, 1\}$. For large but finite U, the lowest order term in a strong coupling perturbative expansion in powers of $\frac{t}{U}$ gives an effective interaction between the localized spins due to the so called 'superexchange' mechanism. The effective spin Hamiltonian is of the form

$$H_{spin} = \frac{4t^2}{U} \sum_{ij} \vec{S}_i \cdot \vec{S}_j. \tag{1.3}$$

For large U, the electrons can gain energy by virtually hopping to neighboring sites if the electron spins are anti-aligned. This effective Hamiltonian is known as the antiferromagnetic Heisenberg model and has an interaction strength given by $J \sim \frac{4t^2}{U}$. Usually in such Mott insulating materials, the spins will orient themselves in some long ranged antiferromagnetic pattern. The approach taken to understand such spin systems was also pioneered by Landau [6, 7], in a theory whereby different orders are classified using the concept of broken symmetry. Within the Landau paradigm, two phases of matter are different because they break different symmetries. The degree of this symmetry breaking is measured using a local variable known as the *order parameter*. In spin systems, this order parameter may give the direction of a net magnetic moment on each site of the lattice. This describes a magnetically ordered state. If the average magnetic moment of the spins on nearby sites point in different

directions, this is known as an antiferromagnet. In these cases, the order parameter is a classical vector. In fact the Landau theory of symmetry breaking is the theory of classical orders. For this reason, a semiclassical theory is often sufficient to capture all the physics of magnetic phases.

Taken together, Landau's Fermi liquid theory and Landau's theory of symmetry breaking can explain most phases of matter that we encounter in nature. On the other hand, the complexity of the quantum wavefunction allows for a great deal of exotic and interesting physics which goes beyond the relatively simple picture painted by these two theories. By searching for Hamiltonians with a combination of the right ingredients, we can find systems where the quantum effects in the ground state wavefunction are enhanced.

In some cases, the phases that result display wildly different properties than that of the constituent matter. This is the case for quantum spin liquids. These are magnetic insulators where at low energies the spin degrees of freedom form a genuine quantum state. Unlike Landau's theory of symmetry breaking, the theory of quantum spin liquids is the theory of quantum orders [8]. These phases are characterized by different patterns of long range entanglement in the ground state wavefunction. This entanglement allows for the existence of exotic forms of collective low energy excitations. In these systems, unlike in the Fermi liquid theory, the emergent effective field theory is formulated using fields which have little relation to the original localized spin degrees of freedom. Instead the low energy theory can be written in terms of emergent fermion matter fields and gauge bosons [2].

The search for spin liquid phases in real materials is one of the great outstanding

[2]Pushing this connection further, one can even attempt to explain all the fundamental physics of the standard model as an emergent theory of some higher energy spin model. This has been the perspective taken, for example, in [9], [10] and [11].

problems in the field. The key ingredients from a theoretical point of view appear to be some combination of low effective spins, magnetic frustration (provided either by the geometry of the lattice or the presence of longer ranged interactions), and spin-orbit coupling. Further, even within the spin liquid classification there exists different classes of states each with their own unique set of phenomena. Xiao Gang Wen's projective symmetry group classification [12] provides a method for studying these different spin liquids based on the symmetry properties of their quasiparticle excitations. This classification comes with a method for constructing the various spin liquid wavefunctions. This can then be adapted into a full fledged numerical algorithm which builds on these wavefunctions and uses them as variational ansatze. This numerical method may be used to assess the feasibility of candidate spin liquid wavefunctions as the ground states of specific Hamiltonians. It can also be adapted to study the properties of spin liquid wavefunctions phenomenologically, which can then be compared to experimental phenomena.

While quantum spin liquids represent one extreme case of exotic quantum matter, it is possible to find interesting physics even when the ground state is a more traditional symmetry broken phase of matter. This is the case in oxide heterostructure materials. These are structures which are formed by layering two or more quasi-two-dimensional materials on top of each other. In recent years, they have become a very popular venue for exploring strongly correlated physics in a highly controlled environment. The main principle is that, although the behavior of the individual materials may be well understood, at the interface between two materials new and interesting physics often emerges. For example, at the interface of two insulating materials a high density two dimensional electron gas appears. The origin of this new physics can often be very mysterious, and understanding the physics of these strongly corre-

lated systems poses a great challenge. These heterostructure materials are a sort of playground for observing strongly correlated phenomena. In this thesis, we explore these heterostructures and show that at the interface between a Mott insulator and a band insulator itinerant ferromagnetism can emerge in a very beautiful way which is governed by the quantum motion of the itinerant interface electrons.

Kondo lattice or heavy fermion systems are a famous example where stable quantum effects have been observed in real materials. In these systems, a lattice of localized spins interact with itinerant electrons. The low energy state that results from this interaction is a Landau Fermi liquid where the effective mass of the quasiparticles can be hundreds or thousands of times greater than that of the physical electrons. A 'screening' of the local spin moments occurs due to local singlet formation between the spins and the nearby itinerant electrons, and so the ground state wavefunction in the microscopic degrees of freedom is a highly entangled state. The low energy effective description can then be written in terms of weakly interacting electrons. This weakly interacting effective theory may in fact be smoothly connected to a band insulator. However, even the seemingly simple band insulators can display exotic physics. This happens in free electron systems when the quantum mechanical phases of the single particle electron states leads to a nontrivial topology in the band structure. Such a band insulator with a nontrivial topology is known as a topological insulator. This topological structure may appear in heavy fermion systems, even if the original itinerant electrons are completely trivial. In this case, we have an emergent topological insulator where interactions must be included *a priori*. We will discuss a particular example of these Kondo topological insulators in chapter 4.

In the rest of this introduction, we will review the most interesting concepts which we will use throughout the rest of this dissertation.

1.2 Background on Quantum Spin Liquids

Quantum spin liquids (QSLs) represent some of the most exotic phases of quantum matter [13, 14, 12, 9]. These are fully quantum phases in which the ordering of the spins cannot be described in terms of a classical symmetry breaking order parameter. Instead, a positive description of the quantum order in spin liquids relies on the fact that these are phases whose ground states intrinsically contain an anomalously high degree of entanglement [15]. More precisely, QSLs are states that cannot be smoothly deformed to a product state while staying within the phase. This can be seen, for example, in gapped spin liquid phases by studying the topological entanglement entropy [16, 17]. This entanglement based definition leads to the intuitive picture whereby a massive superposition of spin configurations produces a quantum disordered spin state. The class of wavefunctions which satisfy this property is very broad, encompassing both gapped phases with topological order and gapless phases where the gaplessness is actually protected by the entanglement structure of the ground state.

The most important *consequence* of this high entanglement is the unique ability of spin liquid wavefunctions to support non-local quasiparticle excitations which cannot exist in traditional symmetry breaking states. For example, these may take the form of the 'fractionalized' spinon excitations which carry spin but not charge and disperse freely throughout the lattice [18, 19]. Roughly speaking, the local singlet formation in the ground state ensures that any defects in the ordering pattern carry nontrivial quantum numbers [20]. When the entanglement is strong enough these defects can propagate freely throughout the lattice. These types of excitations cannot be created individually by any local operator, but only by an infinite number of local

operators. Nevertheless, such excitations cost a finite amount of energy, a feature which is only possible because of the massive entanglement in the wavefunction. As such, the excitations in quantum spin liquids are the ultimate example of *emergent* phenomena, particles which show wildly different properties than the matter from which they are composed and which can only exist in strongly interacting many body quantum systems.

Importantly, the physics of QSLs are well described by gauge theories [21, 22, 23], which gives a natural way to describe non-local excitations. This fact is very closely related to the study of slave-parton mean field theories, which in many cases provides a very simple description of QSLs in terms of their fractionalized excitations. We will rely heavily throughout this chapter on this slave parton construction which also gives a powerful method for classifying spin liquid phases and constructing associated wavefunctions.

While the underlying physics described above is no doubt interesting in its own right, the remarkable aspect of quantum spin liquids is the very real possibility of its existence as the ground state of real spin systems. We will review a few important candidate spin liquid materials, and see what ingredients may be most important in order to stabilize QSL grounds states. We will also describe some important experimental signatures.

1.2.1 Lattice Gauge Theories, Slave Partons and the Projective Symmetry Group

In this subsection, I will give a brief review of the underlying theory behind quantum spin liquids. The purpose is to both give a basis for the rest of the dissertation

and to highlight some of the most interesting properties of highly entangled systems. Much of the physics contained in this subsection is presented in greater depth in the reviews found in Refs [14] and [24]. The overarching theme of this section is that quantum spin liquids contain an effective gauge structure. This structure is manifest in the ground state wavefunction and necessarily leads to exotic behavior. There are many ways to understand the connection between gauge theory and QSLs. In essence, gauge theories provide an effective description of all spin liquid states.

U(1) Lattice Gauge Theory

For concreteness, we will give two familiar examples of lattice gauge theories. The first is the lattice $U(1)$ compact gauge theory on a d-dimensional cubic lattice. On each bond of the lattice we define a conjugate pair of variables $A_{ab} = -A_{ba}$ and $E_{ab} = -E_{ba}$, such that $[A_{ab}, E_{ab}] = i$ and fields on different links commute. Take the Hamiltonian

$$H = -K \sum_p \cos(\nabla \times A)_p + K' \sum_a (\mathrm{div} E)_a^2 + \frac{U}{2} \sum_{\langle ab \rangle} E_{ab}^2 \tag{1.4}$$

where we define the lattice divergence as

$$(\mathrm{div} E)_a = \sum_{b \in nn(a)} E_{ab}, \tag{1.5}$$

and the lattice curl on each plaquette by

$$B_p = (\nabla \times A)_p = \sum_{a \in p} A_{a,a+1}. \tag{1.6}$$

with $a = 1, 2, 3, 4$ labeled sequentially clockwise.

This model is the lattice version of quantum electromagnetism. The E_{ab} variable acts as the electric field and the A_{ab} variable like the vector potential so that B_p behaves as the magnetic field. This model, like usual the usual model of electromagnetism, is invariant under the gauge transformation

$$A_{ab} \to A_{ab} + \chi_a - \chi_b. \tag{1.7}$$

This is an exact local symmetry of the Hamiltonian. Elitzur's theorem [25] states that local symmetries cannot be broken spontaneously. Therefore, the ground state of H must be a superposition over all configurations of A_{ab} which are related by the gauge transformation in Eq. 1.7. Any operator which is not invariant under the gauge transformation must always have a zero expectation value. It is for this reason that it is useful to formulate our theory in terms of the gauge invariant quantities E_{ab} and $(\nabla \times A)$. If we restrict the Hilbert space to only include gauge invariant states, then the gauge transformation is really just an identity operation, which maps a state in the Hilbert space onto itself.

When $V = 0$, both $(\mathrm{div}E)_a$ and $B_p = (\nabla \times A)_p$ commute with H. In this limit, the ground state of H has both $(\mathrm{div}E)_a = 0$ and $B_p = (\nabla \times A)_p = 0$ on all sites and plaquettes. If we take V to be small but nonzero, this term then induces fluctuations in the B_p variable. *If* we assume that these fluctuations are small, then we can expand the cosine in Eq. 1.4 around $B_p = 0$ and take the continuum limit to find the effective Hamiltonian

$$H_{eff} = \int d^3x \left[\frac{\varepsilon}{2} |\vec{E}|^2 + \frac{1}{2\mu} |\vec{B}|^2 \right]. \tag{1.8}$$

When this expansion is valid, we say that the system is in the *deconfined* or *Coulomb* phase. The effective field theory in this case is exactly the same as the usual theory of quantum electromagnetism in a vacuum.

Importantly, $(\mathrm{div}E)_a$ commutes with H for all a, and so its eigenvalues $(\mathrm{div}E)_a |\psi\rangle = q_a |\psi\rangle$ are good quantum numbers. These electric charges are conserved low energy excitations in our theory. Charge excitations in the $U(1)$ lattice gauge theory cannot be created locally by any operator in the theory. This can be seen directly using the fact that electric charges are given by the divergence of E and making use of Gauss's law for some region R

$$Q = \sum_{a \in R} (\mathrm{div}E)_a = \sum_{\langle ab \rangle \in \partial R} E_{ab} \tag{1.9}$$

Then, since the charge in a region can be calculated via the value of the electric field at the boundary, no operator acting solely within the region can change the total electric charge within R. It is, however, possible to create neutral pairs of charge excitations locally within the theory. In the deconfined phase, once these excitations are created they can propagate independently throughout the lattice.

Therefore this theory contains all the usual properties of QED. There exists an energy gap above which charge excitations q_a exist, and multiple charges interact with each other via a long-range $1/r$ coulomb interaction. There also exists an additional excitation which takes the form of a linearly dispersing gapless 'photon' mode. There also exists a third excitation, unique to the lattice model, whereby the flux through a plaquette changes by 2π. This is a topological point defect in three dimensions which is allowed due to the 2π-ambiguity of A. These excitations behave as magnetic charges in the theory, and also interact via a $1/r$ Coulomb interaction.

It turns out that fluctuations of the gapless B_p variable may destroy the order and lead to a phase in which pairs of emergent excitations are bound together[26]. When this occurs, the long range entanglement of the gauge theory is destroyed and we say the system is in a *confined* phase.

$\mathbb{Z}_2$ Lattice Gauge Theory

Now, if instead of the above theory, we restrict the variables A_{ab} so that $A_{ab} \in \{0, \pi\}$ on each site, our theory becomes a $\mathbb{Z}_2$ lattice gauge theory [23]. If we let $\sigma^z_{ab} = e^{iA_{ab}}$, then the curl operator $\cos(\nabla \times A)$ become $P_p = \prod_{\square} \sigma^z_{ab}$, where the product is over all bonds on the plaquette p. Furthermore, the conjugate variable to σ^z_{ab} is $\sigma^x_{ab} = e^{iE_{ab}}$, and the divergence operator $(\mathrm{div}E)_s$ becomes $S_s = \prod_{+} \sigma^x_{ab}$, where the product here is over all bonds emanating from the vertex s. With these new variables, the $\mathbb{Z}_2$ lattice gauge theory is given by the Hamiltonian

$$H_{\mathbb{Z}_2} = -K \sum_p \prod_{\square} \sigma^z - K' \sum_s \prod_{+} \sigma^x - h_z \sum_{\langle ab \rangle} \sigma^z_{ab} - h_x \sum_{\langle pp' \rangle} \sigma^x_{pp'} \qquad (1.10)$$

We can artificially enlarge the degrees of freedom in our model by introducing the spin variables $\tau^x_p = \pm 1$ on each plaquette and $\mu^x_s = \pm 1$ on each bond. We then enforce the constraint that $\mu^x_p = P_p$ and $\tau^x_s = S_s$ on each vertex and plaquette.

$$H_{\mathbb{Z}_2} = -K \sum_p \mu^x_p - K' \sum_i \tau^x_i - h_z \sum_{\langle ab \rangle} \tau^z_a \sigma^z_{ab} \tau^z_b - h_x \sum_{\langle pp' \rangle} \mu^z_p \sigma^x_{pp'} \mu^z_p. \qquad (1.11)$$

In fact this model is exactly the same as the toric code model [27] with the addition of magnetic fields h_z and h_x. The additional variables τ^x and μ^x are completely fixed by the σ configuration, and are therefore redundant. Including these variables allows

us to explicitly cast the σ operators as a gauge field and the μ and τ variables as gradients of this field. Then charges in the gauge theory correspond to spin flips in the μ and τ variables, and it is clear that the magnetic fields h_z and h_x couple to the electric and magnetic excitations respectively in the gauge theory.

Note that Eq. 1.11 has an explicit gauge symmetry generated by $\tau^x_a \prod_{\langle a,b\rangle} \sigma^x_{ab}$. This symmetry can never be broken by Elitzur's theorem. Instead, for large enough h_z the electric excitations will be in a *confined* or *Higgs* phase. In the confined phase, separating pairs of excitations costs an energy which grows linearly with distance. Within this phase, τ^z variables behave similarly to the ordered phase of a transverse field Ising model, but with an important distinction. Within this explicit gauge theory, the two symmetry broken $|\tau^z\rangle$ basis states are related to each other via a gauge transformation. The true ground state must be a superposition over all such gauge related states. Therefore even within the confined phase, the coupling of the τ variables to the σ^z variables results in an entangled phase where the local symmetry of the gauge theory is preserved.

Stability of Gauge Theories

In order for a gauge theory to effectively describe a quantum phase of matter, it must be stable to all perturbations. When all the excitations of an emergent gauge theory are gapped, it is somewhat easy to see that this is true. For example, for the non-gauge-invariant h_x and h_z operators, perturbation theory around the limit where the τ and μ variables in Eq. 1.11 are fully polarized will lead to transverse fluctuations which can be integrated out to obtain an effective pure gauge theory. The situation is more complicated for gapless spin liquids. In [28], it is argued that in gapless spin

liquids which are described by an *emergent* gauge theory, there exists a gap to states which are not gauge invariant. That is, all low energy excitations of the system are gauge invariant. Then, a perturbation which explicitly breaks the gauge invariance will only mix the ground state with the low lying excited states. Since all these states are gauge invariant this system should still have an emergent gauge symmetry even in the presence of perturbations which explicitly break this gauge symmetry.

Slave Parton Theories

We have seen two examples of lattice gauge theories which exist in quantum spin systems. The ground state of these spin models are highly entangled phases of matter and the excitations are nonlocal quasiparticles. The Hamiltonians explicitly possess a local gauge symmetry, which ensures the existence of these interesting properties. The deconfined phases are stable to all weak perturbations, even those which explicitly break the gauge symmetry. In this case, the system possesses an emergent gauge structure. This type of behavior also exists in generic models of spin systems which *a priori* contain no such local symmetries. In these systems, when it is not obvious what is the proper description of the ground state, we need to formulate an effective theory which obeys the known symmetries of the microscopic system. In this case, we may *guess* that this effective theory contains a gauge structure similar to that described above, and formulate a description of the ground state in terms of the emergent quasiparticles of this gauge theory. This guess may be motivated by a type of mean-field theory, or justified later through quantitative or phenomenological approaches.

We start by constructing a theory for a general spin model where the quasiparticle

excitations are fermionic in nature. Fermions are special, in that like the excitations of the deconfined phase of a lattice gauge theory, single fermions cannot be created by any local operator. Therefore, if they are going to be the emergent excitations of a spin system, the ground state of that system must be highly entangled. Deconfined gauge theories are the simplest example we have which can model these systems. Luckily, there exists a simple way to create such theories by making use of Abrikosov fermions.

We write the spin-$\frac{1}{2}$ operator $\vec{S}_i$ in terms of fermion operators $f^\dagger_{i\sigma}$ using the relation

$$\vec{S}_i = f^\dagger_{i\alpha}\vec{\sigma}_{\alpha\beta}f_{i_\beta}. \tag{1.12}$$

In order to ensure that we work with the proper Hilbert space, we must also include the strict constraint

$$\sum_\sigma f^\dagger_{i\sigma}f_{i\sigma} = 1. \tag{1.13}$$

Using this formalism, a proper effective description for the deconfined phase of a spin liquid is one in which the fermion operators $f^\dagger_{i\sigma}$ propagate freely throughout the lattice as low energy quasiparticle excitations of the ground state. The operator $f^\dagger_{i\alpha}$ carry spin but not charge. They are parts of the original spin variables, and therefore are known as 'partons'. This can be motivated through a mean-field theory type analysis [29, 30, 31], whereby a nearest-neighbor spin-spin interaction is written as a four body fermion interaction which is then decoupled in the appropriate channels as

follows:

$$\begin{aligned}\vec{S}_i \cdot \vec{S}_j &= \frac{1}{4} f^\dagger_{i\alpha} f_{i\beta} f^\dagger_{j\gamma} f_{j\delta} \vec{\sigma}_{\alpha\beta} \cdot \vec{\sigma}_{\gamma\delta} \\ &= \frac{1}{2} f^\dagger_{i\alpha} f_{j\delta} f^\dagger_{j\gamma} f_{i\beta} + \text{constant.} \\ &\to \frac{1}{2} \left\langle f^\dagger_{i\alpha} f_{j\delta} \right\rangle f^\dagger_{j\gamma} f_{i\beta} + \frac{1}{2} f^\dagger_{i\alpha} f_{j\delta} \left\langle f^\dagger_{j\gamma} f_{i\beta} \right\rangle + \text{constant.} \end{aligned} \tag{1.14}$$

Decoupling the interaction in this way amounts to a guess that the quasiparticle excitations of this system are freely propagating electrons. We could have equally well decoupled the interaction as

$$\vec{S}_i \cdot \vec{S}_j \to \frac{1}{2} \left\langle f^\dagger_{i\alpha} f^\dagger_{j\gamma} \right\rangle f_{j\delta} f_{i\beta} + \frac{1}{2} f^\dagger_{i\alpha} f^\dagger_{j\gamma} \left\langle f_{j\delta} f_{i\beta} \right\rangle + \text{constant.} \tag{1.15}$$

Likewise, this amounts to a guess that the excitations are Bogoliubov quasiparticles. Obviously there is a huge amount of freedom in how one decouples the spin-spin interaction. If one were to couple fermion operators on the same site together, $f^\dagger_{i\alpha} f_{i\beta} f^\dagger_{j\gamma} f_{j\delta} \to \langle f^\dagger_{i\alpha} f_{i\beta} \rangle f^\dagger_{j\gamma} f_{j\delta}$, this would be equivalent to the conventional magnetic symmetry breaking mean-field theory. In any case, a Lagrange multiplier λ_i is needed to enforce the local constraint of Eq. 1.13, which plays the role of a gauge field [32, 33, 34]. In the case of magnetic order, this gauge theory is in its confined phase.

In fact, we can ignore this mean-field formalism all together, and simply write down a phenomenological *parton* Hamiltonian to describe the behavior of the fermionic quasiparticles

$$\mathcal{H}_{mf} = \sum_{ij} \left[\tilde{u}^{\alpha\beta}_{ij} f^\dagger_{i\alpha} f_{j\beta} + \tilde{\Delta}^{\alpha\beta}_{ij} f^\dagger_{i\alpha} f^\dagger_{j\beta} + \text{h.c.} \right], \tag{1.16}$$

We once again guess at the global symmetry of the fermionic quasiparticles and write down a Hamiltonian as in Eq. 1.16. For concreteness we will focus on the case of a $U(1)$ symmetry. We then notice that the original spin degrees of freedom in Eq. 1.12 are invariant under this symmetry *locally*. Therefore, any spin wavefunction should also be invariant under the local transformation $f^\dagger_{i\sigma} \to e^{i\theta_i \sigma^z} f^\dagger_{i\sigma}$, where $\theta_i \in [0, 2\pi]$ for a $U(1)$ symmetry. We can restore this local symmetry in the quasiparticle theory by adding a gauge field to Eq. 1.16, and including terms in the Hamiltonian which are invariant under the local $U(1)$ symmetry. This equates to studying the parton Hamiltonian

$$\begin{aligned} H &= \sum_{ij} t_{ij}^{\alpha\beta} e^{i\vec{A}_{ij}} f^\dagger_{i\alpha} f_{j\beta} + \text{h.c.} + H_g \\ H_g &= \sum_p \cos[(\nabla \times A)_p] + \sum_i (\text{div} E)_i + \frac{V}{2} \sum_i E_i^2. \end{aligned} \tag{1.17}$$

That is, it is exactly the $U(1)$ lattice gauge theory coupled to fermionic matter fields. In the limit where the gauge field does not fluctuate, one can 'fix a gauge' by setting the value of A_{ij} to any fixed number which satisfies the zero flux condition. In this case, the theory becomes equivalent to the slave-fermion mean-field theory description. Away from this limit, the small fluctuations of the gauge field interact with the matter fields so that the fundamental quasiparticles behave like a 'dressed' version of the Abrikosov fermions, similar to electrons in Landau's Fermi liquid theory. If the gauge field fluctuations are strong enough, the spinon mean-field description may not be valid at all and the system may transition into a confined phase.

For this form of the $U(1)$ lattice gauge theory, the fermionic matter fields may be gapped or gapless. The gapless spinons may take the form of Dirac fermions located at isolated points in momentum space [35] or may even form a gapless Fermi

surface [36]. This state, where the ground state of a local spin system possesses a Fermi surface of gapless excitations which are strongly coupled to a emergent $U(1)$ gauge field is one of the most exotic phases of matter we know of [37, 38] . It is an insulating phase, with a $(d-1)$ dimensional manifold of gapless excitations where the gaplessness is protected only by the entanglement in the ground state.

The Projective Symmetry Group

We saw in the previous section that the physical spin operators may be invariant under symmetry transformations of the parton operators. This symmetry operation therefore cannot be 'real' in the sense that it acts as an identity operator on the physical spin system. Instead, the apparent symmetry of our mean-field Hamiltonian is just a result of our parton description. When this situation occurs, we say that the symmetry acts projectively and the set of symmetry transformations that the *parton* Hamiltonian is invariant under is known as the projective symmetry group [12]. Symmetries are not required in order to have a quantum spin liquid state. However, when symmetries are present in the physical system, the PSG tells us that there exist different classes of spin liquid states which are described by different parton Hamiltonians and which cannot be connected to each other by a gauge transformation. When a symmetry is present, new spin liquid phases appear which cannot be smoothly deformed into each other unless the symmetry is broken or a phase transition occurs. Although the wavefunctions derived from different parton Hamiltonians share the same set of symmetries, the mean-field wavefunctions are invariant under a symmetry transformation followed by a different gauge transformation. Theses different gauge transformations can be used to classify different spin liquid orders [39, 40, 41].

To be concrete, consider the following general form of the quadratic mean-field parton Hamiltonian

$$\begin{aligned} \mathcal{H}_{mf} &= \sum_{i,j,\alpha} \mathrm{Tr}\left[\sigma^{\alpha}\Phi_i u_{ij}^{\alpha}\Phi_j^{\dagger}\right], \\ \Phi_i &= \begin{pmatrix} f_{i\uparrow} & f_{i\downarrow}^{\dagger} \\ f_{i\downarrow} & -f_{i\uparrow}^{\dagger} \end{pmatrix}. \end{aligned} \tag{1.18}$$

A local gauge transformation, such as $f_{i\sigma} \to e^{i\theta_i\sigma^z} f_{i\sigma}$, changes H_{mf} but leaves the physical spin operator $\vec{S}_i = f_{i\alpha}^{\dagger}\vec{\sigma}_{\alpha\beta}f_{i\beta}$ unchanged. Therefore, the set of mean field wavefunctions which are related by such a gauge transformation all map onto the same physical wavefunction. Since the physical wavefunction is unchanged, all mean-field Hamiltonians related by such local gauge transformations must be equivalent. The projective symmetry group is the group of transformations which act on H_{mf} that leave the physical Hamiltonian H invariant. Now, if we let $\theta_i = \theta \,\forall\, i$, there exists a global symmetry which cannot be removed by a gauge transformation. Since the mean-field Hamiltonian is invariant under this global symmetry, this acts as an identity operation in the projective symmetry group. The set of such identity operations is known as the 'invariant gauge group' (IGG).

For example, if H_{mf} contains a global $\mathbb{Z}_2$ symmetry, then this means that H_{mf} is invariant under $f_{i\sigma}^{\dagger} \to f_{i\sigma}^{\dagger}$ and under $f_{i\sigma}^{\dagger} \to -f_{i\sigma}^{\dagger}$. More generally, under a gauge transformation $\Phi_r \to W_r\Phi_r$, the Hamiltonian transforms like $u_{rr'} \to W_r^{\dagger}u_{rr'}W_{r'}$. A global transformation $W_r = W$ is the identity if $W^{\dagger}u_{rr'}W = u_{rr'}$.

Now, a symmetry $\mathcal{S}$ acting on the parton Hamiltonian transforms H_{mf} according

to

$$\mathcal{S} : u_{rr'} \rightarrow u_{\mathcal{S}(r)\mathcal{S}(r')}. \tag{1.19}$$

The parton Hamiltonian is invariant under $\mathcal{S}$ if $u_{\mathcal{S}(r)\mathcal{S}(r')} = u_{rr'}$. But, even if $\mathcal{S}$ is not a symmetry of H_{mf}, the physical wavefunction will still be invariant under $\mathcal{S}$ if there exists a gauge transformation that restores the symmetry. Therefore, physical wavefunctions based on the parton construction are invariant under a symmetry as long as

$$W_r^\dagger u_{\mathcal{S}(r)\mathcal{S}(r')} W_{r'} = u_{rr'}. \tag{1.20}$$

Finding the set of parton Hamiltonians for which the corresponding physical wavefunctions respect a set of symmetries is equivalent to finding the full set of mean field Hamiltonians $u_{rr'}$ and gauge transformations $\{W_r^{(\mathcal{S})}\}$ which satisfy Eq. 1.20.

This task is somewhat simplified by the fact that the properties of a symmetry group imposes certain constraints on the allowed set of gauge transformations. For example, consider the following mirror symmetries on the square lattice using the coordinates $\mathbf{r} = (x, y)$:

$$\begin{aligned} P_x &: \mathbf{r} \rightarrow (-x, y) \\ P_y &: \mathbf{r} \rightarrow (x, -y) \\ P_{xy} &: \mathbf{r} \rightarrow (y, x). \end{aligned} \tag{1.21}$$

As explained in ref.[39], these symmetries are not independent, but instead the set of

symmetries $\mathcal{S} = \{P_x, P_y, P_{xy}\}$ obey the relations

$$\begin{aligned} \mathcal{S}_a^{-1}\mathcal{S}_b^{-1}\mathcal{S}_a\mathcal{S}_b &= \mathcal{I} \quad \forall\, a \neq b \\ \mathcal{S}_a^2 &= \mathcal{I}, \end{aligned} \tag{1.22}$$

where $\mathcal{I}$ is the identity transformation. Each sequence of symmetry transformations also has an associated gauge transformation $G_r^{(\mathcal{S})}$. Then for $\mathcal{O}_{ab} = \mathcal{S}_a^{-1}\mathcal{S}_b^{-1}\mathcal{S}_a\mathcal{S}_b$,

$$G_r^{\mathcal{O}_{ab}} = \left(G^{\mathcal{S}_a}_{\mathcal{S}_b^{-1}\mathcal{S}_a\mathcal{S}_b(r)}\right)^\dagger \left(G^{\mathcal{S}_b}_{\mathcal{S}_a\mathcal{S}_b(r)}\right)^\dagger G^{\mathcal{S}_a}_{\mathcal{S}_a\mathcal{S}_b(r)} G^{\mathcal{S}_b}_{\mathcal{S}_a(r)}. \tag{1.23}$$

When $\mathcal{O}_{ab}$ is the identity, we can use the fact that the identity gauge transformation is any element of the IGG. Therefore, for a $\mathbb{Z}_2$ IGG, we have that $G_r^{\mathcal{O}_{ab}} = \tau^0$ or $G_r^{\mathcal{O}_{ab}} = -\tau^0$, where τ^0 is the zeroth Pauli matrix. For a $U(1)$ spin liquid, $G_r^{\mathcal{O}_{ab}} = e^{i\theta}\tau^0$ for any value of $\theta \in [0, 2\pi]$. Such a choice of identity element can be made for each symmetry relation in a given symmetry group. The different combinations of identity elements give rise to different classes of solutions for the allowed gauge matrices, which in turn lead to different spin states.

In summary, we have seen that the parton Hamiltonian $\mathcal{H}_{mf}$ can ostensibly break the symmetries of H as long as there exists a local gauge transformation which restores the symmetry. In this case, we say that the quasiparticle realizes the symmetry nontrivially. The role of the PSG is to determine the set of allowed mean-field Hamiltonians which cannot be connected to each other by such a gauge transformation. Importantly, $\mathcal{H}_{mf}$ is always invariant under some global transformations $\Phi \to \Phi \cdot W$, where $W \in G$. The group $G \supseteq \mathbb{Z}_2$ of such global transformations is known as the 'invariant gauge group' (IGG) and determines the form of the gauge group around

which fluctuations of the gauge field may occur.

Spin Liquid Wavefunctions from Slave-Partons

We can also use the parton formalism to explicitly construct spin liquid wavefunctions. The parton operators $f_{i\sigma}, f_{i\sigma}^\dagger$ live in a larger Hilbert space than the spins S_i. To remedy this, one must include the strict gauge constraint on the allowed states

$$\sum_\sigma f_{i\sigma}^\dagger f_{i\sigma} = 1. \tag{1.24}$$

This can be done at the level of the wavefunction by applying the Gutzwiller projection operator $\mathcal{P}_G$ to the mean field wavefunction $|\psi_0\rangle$ in the fermionic space:

$$|\Psi\rangle = \mathcal{P}_G |\psi_0\rangle \tag{1.25}$$

$$\mathcal{P}_G = \prod_i n_i(2 - n_i). \tag{1.26}$$

The projected wavefunction $|\Psi\rangle$ lives in the proper Hilbert space of spins and, with a suitable choice of $|\psi_0\rangle$, is highly entangled in real space.

The coefficients of the projected wavefunction are given by the expression

$$|\Psi\rangle = \sum_{\{\sigma_i\}} \Psi_{\sigma_1 \ldots \sigma_N} |\sigma_1 \ldots \sigma_N\rangle \, \Psi_{\sigma_1 \ldots \sigma_N} = \langle 0| \prod_{i=1}^N f_{i\sigma_i} |\psi_0\rangle \tag{1.27}$$

for $\sigma_i = \pm 1$.

To study fermion system, generally one starts from a free-fermion wavefunction

$$|\psi\rangle = \prod_k c_k^\dagger |0\rangle \tag{1.28}$$

where

$$c_k^\dagger = \sum_{i=1}^{N} \sum_{\alpha} A_{k,i}^{(\alpha)} c_{i,\alpha}^\dagger \tag{1.29}$$

and $c_{i\alpha}^\dagger$ creates an electron on site i with quantum numbers α.

This free-fermion wavefunction can be written in a local basis as a single Slater determinant

$$\begin{aligned} |\psi\rangle &= \sum_{\{x\}} \det(A) \, |\{x_1, x_2, \ldots, x_n\}\rangle \\ &= \sum_{\{x\}} \begin{vmatrix} A_{x_1,1} & A_{x_1,2} & \ldots & A_{x_1,N_e} \\ A_{x_2,1} & A_{x_2,2} & \ldots & A_{x_2,N_e} \\ \vdots & \vdots & \ddots & \vdots \\ A_{x_{N_e},1} & A_{x_{N_e},2} & \ldots & A_{x_{N_e},N_e} \end{vmatrix} |\{x_1, x_2, \ldots, x_n\}\rangle \, . \end{aligned} \tag{1.30}$$

where N_e is the number of electrons and $|\{x_n\}\rangle = \prod_i c_{x_i}^\dagger |0\rangle$ is the basis state where electrons are localized at the lattice positions given by the set $\{x_n\}$. We can absorb the spin degree of freedom α into the position label x_i by letting n range from 1 to 2N. The probability amplitude of any given configuration $\{x_n\}$ is therefore $|\det(A_{x_i,j})|^2$.

Once the free-fermion wavefunction is written in real space, the Gutzwiller projection operator $\mathcal{P}_G$ can be applied to $|\psi\rangle$, to create a true spin wavefunction. For the mean-field Hamiltonians which realize physical symmetries nontrivially, the free-fermion wavefunction $|\psi_0\rangle$ will break such a symmetry while the projected wavefunction $|\Psi\rangle = \mathcal{P}_G |\psi\rangle$ will respect it.

1.2.2 Experimental Systems

The most amazing aspect of quantum spin liquids is that this exotic highly entangled phase emerges as the effective low energy description of quite generic many body systems. Many QSL phases can be accessed starting from a simple Hubbard model. For this reason, there exists a very real possibility that real materials may be described by these long range entangled wavefunctions.

Most materials, it turns out, order magnetically at zero temperature and so the quantum nature of the underlying degrees of freedom is somewhat hidden. One therefore must look at systems where the quantum effects are enhanced. This may be achieved in multiple ways. The key is generally to look for sources of frustration of the magnetic order. This is a general term for any aspect of the spin model which doesn't allow for optimal pairwise ordering of the spins on all bonds simultaneously. This may be provided by the geometry of the lattice, the presence of competing longer range interactions in the Hamiltonian or the presence of spin-orbit coupling terms. We will see examples of each of these below.

As an aside, note that for spin-$\frac{1}{2}$ systems, nearly all antiferromagnetic Heisenberg models are technically frustrated since any spin can only exist in the optimal singlet spin configuration $|\uparrow\downarrow\rangle - |\downarrow\uparrow\rangle$ on a single bond. The energy $E = -\frac{3}{4}J$ of this configuration competes with the classical Nèel configuration which has an energy $E = -\frac{1}{4}J$ but may satisfy this on multiple bonds at once. Some lattices, however, are more frustrated than others and do not even allow for spins to optimally satisfy a single component (say the $S_i^z S_j^z$ term) of the Heisenberg interaction. In some cases, the energy of a singlet state may be lowered by taking a superposition of different "dimer coverings" of the lattice, restoring the translational symmetry of the Hamiltonian to the wavefunction. This was the idea behind Anderson's original resonating valence

bond (RVB) state, the first proposed spin liquid wavefunction [42].

We also know of several models with relatively simple interactions where spin liquids are known to be the ground state. We further can identify various materials which appear to be fairly well described by these models. I will briefly review a few of the most promising experimental candidate spin liquid systems and highlight a few key features. We should emphasize that although there is enticing evidence of QSL behavior in all these materials, so far there is yet no conclusive example of a true spin liquid found in nature. The true form of the ground state remains controversial in all known experimental spin liquid candidate systems.

Triangular Lattice Organics

In the organic compounds $\kappa - (ET)_2Cu_2(CN)_3$ and $EtMe_3Sb[Pd(dmit)_2]_2$, organic molecules host single orbitals and appear to form quasi-2D half-filled triangular lattice Mott insulators. The spins in these materials interact with an exchange energy $J \sim 250K$, yet show no order down to $50mK$. The electrons in these organic compounds appear to not be very well localized. The Mott gap in these materials appears to be very small and the system can be driven into a metallic phase by applying a relatively small pressure.

A reasonable description of these materials is a simple single band Hubbard model

$$H_{hub} = -t \sum_{\langle ij \rangle, \sigma} c^{\dagger}_{i\sigma} c_{j\sigma} \; + \; U \sum_{i} n_{i\uparrow} n_{i\downarrow}. \tag{1.31}$$

When U is very large, the electrons are well localized on each site and the system is well described by a Heisenberg model. The Heisenberg model on the triangular lattice was originally the first proposed candidate RVB model. It has since been shown that

the pure Heisenberg case orders magnetically in a 120° pattern [43]. For very small U, the electrons are completely delocalized and the ground state is a metal. The small Mott gap in the organic compounds suggests that U is large enough to localize the electrons, but not so large that they are strictly confined to a single site.

In this case, the full fermion Hilbert space is necessary to describe the true ground state, however one can still project into the spin Hilbert space by expanding the strong coupling expansion to further powers of t/U. To the next leading order, the expansion in $\frac{t}{U}$ gives second- and third-neighbor Heisenberg interactions, plus a 4-site 'ring-exchange' interaction.

$$H_{spin} = \sum_{ij} J_{ij} \vec{S}_i \cdot \vec{S}_j + K \sum_{\square} S_1^+ S_2^- S_3^+ S_4^- + \text{h.c.}, \tag{1.32}$$

where J_{ij} contains first, second and third nearest-neighbor terms J_1, J_2 and J_3. In terms of the Hubbard parameters, we have $J_1 \sim \frac{t^2}{U}$ and $J_2, J_3, K \sim \frac{t^4}{U^3}$. There is numerical evidence [44, 45] that when K is above a certain value, the ground state is a quantum spin liquid. In fact, newer numerical results show that the ring exchange may not be necessary and the spin liquid phase may be stabilized with only a small second-neighbor interaction [46, 47]. Further, both theoretical and numerical work has suggested that this ground state may be a $U(1)$ spin liquid with an emergent gapless Fermi surface [48, 49, 50]. Experimentally, the spinon Fermi surface should exhibit some dramatic behavior owing to the anomalously high number of low energy degrees of freedom for an insulator. The specific heat in these materials has been measured and shows a linear T component. Furthermore, thermal conductivity measurements have been performed and also show a linear contribution. The thermal conductivity measurement in particular can only come from delocalized excitations.

Both of these measurements give results that one would expect in a metallic system, not an insulator. This, together with the theoretical work, has lead to the interpretation of the ground state being a QSL with a spinon Fermi surface.

Kitaev Materials

Another approach in the search for experimental QSLs has been to identify interactions which lead to spin liquid behavior in model systems and search for materials which contain these interactions. This has especially been the case in spin systems with strong spin orbit coupling. In these materials, a large onsite spin-orbit coupling term entangles the spin and orbital degrees of freedom of the local magnetic moments. Starting again from a Hubbard model, we can add a spin-orbit single site ion term which is much stronger than any exchange interactions and therefore determines the low lying magnetic degrees of freedom.

$$\begin{aligned} H &= H_{hub} + H_{ion} \\ H_{ion} &= \lambda \vec{l} \cdot \vec{s}. \end{aligned} \tag{1.33}$$

For d orbital electrons in a lattice with octahedral symmetry, the lowest lying angular momentum orbitals are the three t_{2g} orbitals $|xy\rangle$ with $\ell^z = 0$ and $|xz\rangle \pm i\,|yz\rangle$ with $\ell^z = \pm 1$. Electrons in the xy orbital hop primarily within the xy plane, and similarly for the xz and yz orbitals. When $\lambda = 0$, all the combined spin and orbital states $|\ell^z, \sigma\rangle$ are degenerate. The single ion spin-orbit coupling term breaks the degeneracy

down to a single Kramer's doublet of states

$$|\tilde{\uparrow}\rangle = \frac{1}{\sqrt{3}}\left(|xy,\uparrow\rangle + i\,|xz,\downarrow\rangle + |yz,\downarrow\rangle\right)$$
$$|\tilde{\downarrow}\rangle = \frac{1}{\sqrt{3}}\left(|xy,\downarrow\rangle + i\,|xz,\uparrow\rangle - |yz,\uparrow\rangle\right) \tag{1.34}$$

The *isospin* states $|\tilde{\uparrow}\rangle$ and $|\tilde{\downarrow}\rangle$ are a coherent superposition of different spin and orbital eigenstates, and transform like regular spin-$\frac{1}{2}$ degrees of freedom. The usual superexchange interaction derived from the strong coupling expansion of H_{hub} must now be projected onto the isospin subspace. As shown in [51], this can then lead to interactions among these isospins which are highly anisotropic in real space. In fact, if the spins sit on the sites of a lattice of edge sharing octahedra, there is an exact cancellation of any Heisenberg contribution to the spin-spin interaction, and all that remains is a nearest-neighbor interaction of the form

$$\mathcal{H} = \sum_{ij} S_i^{\gamma_{ij}} S_j^{\gamma_{ij}} \tag{1.35}$$

where $\gamma_{ij} \in \{x, y, z\}$ is the direction perpendicular to the plane containing the bond ij.

This is the form of the famous 'Kitaev' interaction. On the honeycomb lattice, it was shown that this model could be solved exactly and leads to a spin liquid ground state [52]. The solution follows by writing the spin $S_i^\mu = \frac{i}{2} c_i^\mu c_i$ for $\mu = \{x, y, z\}$ where c_i, c_i^μ are Majorana fermion operators with $c_i^\dagger = c_i$. Then, since $u_{ij}^\mu = i c_i^{\gamma_{ij}} c_j^{\gamma_{ij}}$ commutes with $\mathcal{H}$, and also $[u_{ij}, u_{kl}] = 0$, we can fix the value of u_{ij} on each bond.

Then we can write the Hamiltonian as

$$\mathcal{H} = \sum_{ij} u_{ij} c_i c_j. \tag{1.36}$$

In other words, this is a model where the fermionic parton mean-field theory is exact.

It is remarkable that this exactly solvable interaction is in fact generated in real materials via the above described spin-orbit coupling superexchange mechanism. In fact, there exists an entire family of hyper-honeycomb lattices where there is very strong evidence for the presence of the above interaction [53, 54]. However, it appears that in these materials there also exists a Heisenberg interaction of considerable strength, and this term competes with the Kitaev term. So far, it seems that most of these Kitaev materials order magnetically below some critical temperature [55]. Nevertheless, there exist a large family of such materials, and there is considerable hope and activity in finding one where some spin-liquid behavior can be seen.

$\mathbf{YbMgGaO_4}$

Recently, experiments on a new material, $YbMgGaO_4$ have shown very enticing evidence of spin liquid behavior [56, 57]. This material mixes important aspects of both the Kitaev materials and the organic compounds. Like the organics, $YbMgGaO_4$ is a Mott insulator in which effective spin-$\frac{1}{2}$ quantum spins from the Yb ions sit on the sites of a triangular lattice. The spins show no sign of magnetic order down to temperatures below $T < 0.1K$, which is far below the scale of the magnetic interactions (estimated to be around $J \sim 4K$). Also, like the organic compounds, in $YbMgGaO_4$ there is significant evidence of a high density of low energy excitations. The magnetic specific heat shows a $T^{0.7}$ dependence at low temperatures. This power law depen-

dence is very close to the value which is predicted for a metal which is strongly coupled to a $U(1)$ gauge field [49, 44]. This therefore seems like a very strange temperature dependence for an electrical insulator such as this.

Unlike the organic compounds, the electrons in this material appear to be very well localized and so weak Mott insulator physics is not believed to play a role in frustrating the magnetic order. The Yb spins also have much larger magnetic moments and they are much denser than in the organics. This makes $YbMgGaO_4$ a perfect candidate for inelastic neutron scattering experiments. This is the most direct method we have of probing the low energy excitations of a system. These measurements were performed in Refs [56] and [57] and the experiments show a very broad continuum of low energy excitations which has no sharp features and is not peaked around any specific momenta. This is taken to be consistent with the low energy spectrum of a spin liquid where quasiparticle excitations cannot be created singly and so there is no definite energy-momentum relation in the low energy spectrum. In fact, the neutron scattering results appear consistent with the prediction if a Fermi surface of low energy quasiparticle excitations is assumed. This, taken together with the specific heat measurement and lack of magnetic ordering has lead to speculation that the ground state of this material may be a spinon Fermi surface quantum spin liquid. It has since been appreciated that this material contains a significant amount of bond disorder [58], and this may very well play a critical role in determining the ground state physics [59, 60].

This material also has the interesting feature that the effective spins are strongly spin-orbit coupled. Like in the Kitaev materials, strong single ion spin-orbit coupling entangles the spin and orbital degrees of freedom, which in this case lead the Yb^{3+} ions to be in a total angular momentum $J = \frac{7}{2}$ state. Crystal field effects

then break the degeneracy of this spin further down to a Kramer's doublet effective spin-$\frac{1}{2}$ moment. Therefore, in addition to the usual Heisenberg like spin coupling, $YbMgGaO_4$ also contains spin-spin interactions which are highly anisotropic in real space. In Ref. [57], the strength of these spin-orbit interactions were measured to be about 10-15% the strength of the isotropic nearest-neighbor exchange. A small second-neighbor isotropic exchange with $J_2/J_1 \sim 0.22$ was also reported. In chapter 2, we take an in depth look at the possible effects of the interplay between spin liquid physics and spin-orbit coupling in relation to this material.

1.3 Background on Oxide Heterostructures and Itinerant Magnetism

1.3.1 Oxide Heterostructures

Quantum wells are created when the presence of a large potential restricts the motion of electrons in one direction, effectively confining them to a two dimensional plane. This situation can be effectively manufactured in a well controlled way in transition metal oxide heterostructures [61]. The transition metal oxides are created from perovskite derived structures of transition metals which form an ABO_3 structure, where the B site is a transition metal (we will focus on Ti) with a partially filled d orbital and the A site is an alkali earth or rare earth ion (such as Sr or Gd). The B site Ti ions form a cubic lattice of d orbitals with a small overlap-induced hopping between sites which is mediated by the six oxygen atoms which surround each Ti. Heterostructures can be formed from two dimensional layers of transition metal oxides by modulating the chemical composition of the A site ions as one moves

in the third direction perpendicular to the 2D layers. Quantum wells are formed in these heterostructures when a thin layer of one material is sandwiched between thicker layers of a second material. These heterostructures can be created with very high experimental control. Furthermore, the narrow band d orbital electrons are very strongly interacting.

As mentioned, the charge degrees of freedom in these materials live on the cubic lattice of titanium d-orbitals. In isolation, the Ti atoms are rotationally invariant and so the five $\vec{L} = 3$ d orbital angular momentum states are completely degenerate. In the perovskite crystal structure, this rotational symmetry is broken and the degeneracy is split. In particular the octahedral symmetry of surrounding oxygen atoms breaks the degeneracy into a triplet of t_{2g} orbitals and a doublet of e_g orbitals. The three t_{2g} orbitals d_{xz}, d_{yz} and d_{xy} sit at a lower energy than the two e_g orbitals $d_{x^2-y^2}$ and $d_{3z^2-r^2}$. In the oxide heterostructure, near the interface, further tetragonal distortions of the crystal lattice break the symmetry between the xy and z directions. The result is a further splitting of the energy levels whereby the d_{xy} orbital may be at a lower energy than the d_{xz} and d_{yz} orbitals [62]. The symmetry of the electron orbitals determines the strength of the directional hopping of the electrons, and in particular the d_{xy} electrons will hop primarily within the xy plane and have only a weak dispersion in the z direction. Similarly for the d_{xz} and d_{yz} for the xz and yz planes respectively. Meanwhile, the principle role of the A site ions is to donate some number of electrons to these Ti sites, effectively determining which d orbitals are partially filled.

Most of the interesting physics in these heterostructure materials originates from the so called polar discontinuity [63, 64]. This occurs because depending on the A site ion, the individual oxide materials may be either polar or nonpolar. For example, in

$RTiO_3$ materials, the rare earth R ion donates a single electron to the Ti ions, which results in a nonzero electric dipole moment pointing from the now positively charged R layer to the negatively charged Ti layer. On the other hand, in the material $SrTiO_3$, the Sr ions do not donate any electrons to the Ti sites, and so there is no polarization between layers. At the interface between a polar and nonpolar material, exactly half an electron per interface site is donated from the polar material to the nonpolar one. As a result, a very high density two dimensional electron gas (2DEG) becomes trapped in the quantum wells. Experiments in $RTO_3/SrTiO_3$ heterostructures observe a constant carrier density from Hall measurements very close to the theoretical value of $\frac{1}{2}$ electron per unit cell [65, 66, 67]. Furthermore this carrier number scales with the number of interfaces, not the thickness of the layers, indicating that these itinerant electrons do indeed originate from the polar discontinuity.

Therefore, the ability to substitute different A and B site ions allows us to change which d orbitals are partially filled giving some control over the strength of the electron hopping in different directions. By tuning the width of the quantum well, we tune the density of electrons as the $\frac{1}{2}$ e^- donated per interface site are distributed throughout all the sites in the quantum well. Furthermore, the strength of the Hubbard onsite repulsion will vary for different materials. Therefore, in transition metal oxide heterostructures, changing the composition of the constituent materials gives one the capability to tune the physical parameters of the effective strongly interacting electron Hamiltonian.

In this thesis, we will focus on the particular RTO/STO heterostructures, where R is a rare earth ion. $SrTiO_3$ is a band insulator with zero d orbital electrons per site. $RTiO_3$ compounds on the other hand have a single unpaired electron and forms a bulk Mott insulating state. In RTO/STO quantum wells, the d electrons therefore

mainly occupy the single lowest energy d_{xy} orbital. The effective model is one of a strongly interacting single band Hubbard model where the majority of the electron hopping takes place within the two dimensional interface plane. In the experiments, signatures of itinerant magnetism are seen [68, 69], which is taken as evidence of the strongly correlated nature of the 2DEG. Indeed, this magnetism is an example of the emergence of qualitatively new phenomena at the interface in heterostructure materials.

1.3.2 Nagaoka's Theorem of Ferromagnetism

A single band Hubbard model is the starting point for most of the physics explored in this thesis. We have seen that when the onsite repulsion U is very large, a strong coupling expansion at half filling leads to an effective spin model with *antiferromagnetic* exchange coupling $J \sim \frac{t^2}{U}$. It is therefore a very surprising fact that at extremely large U, ferromagnetism actually appears in the ground state wavefunction if the system is doped to be slightly away from half filling. In fact, in one of the few rigorous results which are available in the strongly coupled Hubbard model, Nagaoka proved in 1966 that at $U = \infty$, if a single hole is doped into the half-filled model on a bipartite lattice, the ground state is the fully polarized ferromagnetic state [70]. Since the single hole is then mobile, this is an example of itinerant magnetism. Since the magnetism is caused solely by the kinetic motion of the hole throughout the lattice, this type of phenomenon is known as kinetic magnetism. Recent numerical results have in fact shown that this itinerant ferromagnetism is stable in the infinite U Hubbard model if instead the doping is extended to a small but finite density of holes [71].

Here we will review the key points of Nagaoka's argument. The main point of

emphasis is that when $U = \infty$, the single hole hops freely throughout the lattice if all the spins are fully polarized in one direction. If they are not polarized, minus signs in the wavefunction work to increase the energy of these states.

Starting from the single band Hubbard model

$$H = -t \sum_{\langle ij \rangle, \sigma} c^{\dagger}_{i,\sigma} c_{j\sigma} \; + \; U \sum_{i} n_{i\uparrow} n_{i\downarrow} \tag{1.37}$$

the strong coupling expansion for an arbitrary density of electrons gives the so called $t - J$ model

$$H_{t-j} = -t \sum_{\langle ij \rangle, \sigma} \mathcal{P}_G c^{\dagger}_{i\sigma} c_{j\sigma} \mathcal{P}_G + J \sum_{\langle ij \rangle} \vec{S}_i \cdot \vec{S}_j \tag{1.38}$$

where $\mathcal{P}_G = \prod_i (1 - n_{i\uparrow} n_{i\downarrow})$ is the Gutzwiller projection operator which forbids double occupancy of a site. At half filling this obviously reduces to the usual Heisenberg model for spins. At $U = \infty$, we have that $J = 0$ and the only term in the expansion is the projected hopping term

$$H = -t \sum_{\langle ij \rangle, \sigma} \mathcal{P}_G c^{\dagger}_{i\sigma} c_{j\sigma} \mathcal{P}_G. \tag{1.39}$$

We will sketch the argument that for a bipartite lattice with N sites, when the number of electrons $N_e = N - 1$, the ground state of H in Eq. 1.39 is the fully polarized state with total spin $\vec{S} = S_{max} = \frac{1}{2} N_e$. The first step is to realize that if all the spins have $\sigma = \uparrow$, double occupancy of a site is forbidden automatically and the Hamiltonian is the same as for noninteracting spinless fermions. The ground state wavefunction in this case has energy $E = -zt$, where z is the coordination number.

With a little thought, one can see that this is the lowest energy that is allowed, as the most kinetic energy that can be gained by moving the hole throughout the lattice can only equal that of a freely moving hole. If one attempts to hop the hole in a background of both up and down spins, the fermion will see effective fluxes which can only make it so that the hole is no longer free.

The second part of the argument is to show that the fully polarized phase is the unique ground state wavefunction, up to a degeneracy dictated by the rotational symmetry of the Hamiltonian. In other words, within each S^z sector, the state with $\vec{S}_{tot} = S^z_{max}$ is the unique lowest energy state. The state with $\vec{S}_{tot} = S^z_{max}$ is the positive equal weight superposition of all possible basis states within that S^z sector. In two dimensions, it can be proven that, on a bipartite lattice, any possible basis state can be reached from any other state by hopping the hole to a neighboring site a finite number of times. That is, the basis states in each S^z sector are fully connected in the sense that there is a sequence of nonzero matrix elements connecting any two states $|i\alpha_i\rangle$ and $|j\beta_j\rangle$ (where the state $|i\alpha_i\rangle$ represents the basis state with the hole on site i and spin configuration $\{\alpha_i\}$). Uniqueness of the ground state then follows by proving that this space of connected states obeys a discrete form of Laplace's equation.

To see this, let $j\beta_j = n[i\alpha_i]$ mean that the two states $|i\alpha_i\rangle$ and $|j\beta_j\rangle$ are directly connected by a nonzero matrix element (i.e. by hopping the hole from one site to a neighboring site). Then we have that for a (possibly degenerate) ground state of H

$$|\Phi\rangle = \sum_i \phi(i\alpha_i)\,|\psi_{i\alpha_i}\rangle \tag{1.40}$$

$$\begin{aligned} H|\Phi\rangle &= -zt|\Phi\rangle \\ \Rightarrow -zt\sum_{i\alpha_i}\phi(i\alpha_i)|\psi_{i\alpha_i}\rangle &= -t\sum_{i\alpha_i}\sum_{j\beta_j=n[i\alpha_i]}\phi(i\alpha_i)|\psi_{j\beta_j}\rangle \\ &= \sum_{i\alpha_i}\sum_{j\beta_j=n[i\alpha_i]}\phi(j\beta_j)|\psi_{i\alpha_i}\rangle \end{aligned}$$

$$\Rightarrow \phi(i\alpha_i) - \frac{1}{z}\sum_{j\beta_j=n[i\alpha_i]}\phi(j\beta_j) = 0 \tag{1.41}$$

where z is the coordination number of the lattice. This last line is the discrete version of Laplace's equation, and it guarantees that the set of weights which describe the ground state are unique in this case.

An alternative proof, outlined in Ref. [72] uses the following logic. The amplitudes of all terms in the wavefunction should be positive, because 'nodes' in the probability amplitudes are energetically unfavorable. This is a well known concept in condensed matter physics, where nodes in the probability amplitudes lead to cusps in the probability density which cost kinetic energy. Note that the state with max $\vec{S}_{tot} = S^z_{max}$ is the positive equal weight superposition of all basis states. By symmetry this should have the same energy as the free-fermion wavefunction in the $S^z = S^z_{max}$ sector. Uniqueness then follows from the fact that it is impossible to have two orthogonal states with all positive coefficients.

Therefore, we have "proven" that the fully polarized phase, where $\phi(i\alpha_i)$ are all positive and of equal weight, saturates the ground state energy. This proves that the fully polarized ferromagnet is the unique ground state for the infinite U Hubbard model on a bipartite lattice with a single hole.

1.4 Background on Topological Kondo Insulators

1.4.1 Heavy Fermions and Kondo Lattice Materials

Heavy fermions is a term which describes the effective quasiparticle excitations which can occur in systems where a metal is coupled to a lattice of localized magnetic moments in such a way that the magnetic moments are completely screened [73]. This situation is referred to as a Kondo lattice problem, and the coupling between the local moment and the itinerant fermions is known as the Kondo coupling. Heavy fermion physics occurs when the low energy theory is described by Landau's Fermi liquid theory, where the fermionic quasiparticles have been "dressed" by their interaction with the local moments and have effective masses which can be hundreds or thousands of times the bare electron mass.

Consider first, the situation where a single spin defect $\vec{S}$ located at position R_j interacts antiferromagnetically with nearby conduction electrons, which can be modeled with the Hamiltonian

$$H_K = -t \sum_{\langle ij \rangle} c^\dagger_{i\sigma} c_{j\sigma} + J_K \vec{S} \cdot \vec{s}_j \tag{1.42}$$

$$\text{where} \quad \vec{s}_j = \sum_{k,k'} c^\dagger_{k\alpha} \vec{\sigma}_{\alpha\beta} c_{k'\beta} \, e^{-i(\vec{k}-\vec{k}')\cdot\vec{R}_j}, \tag{1.43}$$

so that the magnetic defect $\vec{S}$ is coupled to an effective spin created by the itinerant electrons near site j. The Kondo effect occurs when $\vec{S}$ and the effective spin $\vec{s}$ form a singlet spin, effectively screening the local moment. This situation obviously occurs when J_K is large, as in this strongly coupled limit the lowest energy state of the Heisenberg like coupling is a singlet state. Anderson showed using his 'poor man's'

scaling procedure [74], that even when the Kondo coupling is weak, the presence of a finite density of states at low energies due to the electron Fermi surface forces the Kondo coupling to flow to the strong coupling regime at low energies. As a result, the magnetic moment is always screened, even at weak coupling, at temperatures below the Kondo temperature $T_K \sim D \exp[1/J\rho]$ where D is the conduction electron bandwidth and ρ is the low energy density of states.

The Kondo lattice problem [75] occurs when there is an entire lattice of magnetic moments S_j, so that the Hamiltonian takes the form

$$H_K = -t \sum_{\langle ij \rangle} c^\dagger_{i\sigma} c_{j\sigma} + J_K \sum_j \vec{S}_j \cdot \vec{s}_j. \tag{1.44}$$

In this case, when such a screening of the local moments occurs, it results in a new quasiparticle which is a bound state of the local moment and the nearby itinerant fermions [76]. These quasiparticles carry the same quantum numbers as the original conduction electrons, but their binding with the local moment can lead to a huge increase in their effective mass. This is most easily seen by considering the following mean field theory.

First, we write the local spin moment using the Abrikosov fermion decomposition

$$\vec{S}_i = f^\dagger_{i\alpha} \vec{\sigma}_{\alpha\beta} f_{i\beta} \tag{1.45}$$

$$\sum_\sigma f^\dagger_{i\sigma} f_{i\sigma} = 1. \tag{1.46}$$

We then write

$$\begin{aligned} H_K &= -t\sum_{\langle ij\rangle} c^\dagger_{i\sigma}c_{j\sigma} \;+\; J_K\sum_j f^\dagger_{j\alpha}f_{j\beta}c^\dagger_{j\gamma}c_{j\delta}\vec{\sigma}_{\alpha\beta}\cdot\vec{\sigma}_{\gamma\delta} \\ &= -t\sum_{\langle ij\rangle} c^\dagger_{i\sigma}c_{j\sigma} \;+\; J_K\sum_j \langle f^\dagger_{j\alpha}c_{j\delta}\rangle f_{j\beta}c^\dagger_{j\gamma} + \langle f_{j\alpha}c^\dagger_{j\delta}\rangle^* f^\dagger_{j\beta}c_{j\gamma} \\ &= \sum_k \varepsilon_k d^\dagger_k d_k. \end{aligned} \tag{1.47}$$

where $d^\dagger_k = u_k c^\dagger_k + v_k f^\dagger_k$ is a coherent superposition of the $c^\dagger$ and $f^\dagger$ operators. In other words, using this mean-field decoupling, the effective theory is still a theory in terms of itinerant fermion operators, but these new operators are a combination of the physical electrons and the 'slave fermions' from the spins.

As in the case of spin liquids, in order for our theory to be valid we must satisfy the constraint of exactly one f fermion per site. In the mean field theory, this can be done approximately by ensuring that $\sum_{i\sigma}\langle f^\dagger_{i\sigma}f_{i\sigma}\rangle = 1$. To find a more precise result, one would need to either introduce a dynamic gauge field or at least Gutzwiller project the resulting free-fermion wavefunction. In this sense, the Kondo phase can be thought of as a confined phase, where the $f^\dagger$ spinons are bound to the physical $c^\dagger$ electrons. One can consider the situation where the $f^\dagger$ spinons are truly deconfined. In this case, the spins form a quantum spin liquid state which is weakly coupled to a fermion state with a Fermi surface. This situation is studied in Refs [77, 78]. The resulting ground state is an exotic conducting state known as the FL* phase.

Furthermore, it can occur that the resulting effective free-fermion theory is a band insulator, even though the original electrons formed a metal. When this occurs the phase is known as a Kondo insulator. Note that although the effective theory is that of noninteracting fermions, interactions are critical if one is to arrive at such an

effective theory. In principle, driving a metal with an odd number of electrons per unit cell into an insulating phase is one of the most dramatic examples of strongly correlated physics. Furthermore, the band insulator of the effective Kondo theory may have an additional topological component. In this case, we say that the system is a topological Kondo insulator [79, 80].

1.4.2 Topological Band Theory

In one of the more surprising and successful developments in the last 20 years it was discovered that even non-interacting fermions can display 'non-trivial' behavior [81, 82]. Bloch's theorem states that the eigenstates of a single electron Hamiltonian in a periodic potential can be written in terms of the Bloch states

$$|\psi_{\mathbf{k}}\rangle = e^{i\mathbf{k}\cdot\mathbf{r}} |u_{\mathbf{k}}\rangle . \tag{1.48}$$

where $|u_k\rangle$ has the same periodicity as the lattice. However, these single particle states have a intrinsic phase ambiguity

$$|u_{\mathbf{k}}\rangle \to e^{i\phi(\mathbf{k})} |u_{\mathbf{k}}\rangle . \tag{1.49}$$

This quantum mechanical phase gives some additional structure to the manifold of single particle eigenstates. We can define the concept of curvature in this manifold using the 'Berry connection'

$$\vec{A}(k) = -i\langle u_{\mathbf{k}}|\vec{\nabla}_{\mathbf{k}} |u_{\mathbf{k}}\rangle . \tag{1.50}$$

The Berry connection acts like a gauge field, since it is invariant under $\vec{A} \to \vec{A} + \vec{\nabla}_{\mathbf{k}}\phi$. This is a consequence of the inherent ambiguity in the phase of a quantum state. The Berry connection is not observable, however, we can also define the 'Berry Curvature' as $F = \vec{\nabla} \times \vec{A}$. The Berry curvature is a well defined gauge-invariant quantity whose value has physical significance. A nonzero Berry curvature acts as a source of flux and modifies the equations of motion of the physical electrons. This leads to the emergence of an anomalous Hall conductivity given by the expression

$$\sigma_{xy} = \frac{e^2}{\hbar} \int_{\partial S} \vec{A}_{\mathbf{k}} \cdot d\mathbf{k} = \int_s \vec{\nabla} \times \vec{A}_{\mathbf{k}} d^2k \tag{1.51}$$

where the integral is taken over the occupied momentum states. The quantity $\int_{\partial S} \vec{A} \cdot d\mathbf{k}$ is known as the Berry phase. If the electron system is a time-reversal invariant band insulator, the Berry phase can only be quantized in integer values of 2π. This gives the band structure a *topological* property. If free-fermion systems are to have a nontrivial topology, each momentum state must have some internal structure. This may be provided, for example, by the internal spin symmetry in time-reversal invariant fermion models. Then, if one is to have a nontrivial winding of the phase, this internal quantum number and the momentum must be coupled in a nontrivial way. In the original proposals of the spin-quantum Hall effect [83, 84], this was provided by a spin-orbit coupling term. The discovery of this topological property in free-fermion systems [85, 86, 87, 88, 89] and the subsequent experimental discovery of the so-called topological insulators [90, 91, 92, 93] opened up completely new avenues of research. An abundance of new phases which can be classified based on their nontrivial topology have been proposed and the search for new topological materials is a very active area of research.

As a final comment, note that if the electron band is only partially filled, the system is a metal. A nontrivial Berry curvature will still have a physical effect on the electrons. In this case, it has been shown that the appearance of a nontrivial anomalous Hall conductivity can be expressed solely in terms of the Berry curvature of the fermionic quasiparticles near the Fermi surface [94]. Therefore, this topological property is fully consistent with Fermi liquid theory and is stable for interacting fermion systems. In general, interacting short-range entangled topological phases have the potential to display even more exotic behavior than the free-fermion phases.

1.5 Outline and Remarks

We finish this section by outlining the remainder of this dissertation. In chapter 2, we very generally explore the relationship between strong spin-orbit coupling and spin liquid physics on the triangular lattice. We broach the topic in numerous ways, combining the projective symmetry group analysis with variational Monte Carlo to look at the competition between magnetically ordered phases and different spin liquid ansätze. We study a very general spin-orbit coupled model of effective spin-$\frac{1}{2}$ moments on the triangular lattice. We relate our model to the spin-orbit coupled material $YbMgGaO_4$ and examine the viability of candidate $U(1)$ quantum spin liquid wavefunctions. We are able to map out the entire phase diagram of this model when both spin-orbit coupling terms and second- and third-neighbor Heisenberg interactions are present. In this way we are able to make connections to spin liquid studies of rotationally invariant models with further-neighbor interactions on the triangular lattice. We also develop a method to numerically study phenomenological effects in the spinon Fermi surface spin liquid states in the presence of spin-orbit interactions

which are beyond the effects seen in the standard Gutzwiller wavefunctions. We find several new and interesting features which one may expect to see in such a system. In particular, we find that the spinon metal QSL with spin-orbit interactions may have a large thermal Hall conductivity term which emerges due to an intrinsic Berry curvature which is induced near the spinon Fermi surface.

In chapter 3, we study the physics which emerges at the interface between a Mott insulator and a band insulator. This situation is seen experimentally in $GTiO_3/SrTiO_3$ oxide heterostructures. We take a distinct view of the interface, proposing that the nearby Mott insulating spin degrees of freedom in the $GTiO_3$ layer will interact with the high density 2DEG in the $SrTiO_3$. In $GTiO_3$, the onsite Hubbard repulsion is of order $U \sim 4 - 8eV$, which is very large, while $t \sim 0.3eV$. This implies that the magnetic exchange $J \sim t^2/U \ll t, U$ is very small. With this in mind, we model the Mott insulator/band insulator interface in this model with a two layer infinite U Hubbard model, adding a chemical potential offset between the two layers. When this offset is large, we can truly think of the two layers independently as a layer of localized spins and an itinerant fermion layer. This allows us to show that magnetism emerges in this model due entirely to the *interplay* between the Mott insulating and itinerant electron degrees of freedom. This should be taken in the context of the huge and growing amount of research on oxide interfaces, and in which, in several examples, such magnetism has been observed. We show that itinerant ferromagnetism appears in our model. We relate this ferromagnetism quite rigorously to the long standing idea of kinetic magnetism. Our model provides one of the first examples of a qualitatively new phenomenon that can be pinpointed to emerge entirely due to the introduction of a Mott insulator/band insulator interface. We further strengthen our analytic arguments with well-controlled numerical calculations. This gives us unprecedented

insight into the strongly interacting regime of these interface materials.

In chapter 4, we study a model of graphene which interacts via a Kondo coupling with a lattice of localized magnetic moments. Spin-orbit coupling in the local moments then induces spin-orbit effects in the hybridized fermions in the Kondo phase. This leads to a topological Kondo insulator phase appearing in this model. We study the full phase diagram looking specifically at the competition between topological Kondo order and magnetic order. The most dramatic consequence of a nontrivial topology in two-dimensional insulating phases is the existence of symmetry protected gapless edge states. We look at the effect of interactions on these edge states and look specifically at the possibility that the Kondo interaction leads to edge states which spontaneously break time-reversal symmetry, while preserving the symmetry within the bulk.

Chapter 2

Spin Liquid versus Spin Orbit Coupling on the Triangular Lattice

2.1 Introduction

Quantum spin liquids (QSLs) are exotic phases of correlated electrons possessing highly entangled ground states, exotic fractionalized excitations, and typically, the absence of any magnetic order [13, 14]. Historically, studies of QSLs focused on spin-rotationally invariant Heisenberg models, but in recent years, strongly anisotropic interactions arising from spin-orbit coupling have come under focus [95]. In the famous Kitaev honeycomb model, bond-dependent interactions lead to an exactly solvable model with a spin liquid ground state [52]. Remarkably, it was later shown that these directional interactions can be generated in real materials when spin-orbit effects are present [96, 51]. In turn, this has led to the recent discoveries of many candidate 'Kitaev' materials and has paved the way for the study of spin liquid physics in spin-orbital systems. One recent example of particular interest is the

material $YbMgGaO_4$ [97, 98, 56, 99, 57]. This system very likely contains directional interactions of significant strength. Moreover, thermodynamic and inelastic neutron scattering measurements have been interpreted as supporting a QSL state with a Fermi surface of neutral spin-1/2 excitations, "spinons", in this material.

Spin-orbit generated interactions invariably lead to a strong breaking of spin-rotation symmetry. A consideration of this symmetry in spin liquids can then reveal new and unexpected physics. One striking feature is that the lowered symmetry allows for new distinct spin-liquid phases which do not exist in the rotationally invariant case [41, 39]. There exists a systematic method of classifying these phases, given by the so-called projective symmetry group (PSG) [12]. This approach also gives a method for constructing a wavefunction for each phase, as a Gutzwiller projection of a free-fermion state.

We will study a very general spin-orbit coupled model on a triangular lattice which is believed to describe $YbMgGaO_4$ [100, 101, 102] and focus specifically on the possibility that this model contains spin liquid physics. We look at the allowed spin liquid phases and use the PSG as a starting point of our analysis. However, our main tool throughout this work is the variational Monte Carlo (VMC) technique. With this numerical technique, one performs Monte Carlo sampling of the quantum wavefunction in the many-body basis where electrons are localized on each site, allowing one to work with trial states which would otherwise be intractable.

In this chapter, we broadly address three points. First, we expound on the relationship between our model and the PSG wavefunctions. The VMC allows us to quantitatively compare the energies of the different candidate QSL phases. This approach complements recent studies that work with the states phenomenologically [103, 104]. We focus on gapless spin liquids with emergent fermionic excitations and

highlight the differences between states with isolated Dirac-like quasiparticles and those with a Fermi surface of gapless excitations.

Second, we compare the QSL states to magnetically ordered states, seeking the region of stability of the former ones. We show that a QSL is favored if we allow for second-neighbor interactions, but that spin-orbit effects work to reduce the size of this phase, in agreement with Ref. [59]. We then go further and show that, if a natural third-neighbor interaction is also included, then the spin liquid phase is energetically competitive, even in the presence of significant spin-orbit interactions.

Finally, we look at how spin-orbit coupling modifies the properties of a QSL, and how this may lead to distinct observables for experiment. We develop a novel method to incorporate modifications beyond the simplest Gutzwiller projected free-fermion state into our trial wavefunction. This method proceeds by calculating many-body corrections order by order in perturbation theory, and sampling these using VMC. We find that this technique is particularly useful for our problem where spin-orbit interactions introduce qualitative differences between the ground state and our trial states. In particular, we study the effect of spin-orbit coupling on the energies of certain trial states and also demonstrate how unique properties of these wavefunctions appear in the spin structure factor and in thermal transport properties.

The remainder of this chapter is structured as follows. In section 2.2, we define the general spin model on the triangular lattice that we study in our work. In section 2.3, we introduce the variational wavefunctions given by the PSG analysis, which will form the basis for the rest of our discussion. We first calculate the energies of the different candidate spin liquid ansätze using variational Monte Carlo, then allow for the possibility of magnetic order in our simulation, and finally plot the full variational phase diagram for our Hamiltonian. In section 2.4, we introduce our new method for

improving the simple PSG wavefunctions. We calculate the corrections to the energy and the spin structure factor of the spinon Fermi surface spin liquid state. We also show how the spin-orbit interactions may result in an appreciable thermal Hall conductivity in this system. Finally, in section 2.5, we summarize our results and discuss the relevance of our work to the material $YbMgGaO_4$.Quantum spin liquids (QSLs) are exotic phases of correlated electrons possessing highly entangled ground states, exotic fractionalized excitations, and typically, the absence of any magnetic order [13, 14]. Historically, studies of QSLs focused on spin-rotationally invariant Heisenberg models, but in recent years, strongly anisotropic interactions arising from spin-orbit coupling have come under focus [95]. In the famous Kitaev honeycomb model, bond-dependent interactions lead to an exactly solvable model with a spin liquid ground state [52]. Remarkably, it was later shown that these directional interactions can be generated in real materials when spin-orbit effects are present [96, 51]. In turn, this has led to the recent discoveries of many candidate 'Kitaev' materials and has paved the way for the study of spin liquid physics in spin-orbital systems. One recent example of particular interest is the material $YbMgGaO_4$ [97, 98, 56, 99, 57]. This system very likely contains directional interactions of significant strength. Moreover, thermodynamic and inelastic neutron scattering measurements have been interpreted as supporting a QSL state with a Fermi surface of neutral spin-1/2 excitations, "spinons", in this material.

2.2 The Model

In many physical systems, the spin and orbital degrees of freedom of the localized electrons are highly entangled. In these cases, when the rotation symmetry is broken

by the surrounding crystal structure, the spin-rotation symmetry is broken as well. Superexchange processes then lead to the generation of highly anisotropic terms in the effective spin Hamiltonian. In these strongly spin-orbit coupled systems, lattice symmetry transformations are accompanied by an equivalent transformation in spin space. Following Ref. [100], we consider the Hamiltonian

$$\begin{aligned} H &= H_{\pm} + H_z + H_{\pm\pm} + H_{\pm z}, \\ \\ H_{\pm} &= J_{\pm}\mathsf{H}_{\pm} = J_{\pm}\sum_{\langle ij\rangle}\left(S_i^+S_j^- + S_i^-S_j^+\right), \\ H_z &= J_z\mathsf{H}_z = J_z\sum_{\langle ij\rangle}S_i^zS_j^z, \\ H_{\pm\pm} &= J_{\pm\pm}\mathsf{H}_{\pm\pm} = J_{\pm\pm}\sum_{\langle ij\rangle}\left(\gamma_{ij}S_i^+S_j^+ + \gamma_{ij}^*S_i^-S_j^-\right), \\ H_{\pm z} &= J_{\pm z}\mathsf{H}_{\pm z} \\ &= iJ_{\pm z}\sum_{\langle ij\rangle}\left[(\gamma_{ij}^*S_i^zS_j^+ - \gamma_{ij}\,S_i^zS_j^-) + (i\leftrightarrow j)\right], \end{aligned} \tag{2.1}$$

where $\gamma_{ij} = 1, e^{2\pi i/3}, e^{-2\pi i/3}$ for bonds $\langle ij\rangle$ along the $\vec{a}_1, \vec{a}_2, \vec{a}_3$ directions, respectively (see Fig. 2.1a)). This is the most general nearest-neighbor Hamiltonian which is invariant under the symmetry generators of the system: the translations $\mathcal{T}_{1,2}$ along the $\vec{a}_{1,2}$ directions, the sixfold roto-reflection $\mathcal{S}_6$ within the plane of the lattice, the twofold rotation $\mathcal{C}_2$ around a bond in the $\vec{a}_3$ direction, and time reversal Θ. (Note that the threefold rotation $\mathcal{C}_3 = \mathcal{S}_6^2$ and the inversion $\mathcal{I} = \mathcal{S}_6^3$ are both generated by the sixfold roto-reflection.) The symmetry generators are all discrete and act simultaneously in real space and spin space. In particular, they transform the coordinates x_1, x_2 of a

general lattice point $\vec{r} = x_1\vec{a}_1 + x_2\vec{a}_2$ as

$$\begin{aligned}
\mathcal{T}_1 : &\quad (x_1, x_2) \to (x_1 + 1, x_2), \\
\mathcal{T}_2 : &\quad (x_1, x_2) \to (x_1, x_2 + 1), \\
\mathcal{C}_2 : &\quad (x_1, x_2) \to (x_2, x_1), \\
\mathcal{S}_6 : &\quad (x_1, x_2) \to (x_1 - x_2, x_1), \\
\Theta : &\quad (x_1, x_2) \to (x_1, x_2).
\end{aligned} \tag{2.2}$$

while they transform the spin components (S^x, S^y, S^z) as

$$\begin{aligned}
\mathcal{T}_{1,2} : &\quad (S^x, S^y, S^z) \to (S^x, S^y, S^z), \\
\mathcal{C}_2 : &\quad (S^x, S^y, S^z) \to (-\frac{1}{2}S^x + \frac{\sqrt{3}}{2}S^y, \frac{\sqrt{3}}{2}S^x + \frac{1}{2}S^y, -S^z), \\
\mathcal{S}_6 : &\quad (S^x, S^y, S^z) \to (-\frac{1}{2}S^x + \frac{\sqrt{3}}{2}S^y, -\frac{\sqrt{3}}{2}S^x - \frac{1}{2}S^y, S^z), \\
\Theta : &\quad (S^x, S^y, S^z) \to (-S^x, -S^y, -S^z).
\end{aligned} \tag{2.3}$$

Importantly, the Hamiltonian does not generically have a continuous spin-rotation symmetry because the XXZ terms $\mathsf{H}_\pm$ and H_z break the $SU(2)$ spin symmetry down to an in-plane $U(1)$ spin symmetry, while the remaining terms $\mathsf{H}_{\pm\pm}$ and $\mathsf{H}_{\pm z}$ further break the $U(1)$ spin symmetry down to discrete spin symmetries that are intertwined with appropriate lattice symmetries.

It is helpful to write the $\mathsf{H}_{\pm\pm}$ and $\mathsf{H}_{\pm z}$ terms in a slightly different form to further

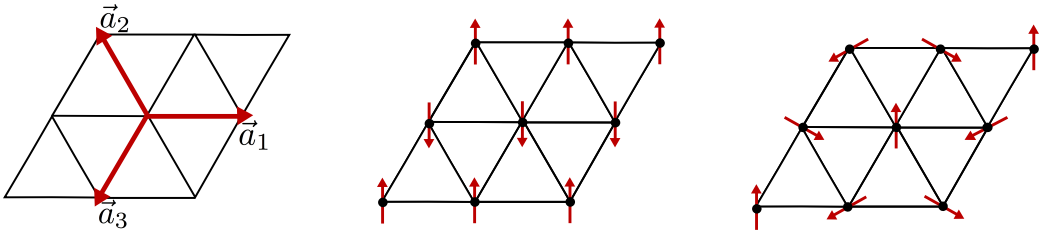

Figure 2.1: **a)** The three lattice bonds a_1, a_2, and a_3. The two commensurate magnetic orders we consider are **b)** stripe order and **c)** 120° antiferromagnetic order.

expose the symmetries:

$$\begin{aligned}
\mathsf{H}_{\pm\pm} &= \sum_{\langle ij\rangle}(\gamma_{ij}S_i^+S_j^+ + \text{h.c.}) \\
&= 4\sum_{\langle ij\rangle}\left[(\vec{S}_i\cdot\hat{n}_{ij})(\vec{S}_j\cdot\hat{n}_{ij}) - \frac{1}{2}(S_i^xS_j^x + S_i^yS_j^y)\right], \\
\mathsf{H}_{\pm z} &= \sum_{\langle ij\rangle}\left[(i\gamma_{ij}S_i^+S_j^z + \text{h.c.}) + (i\leftrightarrow j)\right] \\
&= 2\sum_{\langle ij\rangle}\left[\{(\vec{S}_i\times\hat{n}_{ij})\cdot\hat{z}\}\,S_j^z + (i\leftrightarrow j)\right].
\end{aligned} \tag{2.4}$$

where $\hat{n}_{ij}$ is the unit vector pointing from site i to site j. The term $\mathsf{H}_{\pm\pm}$ has a 'clock' structure where spins would like to align along the 120° bond directions, and the term $\mathsf{H}_{\pm z}$ also has a bond dependent structure that incorporates the $\hat{z}$ direction.

There are several cursory reasons one may expect to find spin liquid physics in this model. For one, due to its strong frustration, the triangular lattice has a long and storied history as a spin liquid candidate [44, 105, 106, 46, 47]. Beyond that, the form of the anisotropic part of H is highly reminiscent of the interactions in the Kitaev honeycomb model [52], where the direction-dependent spin-spin interactions frustrate the coupling in a way which renders all magnetic orders energetically unfavorable.

2.3 Spin Liquid Wave functions

2.3.1 Generalities of parton wavefunctions

The ground state wavefunction in a quantum spin liquid is completely symmetric under all the symmetries of the Hamiltonian. The PSG gives a systematic classification of the allowed spin liquid phases under such a set of symmetries [12]. In the process, it also gives a construction of a representative wavefunction for each phase. It is a surprising fact that, in many cases, the number of allowed spin liquid phases increases as the symmetry is reduced [39, 41]. Spin liquids are fundamentally defined by their fractionalized quasiparticle excitations, whose behavior can be described phenomenologically by a mean-field Hamiltonian. The PSG classifies the fractionalized symmetry by identifying the allowed form of the mean-field Hamiltonians. In general, these excitations can realize the symmetries of the original Hamiltonian in a nontrivial manner.

One starts by writing the physical spin operator $\vec{S}_i$ in terms of fermionic parton operators:

$$\vec{S}_i = \frac{1}{2} f^\dagger_{i\alpha} \vec{\sigma}_{\alpha\beta} f_{i\beta}. \tag{2.5}$$

The parton operators $f_{i\sigma}, f^\dagger_{i\sigma}$ live in a larger Hilbert space than the spins S_i. To remedy this, one must also include the strict gauge constraint on the allowed states:

$$\sum_\sigma f^\dagger_{i\sigma} f_{i\sigma} = 1. \tag{2.6}$$

In this chapter, we enforce Eq. (2.6) at the level of the wavefunction. This is ac-

complished by applying the Gutzwiller projection operator $\mathcal{P}$ to a state $|\psi_0\rangle$ in the fermionic space:

$$|\Psi\rangle = \mathcal{P}\,|\psi_0\rangle\,, \tag{2.7}$$

$$\mathcal{P} = \prod_i n_i(2-n_i). \tag{2.8}$$

The projected wavefunction $|\Psi\rangle$ lives in the proper Hilbert space of spins and, with a suitable choice of $|\psi_0\rangle$, is highly entangled in real space. Furthermore, with some minor improvements, such an ansatz can be made to give variational energies which are competitive with the most state of the art 2D DMRG calculations [106].

For the state $|\psi_0\rangle$, we take a "mean field" wavefunction, which is the ground state of some quadratic fermion Hamiltonian. The parameters of that fiduciary Hamiltonian then become variational parameters in the ansatz. When the fermions are allowed to hop in the mean field Hamiltonian, the partons become deconfined in the corresponding spin liquid phase. In general, the quadratic mean-field Hamiltonian can be written as

$$\mathcal{H}_{mf} = \sum_{i,j,\alpha} \mathrm{Tr}\left[\sigma^\alpha \Phi_i u_{ij}^\alpha \Phi_j^\dagger\right], \tag{2.9}$$

$$\Phi_i = \begin{pmatrix} f_{i\uparrow} & f_{i\downarrow}^\dagger \\ f_{i\downarrow} & -f_{i\uparrow}^\dagger \end{pmatrix}, \tag{2.10}$$

where $\alpha = 0, x, y, z$. A local gauge transformation, such as $f_{i\sigma} \to e^{i\theta_i\sigma^z} f_{i\sigma}$, changes H_{mf} but leaves the physical spin operator $\vec{S}_i$ unchanged. Since the physical wavefunction is unchanged, all mean-field Hamiltonians related by such local gauge transformations must be equivalent. The parton Hamiltonian $\mathcal{H}_{mf}$ can therefore ostensibly break

the symmetries of H as long as there exists a local gauge transformation which restores the symmetry. In this case, we say that the quasiparticle realizes the symmetry nontrivially. The role of the PSG is to determine the set of allowed mean-field Hamiltonians which cannot be connected to each other by such a gauge transformation. Importantly, $\mathcal{H}_{mf}$ is always invariant under some global transformations $\Phi \to \Phi \cdot W$, where $W \in G$. The group $G \supseteq \mathbb{Z}_2$ of such global transformations is known as the 'invariant gauge group' (IGG) and determines the form of the gauge group around which fluctuations of the gauge field may occur. In this work, we consider $U(1)$ spin liquids with IGG $= U(1)$.

A more complete study would also include $\mathbb{Z}_2$ spin liquids (IGG $= \mathbb{Z}_2$). However, even restricting to nearest-neighbor couplings, there are at least 18 different mean-field ansätze. To avoid this complexity, we neglect these candidate QSLs for the present work. This is at least consistent with recent work on several related triangular lattice spin systems, for which the $U(1)$ spin liquids have proven to have competitive energies [44, 106]. Furthermore, the spinon Fermi surface QSL suggested by several previous papers for $YbMgGaO_4$ falls into the $U(1)$ class.

2.3.2 Six specific parton states

The PSG classification of $U(1)$ QSLs for the space group of our model was done in Ref. [103]. There are 6 distinct nearest-neighbor mean-field Hamiltonians:

$$\mathcal{H}_{mf}^{(1)} = \sum_{\langle ij\rangle,\sigma} \left[t_{ij} f_{i\sigma}^{\dagger} f_{j\sigma} + \text{h.c.} \right], \tag{A1/B1}$$

$$\mathcal{H}_{mf}^{(2)} = i \sum_{\langle ij\rangle} \left[t_{ij} f_{i\alpha}^{\dagger} (\vec{\sigma}_{\alpha\beta} \cdot \vec{n}_{ij}) f_{j\beta} + \text{h.c.} \right], \tag{A2/B2}$$

$$\mathcal{H}_{mf}^{(3)} = i \sum_{\langle ij\rangle} \left[t_{ij} f_{i\alpha}^{\dagger} \{ (\vec{\sigma}_{\alpha\beta} \times \vec{n}_{ij}) \cdot \hat{z} \} f_{j\beta} + \lambda_{ij} f_{i\alpha}^{\dagger} \sigma_{\alpha\beta}^{z} f_{j\beta} + \text{h.c.} \right]. \tag{A3/B3}$$

The ground state of each mean-field Hamiltonian defines $|\psi_0\rangle$ for the corresponding type of QSL. We distinguish two versions for each mean-field Hamiltonian $\mathcal{H}_{mf}^{(n)}$, which differ only in the way translation symmetry is realized. In the A states, translation acts in the usual way as $t_{ij} = -1$ for all nearest-neighbor bonds $\langle ij\rangle$. Conversely, in the B states, translation acts nontrivially; this is achieved by setting $t_{ij} = \pm 1$ such that the unit cell is doubled and a π flux is thread through every other triangle. In the A1/B1/A2/B2 cases, there are no variational parameters (since the overall scale of the Hamiltonian leaves its ground state unchanged), while in the A3/B3 cases, there is a single variational parameter λ/t.

We note that, importantly, the spinon band structure determines the physical properties of the wavefunctions and that it is gapless in all 6 states. This is necessary for a U(1) spin liquid to be stable in two dimensions. We now discuss some aspects of these states.

The (A1) state has no mixing between the up and down spin states. In order to satisfy the constraint $\langle f_i^{\dagger} f_i \rangle = 1$, the band structure then must contain a large Fermi surface. We refer to this state as the **uniform Fermi surface (uFS)** or

spinon metal state. Notably, although the microscopic Hamiltonian H has only discrete symmetries, the mean-field Hamiltonian of this uFS state is spin-rotationally invariant. This accidental "emergent SU(2) symmetry" is surprisingly robust, and is not an accident of assuming a nearest-neighbor form for $\mathcal{H}_{mf}$. In fact, all spin-dependent quadratic terms are prohibited from appearing in $\mathcal{H}_{mf}$ by the PSG, even for hoppings of arbitrary distance. The argument for this hinges on the fact that both time-reversal (Θ) and inversion ($\mathcal{I}$) symmetries act trivially in this class. First, the operators which implement these symmetries both involve a complex conjugation, time-reversal by definition and inversion due to a site-exchange which corresponds to a Hermitian conjugation. Then, since spin is even under inversion and odd under time reversal, it is odd under their combination, and so a spin-dependent term with any complex coefficient is forbidden in the presence of such a combined symmetry.

The (B1) state also has no mixing of the spin states, but translations act nontrivially on the spinons. The unit cell is then doubled and the band structure contains two Dirac cones. We therefore refer to this state as the **Dirac spin liquid** state. The uFS and Dirac states are the two $U(1)$ spin liquids that can also occur in rotationally invariant systems. Note, however, that spin-dependent quadratic terms are not generically prohibited in the case of the (B1) state and that they in fact appear at the level of third-nearest-neighbor hoppings.

The (A2) and (B2) states are called the **120° clock spin liquid (ClSL)** and the **120° clock + π spin liquid (ClπSL)**, respectively. These ansätze do mix the spin flavors and orbital degrees of freedom by including bond dependent hoppings. The band structures in both cases contain protected Dirac cones at the Γ, M, and K points in the Brillouin zone.

The (A3) state, called the **Rashba spin liquid (RSL)**, also has Dirac cones at

the Γ, M, and K points when $\lambda = 0$ or $t = 0$, and a gap opens at the Γ point for intermediate values of λ/t. Finally, the (B3) state, called the **Rashba + π spin liquid (RπSL)**, contains 4 bands and a small Fermi surface for intermediate values of λ/t.

2.3.3 Energetics of PSG Wave Functions

The PSG method gives us the full set of allowed free-fermion wavefunctions that are invariant under the symmetries of the system once the gauge constraint, Eq. (2.6), is enforced. It tells us nothing, however, about the energies of these wavefunctions. The PSG gives us a starting ansatz, but is completely agnostic about which state may actually be the ground state.

One simple way to proceed is to work directly with the single particle wavefunctions by satisfying Eq. (2.6) on average: $\frac{1}{N}\sum_{i,\sigma}\langle f^\dagger_{i\sigma} f_{i\sigma}\rangle = 1$. However, such a mean field approach requires an infinite number of approximations, the resulting wavefunctions do not even live in the proper Hilbert space, and thus it cannot give reliable energy estimates. Instead, we carry out a variational analysis based on the fully projected wavefunctions in Eq. (2.7). We calculate the variational energy $E_s = \langle\Psi_s|H|\Psi_s\rangle$, where s indicates one of the six QSL ansätze.

The results are highly constrained by how the projective symmetries are implemented in the given mean-field Hamiltonian. In particular, the uniform Fermi surface and Dirac spin liquid states are completely $SU(2)$ invariant, and therefore the expectation values of the $J_{\pm\pm}$ and $J_{z\pm}$ terms vanish in these states. Similarly, while both the 'clock' and 'Rashba' Hamiltonians have some spin-orbit terms, only the Rashba Hamiltonians include spin-orbit terms both within and perpendicular to the xy plane. Consequently, the 'clock' wavefunctions also yield vanishing expectation values for the

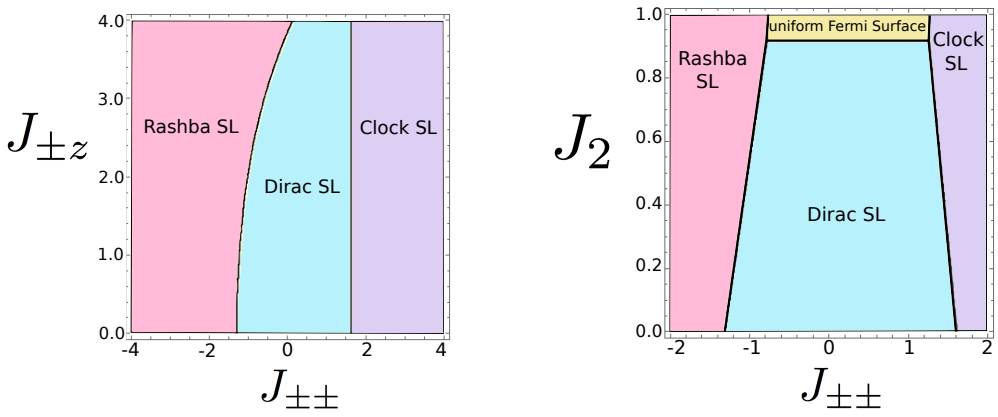

Figure 2.2: The phase diagram showing only the lowest-energy spin liquid ground states **a)** in the $J_{\pm\pm} - J_{\pm z}$ plane with $J_2 = 0$, and **b)** in the $J_{\pm\pm} - J_2$ plane when $J_{\pm z} = 0$. We set the third-neighbor coupling $J_3 = 0$. All energies are measured in units of $J_\pm = 1$. See the main text for a description of the further-neighbor terms J_2 and J_3.

$J_{\pm z}$ terms.

We performed a variational Monte Carlo simulation and measured the energies of each of our trial wavefunctions on finite size lattices for system sizes up to $N = 32 \times 32$ sites. Each mean-field wavefunction, when projected, gives a different pattern of entangled spins, giving rise to different spin correlations. When $\lambda = 0$, none of the wavefunctions have any free parameters. Setting $J_\pm = 1$ and scaling to the thermodynamic limit, the corresponding energy densities are then given by

$$\begin{aligned} E_{Dirac}/N &= -0.7050(1)[1 + J_z/4], \\ E_{uFS}/N &= -0.4682(5)[1 + J_z/4], \\ E_{Clock}/N &= -0.0645(2) + 0.325(1)J_z - 0.716(1)J_{\pm\pm}, \\ E_{Rashba}/N &= -0.1663(4) + 0.258(1)J_z + 0.741(1)J_{\pm\pm}, \\ E_{Cl\pi}/N &= -0.0619(6) - 0.321(1)J_z - 0.582(1)J_{\pm\pm}, \\ E_{Rsh\pi}/N &= +0.1173(4) + 0.256(1)J_z + 0.525(1)J_{\pm\pm}. \end{aligned} \tag{2.11}$$

A few observations are apparent. First, we see that the (ClπSL) and (RπSL) ansätze are never competitive energetically in our regimes of interest. While the Dirac state has the lowest energy at $J_{\pm\pm} = 0$, the clock and Rashba spin liquid states become energetically favorable for large positive and negative $J_{\pm\pm}$, respectively. The Rashba states (and only the Rashba states) have an energy which is modified by including $\lambda \neq 0$, which is beneficial only when $J_{\pm z} \neq 0$. In this case, we determine the optimal Rashba state for a given value of $J_{\pm z}$ by numerically minimizing the energy with respect to λ/t.

The results for a full comparison of energies are presented in Fig. 2.2a), which shows the state of lowest variational energy amongst the 6 QSLs for all values of $J_{\pm\pm}$ and $J_{\pm z}$. (Note that the phase diagram is qualitatively similar for all values of J_z.) Looking ahead, it has been suggested [57] that next-nearest-neighbor interactions may be important in stabilizing a spin liquid ground state for our model. We therefore also looked at the variational energies of our ansätze when XXZ-like next-nearest-neighbor interactions are added, (See Eq. 2.14 in Sec. 3.4.2). In Fig. 2.2b), we plot the lowest energy states as a function of the next-nearest-neighbor coupling J_2 for $J_{\pm z} = 0$. Notice that the Fermi surface state only becomes competitive in energy for very large next-nearest-neighbor coupling.

2.3.4 Magnetic Order

Parton formulation of ordered states

The PSG wavefunctions can be used as a starting point on which magnetic order can be added. This is done by adding a site dependent magnetic field $\vec{h}_i$ to the

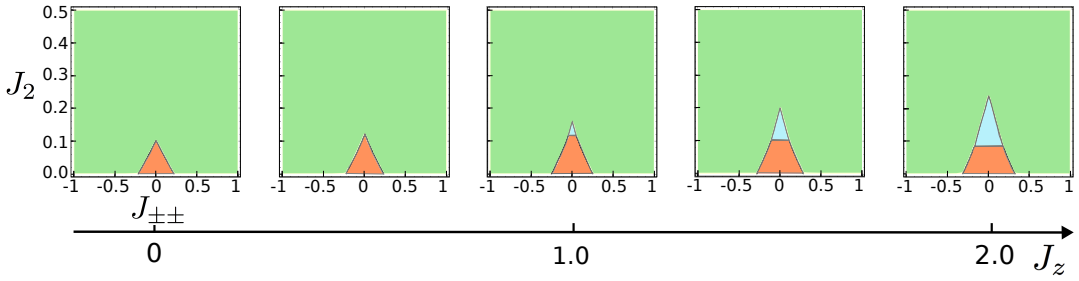

Figure 2.3: The full $J_{\pm\pm} - J_2 - J_z$ magnetic phase diagram for $J_3 = J_{\pm z} = 0$. Green is stripe order, red is 120° AFM order, and blue is the Dirac spin liquid phase. Stripe order dominates the phase diagram, except for small J_2 and $J_{\pm\pm}$. The spin liquid regime also depends strongly on the value of J_z and is greatly reduced when J_z moves away from the isotropic point $J_z = 2$. The horizontal axis on each subplot gives the value of $J_{\pm\pm}$. All energies are measured in units of $J_\pm = 1$.

mean-field Hamiltonians, which define our trial states:

$$\mathcal{H}_{mo} = \mathcal{H}_{mf} - \sum_i \vec{h}_i \cdot \vec{S}_i. \tag{2.12}$$

Magnetic order can be induced in this way on top of any of the 6 QSL states. In practice, the lowest energies are found by using $\mathcal{H}_{mf}^{(1B)}$, i.e., by perturbing the Dirac spin liquid. Notably, the Zeeman term in this case fully gaps the partons. Consequently, the usual Polyakov argument, which applies to an emergent $U(1)$ gauge theory with fully gapped Dirac fermions in two dimensions, implies that monopole instantons proliferate and the Dirac spinons are confined. Thus, the projected wavefunction built from $\mathcal{H}_{mo}$ describes a state adiabatically connected to a conventional magnetically ordered one.

If $|\vec{h_i}| \to \infty$, Eq. (2.12) describes classical magnetic order with $|\langle \vec{S}_i \rangle| = 1/2$ on each site. If instead a finite field is used, the value of the magnetic moment can be greatly reduced. In general, the energy should be optimized with respect to the full

set of Zeeman fields $\vec{h}_i$ on all sites. In practice, such an optimization would have too many parameters. Instead, we guess an appropriate pattern for these fields, and then optimize $|h|/t$ to give the lowest variational energy. For example, in the Heisenberg limit, we choose the field to have a constant magnitude but an orientation with a three-sublattice structure of total vector sum zero (the symmetry pattern of the 120° state):

$$\vec{h}_i = |h|(\cos(\vec{q}\cdot\vec{r}_i + \phi), \sin(\vec{q}\cdot\vec{r}_i + \phi), 0), \tag{2.13}$$

where $\vec{q}$, $|h|$ and a phase ϕ are variational parameters. In this case, the optimal magnetic field of our simple ansatz gives a staggered magnetic moment $|\langle\vec{S}_i\rangle| \approx 0.30$, while DMRG calculations find a staggered magnetic moment $M \sim 0.20$ [46]. Including local correlations in our variational state, for example, by including Jastrow factors, will in general reduce the value of $\langle S\rangle$ further. It is interesting that our PSG analysis provides a general way to construct any ansatz satisfying the constraint of Eq. (2.6), even allowing us to construct energetically competitive *magnetic* states in addition to giving a general classification of all spin liquid states.

Extended model

Implementation of the above method shows that the nearest-neighbor Hamiltonian H_{nn} in Eq. (4.6) is dominated by magnetic order. To find actual spin liquid physics, we therefore extend the model to include second- and third-neighbor interactions.

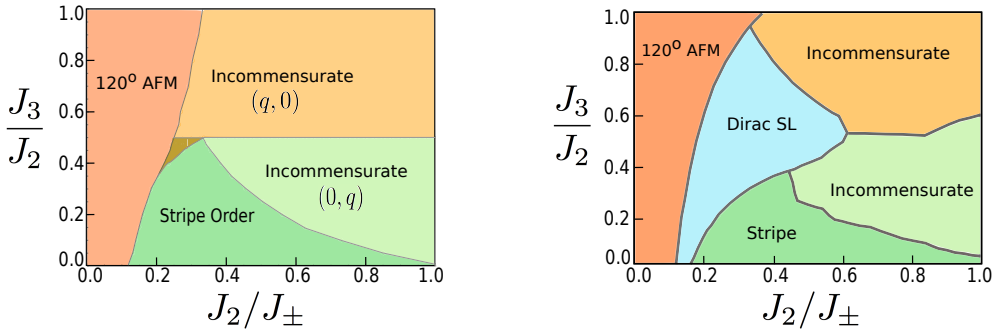

Figure 2.4: **a)** The classical phase diagram from the Luttinger-Tisza method and **b)** the same quantum phase diagram from variational Monte Carlo at $J_z/J_\pm = 1$ and $J_{\pm\pm} = J_{\pm z} = 0$.

Keeping the same relative XY anisotropy, we study the Hamiltonian:

$$\begin{aligned} H &= H_{nn} + J_2 \sum_{\langle\langle ij\rangle\rangle} \left(S_i^+ S_j^- + S_i^- S_j^+ + \frac{J_z}{J_\pm} S_i^z S_j^z \right) \\ &\quad + J_3 \sum_{\langle\langle\langle ij\rangle\rangle\rangle} \left(S_i^+ S_j^- + S_i^- S_j^+ + \frac{J_z}{J_\pm} S_i^z S_j^z \right). \end{aligned} \tag{2.14}$$

To avoid complications involving canted magnetic orders, we restrict our attention to the case of $J_{\pm z} = 0$. With this in mind, in this section, we undertake the somewhat ambitious goal of describing the entire four-dimensional phase diagram in terms of the free parameters J_z, $J_{\pm\pm}$, J_2, and J_3, all relative to $J_\pm = 1$.

We first review what is already known about the ground state phase diagram of Eq. (2.14):

- In the absence of second- and third- neighbor interactions ($J_2 = J_3 = 0$), the Luttinger-Tisza analysis of Ref. [100] tells us the magnetic order when $\vec{S}$ is treated as a classical vector. In that case, there is a phase transition from the 120° staggered antiferromagnetic state [ordered at wave-vector $\vec{q}_{120} = (\frac{4\pi}{3}, 0)$] at small $|J_{\pm\pm}|$ to a striped phase [ordered at wave-vector $\vec{q}_s = (0, \frac{2\pi}{\sqrt{3}})$] for

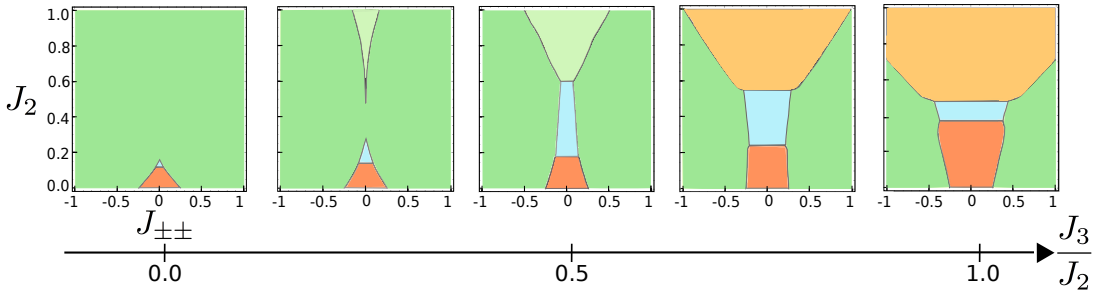

Figure 2.5: The full $J_{\pm\pm} - J_2 - J_3$ quantum phase diagram for $J_z = 1$ and $J_{\pm z} = 0$. Note that the color scheme is the same as in Fig. 2.4. Third-neighbor interactions J_3 strongly disfavor stripe order (dark green) and increase the range of the spin liquid phase (light blue). The horizontal axis on each subplot gives the value of $J_{\pm\pm}$. All energies are measured in units of $J_\pm = 1$.

$|J_{\pm\pm}| \gtrsim 0.25$.

- There is also a great deal of literature on the quantum $J_1 - J_2$ model ($J_{\pm\pm} = J_3 = 0$), in the Heisenberg limit ($J_z = 2J_\pm$) [47, 46]. In this case, growing evidence suggests that a spin liquid phase interpolates between the 120° phase for small J_2 and the stripe phase at large J_2.

VMC results

The advantage of using variational Monte Carlo with simple trial wavefunctions is that we are able to explore a huge phase space of our Hamiltonian. We consider several ansätze for magnetic order, taking the Zeeman field in the form of Eq. (2.13) with wave-vector $\vec{q}_v = (q, 0)$ or $\vec{q}_v = (0, q)$, where q, $|h|$, and a phase ϕ are variational parameters, which allows for both commensurate and incommensurate ordering. In practice, we find that the energies of all our ansätze, except for the striped phase with $\vec{q}_s = (0, \frac{2\pi}{\sqrt{3}})$, are independent of ϕ, even when the $U(1)$ symmetry is broken by $H_{\pm\pm}$. In the stripe phase, we find that the minimum energy is always obtained for

$\phi = 0$ when $J_{\pm\pm} > 0$, giving the ordering pattern seen in Fig. 2.1b), and for $\phi = \pi/2$ when $J_{\pm\pm} < 0$, which rotates all spins by 90°. In Fig. 2.3, we present our result for the full quantum $J_z - J_{\pm\pm} - J_2$ phase diagram. Notice that our results agree well with the previously understood limits. When $J_2 = 0$, the system acts very similar to the classical case, with a transition between the 120° and stripe orders around $J_{\pm\pm} \approx 0.20 + 0.05 J_z$. When a second-neighbor interaction is added, we indeed see that a Dirac spin liquid appears between the 120° and stripe phases. This phase is stable for small $J_{\pm\pm}$, but both large J_2 and $J_{\pm\pm}$ favor stripe order, leading to the triangular shape of the spin liquid regime which we see in Fig. 2.3. It is also notable that the extent of the spin liquid phase shrinks dramatically when J_z is lowered from the Heisenberg point. This is in agreement with the DMRG results on this model in Ref. [59].

We are also able to go beyond this model to look at the effect of the third-neighbor XXZ interaction J_3. Since both the second- and third-neighbor sites are separated by two lattice bonds, a simple superexchange picture implies that such a term would be present in materials with $J_3 \sim 0.5 J_2$. We will see that the effect of such a term is to enhance the size of the spin liquid regime.

First, we present the results in the classical limit. When $J_{\pm\pm} = 0$, the system has $U(1)$ symmetry and we can solve for the classical magnetic order using the Luttinger-Tisza method since any coplanar magnetic order with a single ordering wave-vector will satisfy the hard constraint that $\vec{S}_i = 1/2$ on every site. The result is that, in addition to the usual 120° and stripe phases, J_3 favors two additional incommensurate magnetic phases, with ordering wave-vectors at $(q, 0)$ and $(0, q)$. These phases can be thought of as the incommensurate versions of the 120° and stripe phases, respectively. A third incommensurate order with wave-vector (q, q) also appears classically, but we

will ignore this as such a phase never appears in the quantum case. The full classical phase diagram is shown in Fig. 2.4a) and is independent of J_z since the ordering is always in the xy plane.

Our VMC results on the quantum model agree remarkably well with the classical phase diagram, considering we have used completely different methods. Fig. 2.4b) shows the results for $J_z = 1.0$. We see that the shapes of the magnetic phases are largely the same as in the classical case, but the intermediate region where the phases meet is occupied by a broad spin liquid regime.

In Fig. 2.5, we show the full $J_2 - J_3 - J_{\pm\pm}$ phase diagram for $J_z = 1.0$. In addition to the presence of incommensurate magnetic order, the major feature of the data is that the spin liquid regime is enhanced with respect to the $J_3 = 0$ case. The third-neighbor interaction provides further frustration and finds stripe order particularly unfavorable. The spin liquid phase therefore survives to a large value of $J_{\pm\pm}$ when J_3 is included.

As mentioned previously, more accurate energies can be found by adding further variational parameters to the wavefunction, such as allowing for Jastrow factors [107, 108] or performing a small number of Lánczos steps [109]. However, we find that supplementing the PSG wavefunctions in this way only gives small improvements in the energies, leading to very small shifts of the phase boundaries. In section 2.4, we look at how we can make *qualitative* changes to the spin liquid ansätze.

In summary, our variational Monte Carlo calculation allowed us to explore a huge parameter space of the Hamiltonian in Eq. (2.14) and to obtain quantitative results for the ground state in each parameter regime. When a second-neighbor interaction is added, the *Dirac* spin liquid appears as the ground state between the 120° and stripe phases. This phase shrinks dramatically away from the Heisenberg limit, but

is in fact enhanced when a small third-neighbor interaction is included.

2.4 Beyond the PSG Wave Function

2.4.1 Perturbative Correction to the Wave function

In this section, we take a more phenomenological approach to studying a quantum spin liquid in the presence of strong spin-orbit coupling. We propose modifications to the mean-field ansätze which can be implemented numerically in the variational wavefunctions.

The plain mean field ansätze are limited in the amount of complexity they can accommodate. The main issue with the VMC simulation in this context is that the two most energetically competitive states, the Fermi surface and the Dirac spin liquid ones, possess *too* much symmetry. Our trial wavefunctions have no coupling between the spin and orbital degrees of freedom, which is a feature one would expect to find in the Hamiltonian's true ground state. Furthermore, according to the PSG analysis, no fermion bilinear operators inducing such spin orbit coupling can be added to the uniform Fermi surface Hamiltonian, not even at the further-neighbor level.

Instead, we formulate a method to incorporate *many-body* effects which modify our wavefunctions. Inspired by the path integral formulation for an interacting quantum field theory, we consider the variational state

$$|\Psi\rangle = e^{-\alpha \mathsf{H}} \mathcal{P} |\psi_0\rangle , \tag{2.15}$$

where $\mathsf{H} = \mathsf{H}_{\pm\pm}$ is defined in Eq. (4.6). This form is reminiscent of the Lánczos algorithm, where applications of large powers of an operator project a trial state

into the ground state of the given operator. Indeed, if we let $\alpha \to \infty$, this operator projects into the ground state of H. Instead, however, we take a slightly different approach, and let α be a small perturbation on $\mathcal{P}\left|\psi_0\right\rangle$, treating $\left|\Psi\right\rangle$ as a variational wavefunction.

There have been previous works combining the Lánczos algorithm with variational Monte Carlo [106, 109]. This proceeds by applying a finite number of Lánczos steps and working with the wavefunction $\left|\Psi^{(n)}\right\rangle = (1+\sum_{p=1}^{n}\alpha_p H^p)\left|\psi_0\right\rangle$, where the series is truncated for some small n, and the α_p are left as variational parameters. While this works well if the initial state is very close to the ground state of H, it is less effective as a phenomenological tool. The reason is that corrections at any finite order n necessarily scale to zero in the thermodynamic limit. When calculating the *correction* to an expectation value using $\left|\Psi^{(n)}\right\rangle$, "disconnected" powers of the Hamiltonian are subtracted off in the numerator, but not in the denominator. The normalization factor in the denominator therefore necessarily grows faster than the numerator with system size. Additional powers of n are then needed to compensate for this fact, but a fully extensive correction is only found at $n \sim N$.

Instead, we have found that the best way to work with the wavefunction in Eq. (2.15) numerically is to implement the correction perturbatively in α, but to all powers in n. To do this, we realize that the expectation value of any operator with respect to our improved wavefunction can be written as

$$\left\langle \mathcal{O} \right\rangle = \frac{\left\langle e^{-\alpha \mathsf{H}} \mathcal{O} e^{-\alpha \mathsf{H}} \right\rangle_0}{\left\langle e^{-2\alpha \mathsf{H}} \right\rangle_0}, \tag{2.16}$$

where $\left\langle \cdots \right\rangle_0$ is the expectation value taken with respect to the unperturbed wavefunction $\mathcal{P}\left|\psi_0\right\rangle$.

It is now possible to expand Eq. (2.16) analogously to diagrammatic perturbation theory. For any Hermitian operator $\mathcal{O}$, the correction to order α^2 reads

$$\langle \mathcal{O} \rangle = \frac{(\langle \mathcal{O} \rangle_0 - 2\alpha \,\mathrm{Re}[\langle \mathcal{O}\mathsf{H} \rangle_0] + \alpha^2 (\langle \mathsf{H}\mathcal{O}\mathsf{H} \rangle_0 + \mathrm{Re}[\langle \mathsf{H}^2\mathcal{O} \rangle_0]))}{(1 - 2\alpha \langle \mathsf{H} \rangle_0 + 2\alpha^2 \langle \mathsf{H}^2 \rangle_0)}. \tag{2.17}$$

The subtle difference is that now, by including all powers of n, all terms in the denominator exactly cancel the higher order "disconnected" pieces in the numerator. In the VMC calculation, this is expressed by the fact that $\langle H_{ij} H_{k\ell} \rangle \approx \langle H_{ij} \rangle \langle H_{k\ell} \rangle$ as $|(ij) - (kl)| \to \infty$. This way, we are able to measure, in our numerical simulation, many-body corrections to the wavefunction which survive in the thermodynamic limit.

In principle, applying the operator $\exp[-\alpha \mathsf{H}]$ to our unperturbed trial wavefunction could cause a phase transition, and we would no longer be working with a spin liquid state. For small α, however, we expect that the spin liquid ground state should be stable to such a perturbation. In the spinon metal, in a similar vein to Fermi liquid theory, we expect that these terms only give a correction to the self-energy of spinons near the Fermi surface [5].

2.4.2 Correction to the Energy

To begin, we measure the correction to the energy of the Dirac and uniform Fermi surface states, which arises from including the spin-orbit interaction in our variational wavefunction. We can directly measure the first and second order corrections numerically.

For any operator $\mathcal{O}$, we write the n^{th} order correction to the expectation value

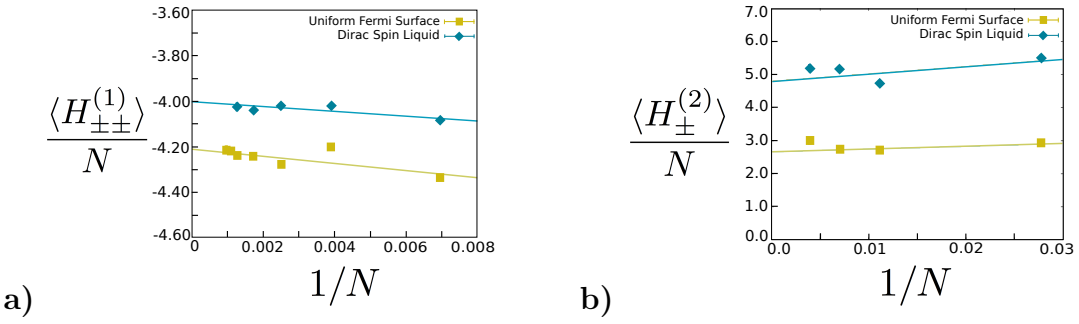

Figure 2.6: Finite size scaling of the lowest-order correction to **a)** $\langle \mathsf{H}_{\pm\pm}\rangle$ and **b)** $\langle \mathsf{H}_{\pm}\rangle$, for both the uFS (yellow) and Dirac (blue) spin liquid states. The corresponding change in energy is $\Delta E \sim \alpha J_{\pm\pm}\langle \mathsf{H}_{\pm\pm}\rangle + \alpha^2 J_{\pm}\langle \mathsf{H}_{\pm}\rangle$.

$\langle \mathcal{O}\rangle$ from applying $\exp[-\alpha \mathsf{H}]$ as $\alpha^n \langle \mathcal{O}^{(n)}\rangle$. Expanding Eq. (2.17) gives

$$\begin{aligned} \langle \mathcal{O}^{(1)}\rangle &= -2(\mathrm{Re}[\langle \mathsf{H}\mathcal{O}\rangle_0] - \langle \mathsf{H}\rangle_0\langle \mathcal{O}\rangle_0), \\ \langle \mathcal{O}^{(2)}\rangle &= \langle \mathsf{H}\mathcal{O}\mathsf{H}\rangle_0 + \mathrm{Re}[\langle \mathsf{H}^2\mathcal{O}\rangle_0] - 4\mathrm{Re}[\langle \mathsf{H}\rangle_0\langle \mathcal{O}\mathsf{H}\rangle_0] \\ &\quad -2\langle \mathsf{H}^2\rangle_0\langle \mathcal{O}\rangle_0 + 4\langle \mathsf{H}\rangle_0^2\langle \mathcal{O}\rangle_0. \end{aligned} \tag{2.18}$$

In our case, $\mathsf{H} = \mathsf{H}_{\pm\pm}$ and $\langle \mathsf{H}_{\pm\pm}\rangle_0 = \langle \mathsf{H}_{\pm\pm}\mathsf{H}_{\pm}\rangle_0 = 0$. Therefore, the spin-orbit part of the Hamiltonian is altered at order α, while the rotationally invariant part is corrected at order α^2:

$$\begin{aligned} \langle \mathsf{H}^{(1)}_{\pm\pm}\rangle &= -2\langle \mathsf{H}^2_{\pm\pm}\rangle_0, \\ \langle \mathsf{H}^{(2)}_{\pm}\rangle &= \mathrm{Re}[\langle \{\mathsf{H}_{\pm\pm}, \mathsf{H}_{\pm}\}\mathsf{H}_{\pm\pm}\rangle_0] - 2\langle \mathsf{H}^2_{\pm\pm}\rangle_0\langle \mathsf{H}_{\pm}\rangle_0, \\ \langle \mathsf{H}^{(2)}_{z}\rangle &= \mathrm{Re}[\langle \{\mathsf{H}_{\pm\pm}, \mathsf{H}_{z}\}\mathsf{H}_{\pm\pm}\rangle_0] - 2\langle \mathsf{H}^2_{\pm\pm}\rangle_0\langle \mathsf{H}_{z}\rangle_0. \end{aligned} \tag{2.19}$$

In Fig. 3.1, we show the resulting scaling of $\langle \mathsf{H}^{(1)}_{\pm\pm}\rangle$ and $\langle \mathsf{H}^{(2)}_{\pm}\rangle$ to the thermodynamic limit. The result is that the spinon metal is more susceptible, compared to the Dirac

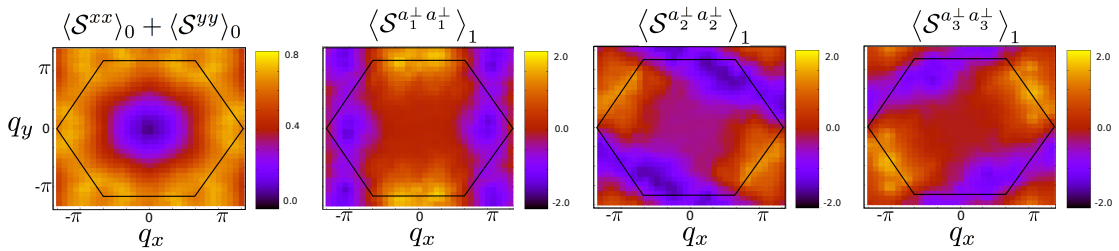

Figure 2.7: The rotationally invariant spin structure factor (top left) and the perturbative corrections to the spin-polarized structure factors measured with spins pointing perpendicular to the three lattice bond directions $\vec{a}_1, \vec{a}_2$, and $\vec{a}_3$, within the plane of the triangular lattice.

state, to energetically beneficial corrections to $\mathsf{H}_{\pm\pm}$ and less susceptible to detrimental corrections to $\mathsf{H}_{\pm}$ and H_z. Putting this together, we find that the optimal value of the variational parameter is $\alpha_{min} \sim J_{\pm\pm}/(J_\pm + J_z)$, which gives an energy correction $\Delta E \sim -J_{\pm\pm}^2/(J_\pm + J_z)$. More precisely, we find that the energy densities after the lowest-order corrections are given by

$$\begin{aligned} \mathrm{E}_{uFS}/N &= -0.4682(1 + J_z/4) - \frac{1.56\, J_{\pm\pm}^2}{J_\pm + 1.42 J_z}, \\ \mathrm{E}_{Dirac}/N &= -0.7050(1 + J_z/4) - \frac{0.84\, J_{\pm\pm}^2}{J_\pm + 0.87 J_z}. \end{aligned} \tag{2.20}$$

This implies that that the Fermi surface state becomes energetically superior to the Dirac state between $J_{\pm\pm} = 0.57$ at $J_z = 0$ and $J_{\pm\pm} = 1.54$ at $J_z = 2.0$. One caveat, of course, is that these values of $J_{\pm\pm}$ may fall outside the perturbative regime. Also, while smaller J_z appears to be more favorable for the spinon Fermi surface, this is also the parameter regime which is more susceptible to magnetic order.

2.4.3 Correction to the Spin Structure Factor

Studying the improved variational wavefunction makes it clear that the spinon metal state in a spin-orbit coupled environment has several unique properties, despite the fact that the mean-field Hamiltonian retains its rotational invariance. Taking our analogy to Fermi liquid theory seriously, the spin-orbit interaction gives a momentum and spin dependent correction to the self energy. This appears as a momentum dependent correction to the structure factor, which we can again measure directly in our simulation.

We differentiate between the various spin polarized contributions to the spin-spin correlation function:

$$\mathcal{S}^{\alpha\beta}(\vec{q}) = \sum_i e^{i\vec{q}\cdot\vec{r}_i}\langle S_i^\alpha S_0^\beta\rangle. \tag{2.21}$$

The first-order correction to the correlation function is

$$\langle S_i^\alpha S_j^\beta\rangle_1 = -2\left[\mathrm{Re}[\langle S_i^\alpha S_j^\beta \mathsf{H}_{\pm\pm}\rangle_0] - \langle S_i^\alpha S_j^\beta\rangle_0\langle \mathsf{H}_{\pm\pm}\rangle_0\right]. \tag{2.22}$$

The results are shown in Fig. 3.2. The corrections to the spin-polarized structure factor are direction-dependent broad peaks at the M points of the Brillouin zone which appear at order $\alpha \sim J_{\pm\pm}/(J_\pm + J_z)$. Therefore, in a spinon metal with spin-orbit coupling, spin-spin correlations when measured with different spin polarizations are direction dependent. This type of measurement could prove to be an important test to show both the presence of spin-orbit interactions and the absence of spontaneous symmetry breaking. Similar directional peaks can be seen in related models when spin-orbit terms are directly included in the ground state ansatz [110]. We note

that these kinds of direction-dependent structure factors have already been measured experimentally by resonant elastic x-ray scattering in the honeycomb lattice iridate Na_2IrO_3 [111].

2.4.4 Thermal Hall Conductivity

General considerations

Thermal transport measurements can be a powerful tool for studying magnetic insulators. The idea is to set up a thermal gradient ∇T (which is analogous to an electric field) and then measure the heat current j^{th} in response to it (which is analogous to an electric current). Any heat current in the insulator must be carried by the emergent quasiparticles, giving us a probe of the low energy excitations. The thermal conductivity, κ, can be defined within linear response as

$$j^{\text{th}}_{\mu} = -\kappa_{\mu\nu}\partial_{\nu}T. \tag{2.23}$$

The spinon Fermi surface QSL is unusual due to the large number of gapless excitations. This leads to a predicted linear T term appearing in the diagonal component of κ, similar to what one would expect in a metal. The deconfined spinons carry heat in the same way physical electrons carry charge in an electrical conductor. A major difficulty is that many degrees of freedom, most notably phonons, can contribute to the diagonal thermal conductivity, making the measurement challenging.

The thermal *Hall* conductivity, however, given by the off-diagonal component of κ, should not contain a phonon term. Furthermore, as explained in Ref. [112], it is very difficult to find an effect generated by magnons on the triangular lattice due to a cancellation of the contributions from neighboring edge sharing plaquettes.

A large nonzero thermal Hall conductivity could therefore be a strong indicator of exotic physics. Indeed, in Ref. [112], the authors also predict that a spinon metal would display such an effect. However, the reasoning is very subtle, depending on a coupling of the *orbital* motion of the spinons to the external electromagnetic field through the interaction with the internal gauge field.

Here, we argue that there exists a distinct contribution to the thermal Hall conductivity in the spinon metal which is unique to spin-orbit coupled systems and relies only on a Zeeman coupling to the external electromagnetic field. For itinerant fermions with conserved charge, the presence of spin-orbit coupling can lead to a nontrivial Berry curvature which may induce an anomalous component of the charge Hall conductivity, in the absence of any Lorentz force. This mechanism of anomalous Hall conductivity was explored intensely for Rashba two-dimensional electron gases and in many other models. In the following, we adapt this idea to study the *thermal* conductivity of the Fermi surface QSL state.

The U(1) QSL states studied here have an *emergent* conserved charge, which is the fermion number associated with the emergent U(1) gauge symmetry. Consequently, at the parton level, we can define a current associated with this charge, and we may consider, formally, the emergent conductivity tensor $\sigma^{qp}_{\mu\nu}$ defined with respect to the emergent current and a potential coupling to the associated emergent charge density. This is not the true electrical conductivity, since this is an insulator, and it is also not the thermal conductivity. Thus we proceed in two stages. First, we consider the anomalous emergent Hall conductivity of the spinons. Then, we relate it to the more easily measurable *thermal* Hall conductivity (in principle, the emergent conductivity should also be measurable, but it is not obvious how to do so).

Effective quasiparticle Hamiltonian

At the mean field level, the emergent Hall conductivity can be extracted as an integral over the Berry curvature of the occupied spinon bands. Within the simple PSG wavefunction, the spinon metal is spin-rotationally invariant and therefore has zero Berry curvature. On symmetry grounds, however, we expect that a Hall conductivity should microscopically arise. To estimate it, we consider the 'improved' wavefunction, and infer a self-energy correction which breaks spin-rotational symmetry and induces a non-zero Berry curvature.

The Berry gauge field (Berry connection) is defined for a single particle system as

$$\vec{A}(k) \;=\; -i\,\langle u_k|\vec{\nabla}_k|u_k\rangle, \tag{2.24}$$

where $|u_k\rangle$ is defined as in the Bloch wavefunction. The anomalous Hall conductivity is then given by

$$\sigma_{xy}^{qp} \;=\; \oint_{\partial S}\vec{A}(k)\cdot d\vec{k} \;=\; \int_S [\vec{\nabla}_k\times\vec{A}(k)]\,d^2k, \tag{2.25}$$

where the first (line) integral is taken around the Fermi surface ∂S, while the second (area) integral is taken over the area S spanned by it. This physical quantity is invariant under $U(1)$ gauge transformations, as is immediately evident from its expression in terms of the Berry curvature $\mathcal{B}(k) = \vec{\nabla}_k \times \vec{A}(k)$.

To obtain the Berry curvature, we suppose that the system is described by an effective quasiparticle Hamiltonian including a self-energy correction $\Sigma(k)$ and a Zee-

man coupling to an external magnetic field $\vec{B} = h\hat{z}$:

$$\mathcal{H}_{\text{eff}}(k) \;=\; \left(f^{\dagger}_{k\uparrow}\, f^{\dagger}_{k\downarrow}\right) \begin{pmatrix} \varepsilon(k) - h & \Sigma^{*}(k) \\ \Sigma(k) & \varepsilon(k) + h \end{pmatrix} \begin{pmatrix} f_{k\uparrow} \\ f_{k\downarrow} \end{pmatrix}. \tag{2.26}$$

We determine the self-energy $\Sigma(k)$ by requiring that the off-diagonal expectation value $\Pi_{\uparrow\downarrow}(k) \equiv \langle f^{\dagger}_{k\uparrow} f_{k\downarrow}\rangle$ calculated using the improved wavefunction *matches* that calculated using the effective Hamiltonian $\mathcal{H}_{\text{eff}}(k)$.

To proceed, we consider an improved wavefunction similar to that in Eq. (2.15):

$$|\Psi\rangle = e^{-\tilde{\alpha}\tilde{\mathsf{H}}}\,\mathcal{P}\,|\psi_0\rangle\,, \tag{2.27}$$

where now we take $\tilde{\mathsf{H}} = \mathsf{H}_{\pm z}$. The reason for this change is that the previously-considered correction due to $\mathsf{H}_{\pm\pm}$ gives exactly zero contribution to $\Pi_{\uparrow\downarrow}$ because it conserves the total spin S^z modulo 2. The analogous contribution due to $\mathsf{H}_{\pm z}$, however, does contribute. We expect that the energetically optimal value of the variational parameter is $\tilde{\alpha} \sim J_{\pm z}/J_0$, where J_0 is on the order of the other exchange couplings ($J_{\pm}$ and J_z).

Using the same perturbative expansion as above, the first-order form of $\Pi_{\uparrow\downarrow}(k)$ becomes

$$\begin{aligned} \Pi_{\uparrow\downarrow}(k) \;&=\; \left\langle e^{-\tilde{\alpha}\tilde{\mathsf{H}}} f^{\dagger}_{k\uparrow} f_{k\downarrow} e^{-\tilde{\alpha}\tilde{\mathsf{H}}}\right\rangle_0 \\ &= -\tilde{\alpha}\Big(\langle f^{\dagger}_{k\uparrow} f_{k\downarrow}\tilde{\mathsf{H}}\rangle_0 + \langle \tilde{\mathsf{H}} f^{\dagger}_{k\uparrow} f_{k\downarrow}\rangle_0\Big) \\ &\equiv \Pi^{(1)}_R(k) + \Pi^{(1)}_L(k). \end{aligned} \tag{2.28}$$

If we represent the spin-spin interaction in momentum space with a momentum-dependent form factor

$$\tilde{\gamma}(k) \;=\; \frac{i}{2}\sum_{\mu=1}^{3}\sum_{\pm}\gamma_{\mu}e^{\pm i\vec{k}\cdot\vec{a}_{\mu}}, \qquad \gamma_{\mu}\equiv\gamma_{\vec{0},\vec{a}_{\mu}}, \tag{2.29}$$

the first expectation value $\Pi_R^{(1)}(k)$ takes the form

$$\begin{aligned}
\Pi_R^{(1)}(k) \;&=\; i\tilde{\alpha}\Big\langle f_{k\uparrow}^{\dagger}f_{k\downarrow}\sum_{\langle mn\rangle}\left[\gamma_{mn}S_m^zS_n^- + (m\leftrightarrow n)\right]\Big\rangle_0 \\
&= \frac{\tilde{\alpha}}{N}\sum_{k_1,k_2,k_3}\Big[\langle f_{k\uparrow}^{\dagger}f_{k\downarrow}f_{k_1\uparrow}^{\dagger}f_{k_2\uparrow}f_{k_3\downarrow}^{\dagger}f_{(k_1-k_2+k_3)\uparrow}\rangle_0 \\
&\quad - \langle f_{k\uparrow}^{\dagger}f_{k\downarrow}f_{k_1\downarrow}^{\dagger}f_{k_2\downarrow}f_{k_3\downarrow}^{\dagger}f_{(k_1-k_2+k_3)\uparrow}\rangle_0\Big]\,\tilde{\gamma}(k_1-k_2) \\
&= -\frac{\tilde{\alpha}}{N}\sum_{q}\Big[\langle f_{k\uparrow}^{\dagger}f_{k\uparrow}f_{q\uparrow}^{\dagger}f_{q\uparrow}\rangle_0\,\langle f_{k\downarrow}f_{k\downarrow}^{\dagger}\rangle_0 \\
&\quad + \langle f_{k\uparrow}^{\dagger}f_{k\uparrow}\rangle_0\,\langle f_{k\downarrow}f_{k\downarrow}^{\dagger}f_{q\downarrow}f_{q\downarrow}^{\dagger}\rangle_0\Big]\,\tilde{\gamma}(k-q),
\end{aligned} \tag{2.30}$$

where we arrive at the last line after conserving spin and momentum in the zeroth-order expectation values as well as using $\tilde{\gamma}(-k)=\tilde{\gamma}(k)$ and $\tilde{\gamma}(0)=0$.

Performing similar manipulations on $\Pi_L^{(1)}(k)$ and combining the two contributions

gives

$$\Pi_{\uparrow\downarrow}(k) = \Pi_R^{(1)}(k) + \Pi_L^{(1)}(k) = -\tilde{\alpha}\Lambda\tilde{\gamma}(k)\Gamma(k),$$

$$\begin{aligned}\Gamma(k) &= \langle n_{k\uparrow}\rangle_0\langle 1-n_{k\downarrow}\rangle_0 + \langle n_{k\downarrow}\rangle_0\langle 1-n_{k\uparrow}\rangle_0 \\ &= \coth(h/T)\left[\langle n_{k\uparrow}\rangle_0 - \langle n_{k\downarrow}\rangle_0\right], \end{aligned} \tag{2.31}$$

$$\begin{aligned}\Lambda &= \frac{1}{N}\sum_q e^{\pm i\vec{q}\cdot\vec{a}_\mu}\left[\langle n_{q\uparrow}\rangle_0 + \langle 1-n_{q\downarrow}\rangle_0\right] \\ &\sim a^2\int d^2q\, e^{\pm i\vec{q}\cdot\vec{a}_\mu}\left[\langle n_{q\uparrow}\rangle_0 - \langle n_{q\downarrow}\rangle_0\right],\end{aligned}$$

where $n_{k\sigma} = f_{k\sigma}^\dagger f_{k\sigma}$ is a number operator and $a = |\vec{a}_\mu|$ is the lattice constant. Importantly, Λ is real and independent of both μ and $\pm$ due to the sixfold symmetry $\mathcal{S}_6$. Furthermore, in the limit of $T \ll |h|$, the integrand is only non-zero in an annulus of thickness $\sim h/(aJ_0)$ around the Fermi surface of radius $\sim 1/a$, and the integral can then be estimated as $\Lambda \sim h/J_0$.

Let us also calculate $\Pi_{\uparrow\downarrow}(k)$ from the effective Hamiltonian in Eq. (2.26). In the limit of $|\Sigma(k)| \ll |h|$, we obtain

$$\begin{aligned}\Pi_{\uparrow\downarrow}(k) &= -\frac{\mathrm{sgn}(h)\,\Sigma(k)}{2\sqrt{h^2+|\Sigma(k)|^2}}\left[\langle n_{k\uparrow}\rangle_0 - \langle n_{k\downarrow}\rangle_0\right] \\ &= -\frac{\Sigma(k)}{2h}\left[\langle n_{k\uparrow}\rangle_0 - \langle n_{k\downarrow}\rangle_0\right].\end{aligned} \tag{2.32}$$

Finally, from a comparison of Eqs. (2.31) and (2.32), the self-energy in the limit of $T \ll |h|$ becomes

$$\Sigma(k) = 2|h|\tilde{\alpha}\Lambda\tilde{\gamma}(k). \tag{2.33}$$

The real and imaginary parts of $\Sigma(k)$ are plotted in Fig. 3.3. Note that the complex phase of $\Sigma(k) \propto \tilde{\gamma}(k)$ winds by 4π around the Γ point.

Berry curvature and Hall conductivity

Now we are in a position to calculate the emergent Hall conductivity. First, we rewrite the effective quasiparticle Hamiltonian in Eq. (2.26) into the standard form

$$\begin{aligned} \mathcal{H}_{\text{eff}}(k) &= \left(f^{\dagger}_{k\uparrow}\, f^{\dagger}_{k\downarrow}\right)\left[\varepsilon(k)\sigma_0 - h\vec{\beta}(k)\cdot\vec{\sigma}\right]\begin{pmatrix} f_{k\uparrow} \\ f_{k\downarrow}\end{pmatrix}, \\ \vec{\beta}(k) &= \left(-\frac{\mathrm{Re}\,\Sigma(k)}{h}, -\frac{\mathrm{Im}\,\Sigma(k)}{h}, 1\right), \end{aligned} \tag{2.34}$$

where $|\vec{\beta}(k)| \approx 1$ in the limit of $|\Sigma(k)| \ll |h|$. For such a Hamiltonian, the two bands have Berry curvatures of opposite sign and equal magnitude given by

$$\begin{aligned} \mathcal{B}(k) &\sim \vec{\beta}(k)\cdot\left[\partial_{k_x}\vec{\beta}(k)\times\partial_{k_y}\vec{\beta}(k)\right] \\ &\sim \frac{1}{\rho_k}\left\{\vec{\beta}(k)\cdot\left[\partial_{\rho_k}\vec{\beta}(k)\times\partial_{\varphi_k}\vec{\beta}(k)\right]\right\} \\ &\sim \frac{1}{h^2\rho_k}\,\mathrm{Im}\left[\partial_{\rho_k}\Sigma^*(k)\,\partial_{\varphi_k}\Sigma(k)\right], \end{aligned} \tag{2.35}$$

where we use polar coordinates defined by $k_x = \rho_k\cos\varphi_k$ and $k_y = \rho_k\sin\varphi_k$. Due to the 4π phase winding of $\Sigma(k)$ (see Fig. 3.3), there is a finite azimuthal derivative $\partial_{\varphi_k}\Sigma(k) \sim i\Sigma(k)$. From $\partial_{\rho_k}\Sigma^*(k) \sim a\Sigma^*(k)$, the Berry curvature at radius $\rho_k \sim 1/a$ is then on the order of

$$\mathcal{B}(k) \sim \frac{a^2|\Sigma(k)|^2}{h^2} \sim \tilde{\alpha}^2 a^2\left(\frac{h}{J_0}\right)^2. \tag{2.36}$$

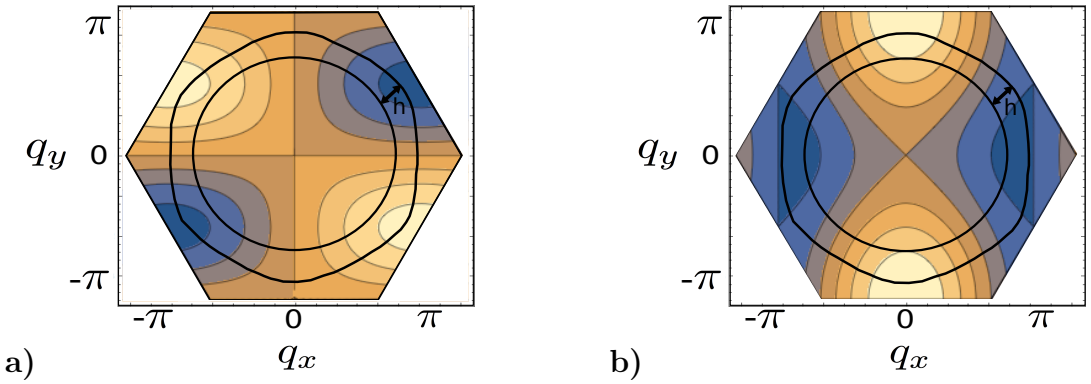

Figure 2.8: The **a)** real and **b)** imaginary components of $\Sigma(k)$ in a magnetic field $\vec{B} = h\hat{z}$. Lighter (darker) contours are positive (negative) contributions. The positions of the spin up and spin down Fermi surfaces in the presence of a nonzero Zeeman field $\propto h$ are also shown.

Next, in terms of the Berry curvatures $\pm\mathcal{B}(k)$ of the two bands, the emergent Hall conductivity takes the form

$$\sigma_{xy}^{qp} = \int d^2k\, \mathcal{B}(k)\, [\langle n_{k\uparrow}\rangle_0 - \langle n_{k\downarrow}\rangle_0]\,. \tag{2.37}$$

In the limit of $T \ll |h|$, the integrand is only non-zero in an annulus of thickness $\sim h/(aJ_0)$ around the Fermi surface of radius $\sim 1/a$, and the Hall conductivity can then be estimated as $\sigma_{xy}^{qp} \sim \tilde{\alpha}^2 (h/J_0)^3$.

Finally, by virtue of the Wiedemann-Franz law that relates the emergent and the thermal conductivities, the quasiparticle contribution to the thermal Hall conductivity is on the order of

$$\kappa_{xy} \sim T\sigma_{xy}^{qp} \sim \tilde{\alpha}^2 T \left(\frac{h}{J_0}\right)^3 \sim \frac{Th^3 J_{\pm z}^2}{J_0^5}. \tag{2.38}$$

Interestingly, κ_{xy} is proportional to the third power of the magnetic field. Note, however, that this result is valid for a relatively large field ($T \ll |h| \ll J_0$). For a small field ($|h| \ll T \ll J_0$), the factor $\coth(h/T)$ in Eq. (2.31) contributes an

additional factor $\sim (T/h)^2$ to κ_{xy}, which is then linearly proportional to the magnetic field.

2.5 Discussion

2.5.1 Relationship to other Work

In this paper, we have provided a comprehensive commentary on the possibility of spin liquid physics in a very general spin-orbit coupled model on the triangular lattice. In the process, we have attempted to consolidate several previous results on this topic. We began by looking at the $U(1)$ PSG wave functions derived in Ref. [103]. Instead of working with these wavefunctions phenomenologically, we go beyond their simple mean-field analysis and find quantitative estimates of the energies of these ansätze using variational Monte Carlo.

We also use VMC to give a complete picture of magnetic order in our model. Our results improve on the classical magnetic phase diagrams presented in Refs. [100, 101]. In those works, a phase transition between the 120° and stripe phases is found in the nearest-neighbor model, and it is conjectured that large spin fluctuations may lead to the presence of a nonmagnetic phase. In our work, by building on the PSG ansätze, we also find a phase transition between the two magnetic phases in a similar parameter regime. We further find that second-neighbor interactions are necessary to create a spin liquid ground state and we identify the Dirac spin liquid as the lowest energy state. This confirms and extends earlier studies of the isotropic Heisenberg model [106].

The only other calculation of the full quantum phase diagram in this model was given by the DMRG analysis in Ref. [113]. Our phase diagram agrees with the DMRG

analysis when second-neighbor interactions are included. The XXZ anisotropy and $J_{\pm\pm}$ interactions both work to limit the spin liquid phase to a very small region of parameter space. However, we go beyond this and also include a third-neighbor interaction, which we believe gives a more complete picture on the behavior of the spin liquid phase. We find that even a very small third-neighbor interaction can greatly stabilize the spin liquid regime.

2.5.2 Relevance to Materials

This model has recently attracted much attention for its potential relevance to the material $YbMgGaO_4$. Experiments find enticing evidence for a spinon Fermi surface state from thermodynamic and inelastic neutron scattering measurements [56, 57]. Our work addressed the theoretical basis for such physics.

Our results support the claim of Ref. [113] that $YbMgGaO_4$ likely falls outside of the spin liquid phase in the presence of only first- and second-neighbor interactions. We found, however, that a very small third-neighbor interaction can greatly increase the size of the spin liquid phase and may appear quite naturally in the material. However, using the simple PSG picture, we always find that the Dirac spin liquid is energetically favored over the spinon Fermi surface state.

While the above results do not support the spinon Fermi surface state, we did find some effects which could tilt the balance in its favor. We saw that the spin-orbit interactions favor the spinon Fermi surface over the Dirac spin liquid state when we include effects beyond the simple projected mean-field wavefunctions. This leaves open the possibility that the spinon metal could be energetically favorable, perhaps assisted by other factors such as disorder or a small ring-exchange interaction.

If we assume that a spinon metal state does exist, interesting features emerge

due to spin-orbit coupling. We showed how the spin-orbit interactions could explain the existence of broad peaks at the M points in the spin structure factor and also predicted that measurements of the spin-polarized structure factors would display specific polarization-dependent peaks reflecting the anisotropic interactions. We also propose that the spin-orbit coupled spinon metal state may have a rather large thermal Hall conductivity which could be a very clear signature of spin liquid physics in such a system.

2.5.3 Future directions and implications

Looking forward, we anticipate a number of implications for the results and techniques developed in this work. For our spin-orbit coupled triangular systems, we showed that the restrictions imposed on the standard Gutzwiller-projected free-fermion states by the PSG are quite severe for several of the $U(1)$ QSL states. Consequently, they are unable to adapt to strongly anisotropic interactions, and this may open the door to competition from $\mathbb{Z}_2$ QSL states in the case of such anisotropic models. In turn, this would be of considerable interest as the Gutzwiller-based approach almost always favors $U(1)$ states in Heisenberg models. The possibility of inducing fully gapped topological QSLs should be explored in the future by VMC techniques.

We argued that the thermal Hall effect should be a key signature of itinerant spinon excitations in spin-orbit coupled systems. While we obtained such an effect for the $U(1)$ spinon Fermi surface state on the triangular lattice, it was in fact suppressed by the PSG-mandated vanishing of effective spin-orbit coupling on the fermionic spinons at the free-particle level. Ultimately, this suppression owes itself to the presence of inversion symmetry, which, in conjunction with time-reversal symmetry, act on the spinons analogously to the way they do on real electrons. As is well

known, the combination of inversion and time reversal in that context imply an exact two-fold Kramers degeneracy of the full electronic band structure, and a similar effect occurs here. When inversion is absent, for example, when an electric field is present normal to a two-dimensional electron gas, spin splitting occurs. The Rashba spin-orbit coupling induced by such a field is known to induce a large anomalous Hall effect in that context [114]. This strongly suggests that one should look for an enhanced thermal Hall effect in two-dimensional magnetic materials in which the magnetic layer has an asymmetric environment. This criteria, along with the requirement of large spin-orbit coupling, should assist in a search for this phenomenon.

Our methodology offers a consistent and quantitative method to compare QSLs and ordered phases for anisotropic magnetic Hamiltonians. This should have broad applicability to other materials such as the Kitaev compounds α-$RuCl_3$, Na_2IrO_3, and Li_2IrO_3 in all its structural variations, and to three-dimensional systems like rare earth pyrochlores and spinels. The ability of VMC-based methods to tackle large systems is a unique numerical advantage. We expect many insights from such studies in the future.

Chapter 3

Kinetic Magnetism at the Interface Between Mott and Band Insulators

Kinetic magnetism is a very old and elegant idea, whereby magnetic order appears solely due to the *motion* of the correlated itinerant electrons. The concept dates back to an argument by Nagaoka from 1966 in which he proved that ferromagnetism must exist in the Hubbard model [70]. While there have been attempts to extend these results to a wide range of models [115, 116], it has become apparent that Nagaoka's ferromagnetism is a subtle effect which seems to be destroyed for any straightforward extension to realistic parameters [117]. It remains an outstanding goal to achieve this effect in an experimentally realizable model.

In this chapter, we consider the relevance of this venerable idea to artificial heterostructures of perovskite transition metal oxides. These systems have emerged as a novel venue to explore correlated electron physics in a highly controlled environment [61]. The dominant motif is that of a cubic lattice of Ti d orbitals, with from 0 to one electron per site. This is a canonical Mott material, with small overlap-induced hop-

ping amongst neighboring d orbitals, and large on-site Hubbard repulsion U. Most of the physics explored experimentally originates from the so-called "polar discontinuity". This produces a high density two-dimensional electron gas (2DEG) at the interface between two such materials with different stacking of polar/non-polar atomic layers, ideally consisting of half an electron per planar Ti unit cell for the case of a unit polar discontinuity. Correlation effects may be observed for these electrons.

Such a 2DEG is in principle induced for any such polar structure, independent of other details of the constituent materials. For example, it should occur at the junction between two band insulators, $LaAlO_3/SrTiO_3$ (LAO/STO), which is the most studied such oxide interface [64, 118, 119]. In practice, the electron concentration observed in LAO/STO is greatly reduced from the expected value, for reasons which are not clear. A polar discontinuity 2DEG is also expected for the interfaces between Mott insulating titanates $R\mathrm{TiO}_3$ (where R is a rare earth) and $SrTiO_3$ (STO), where the proper electron density has been measured experimentally[65, 66, 67]. These latter studies have been interpreted by treating the STO as a quantum well, viewing the $R\mathrm{TiO}_3$ (RTO) as entirely inert and serving only to confine the electrons of the 2DEG. When the 2DEG is sufficiently narrowly confined on both sides by RTO, indications of magnetism in the 2DEG are found [68, 69]. In this chapter, we tentatively connect this observation to the storied problem of kinetic magnetism.

A cautionary note is in order. Ferromagnetism is ubiquitous in theoretical treatments of correlated electron materials [120, 121]. Most theoretical descriptions of magnetism rest on a mean field analysis, which notoriously overestimates the tendency to ferromagnetism. The vast majority of theoretical treatments of oxide heterostructures fit into this category, including all first principles calculations of magnetism, and even sophisticated variants like dynamical *mean field* theory. While such calculations

are useful and suggestive, a controlled approach is desirable.

We take a distinct view of polar Mott Insulator/Band Insulator (MI/BI) interfaces. Unlike a band insulator like LAO, the insulating RTO contains a very high density of correlated *localized* electrons, even higher than in the 2DEG. We suggest that the mobile electrons in STO can have a dramatic effect on these localized electrons, driving magnetism. We introduce a model which takes into account both the Mott insulating and itinerant electron degrees of freedom. We then present a controlled limit whereby kinetic magnetism in the interface emerges independent of the bulk physics of either material. We will further support this analysis with unbiased numerical evidence, which constitutes some of the first exact numerical results on these systems.

3.1 The Model

We consider a minimal model that captures the physics of the MI/BI interface. It consists of a two layer square lattice, with one layer each for the MI and BI. If the two were decoupled, the MI would have "exactly" one electron per site, and the BI a lower concentration n per site, where we expect $n \leq 1/2$, the maximum achievable if all the electrons in the 2DEG are in the first layer of the BI. In reality, inter-layer hopping allows the charge to redistribute, and we include a (large) potential offset Δ to favor more electrons in the MI layer, and fix the total electron concentration to $1 + n$ per two Ti sites. We further stress our use of an *effective* single band model, which captures the effects of orbital splitting at the interface [122, 123] and includes only the electrons which make up the large majority Fermi surface [124, 125, 126].

We model interactions by the extreme limit $U = \infty$, which forbids double oc-

cupancy. The justification is that exchange in the RTO titanates is quite weak, for example the most studied materials with R=Sm, Gd show antiferromagnetism and ferromagnetism, respectively, with $T_c \approx 30K$ in both cases [127], indicating exchange $|J|$ is of order 1 meV, while $t \sim 0.3$ eV and $U \sim 4-8$ eV. Since $J \sim t^2/U \ll t, U$, the very small exchange supports the large U limit.

With this motivation, the $U = \infty$ limit maps the Hubbard model to the so called 't-J model' with $J = 0$:

$$\begin{aligned} H &= -t \sum_{\langle ij \rangle z\sigma} \mathcal{P} c^\dagger_{i\sigma z} c_{j\sigma z} \mathcal{P} - t \sum_{i\sigma} \mathcal{P}(c^\dagger_{i\sigma 1} c_{i\sigma 2} + \text{h.c.})\mathcal{P} \\ &\quad + \sum_{iz\sigma} (\Delta \delta_{z,1} - \mu) n_{i\sigma z}, \end{aligned} \tag{3.1}$$

where $\mathcal{P} = \prod_i (1 - n_{i\uparrow} n_{i\downarrow})$. The only free parameters are the filling $1 + n = \frac{1}{L_x L_y} \sum_{iz\sigma} \langle n_{i\sigma z} \rangle$ (or chemical potential μ) and the ratio of hopping to the potential difference (t/Δ).

The single layer, single band, $U = \infty$ Hubbard model has been the subject of many studies. Nagaoka famously showed in [70] that when the half-filled system is doped with a single hole, the exact ground state is the fully polarized state with maximum S_{total}.

This magnetism is the result of delicate quantum effects arising from the kinetic motion of the single hole through the lattice. The question of whether this ferromagnetism can be extended to finite doping has been attacked via mean field calculations [128], variational studies [129, 130], and unbiased numerical approaches including quantum Monte Carlo [131] and most recently DMRG calculations [71].

While it appears that a ferromagnetic metal is stable over a finite range of filling n, it is clear that at lower densities ($0 \leq n \leq 0.75$), the ground state is a paramagnetic

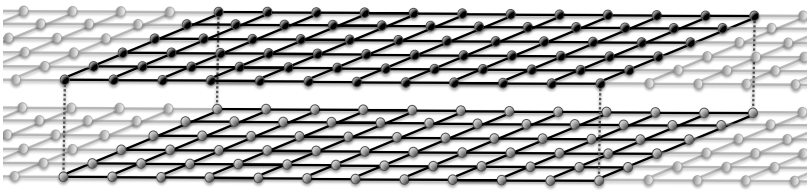

Figure 3.1: The bilayer lattice geometry. For the numerical simulations, an elongated geometry which is optimal for the DMRG algorithm was used.

metal. In this letter we will show that the bilayer model with finite band separation, Δ, contains much richer magnetic structure at all filling densities. In particular, at large band separation we are able to stabilize Nagaoka's ferromagnetism over a wide range of electron densities n.

3.2 Perturbative Regime ($\Delta \gg t$)

In the limit of large Δ we can demonstrate analytic control over the model. At $\Delta = \infty$, the two layers are completely decoupled, where the upper layer is a degenerate spin system and the bottom layer behaves according to the results of Ref.[71]. In particular, for $\langle n \rangle < \frac{3}{4}$, the bottom layer is a paramagnetic metal. If we now tune away from $\Delta = \infty$, we can derive an effective low-energy Hamiltonian perturbatively in (t/Δ). To lowest order in the perturbative expansion,

$$\mathcal{H}_{eff} \;=\; H_{00} + H_{01}\frac{1}{E - H_{11}}H_{10}. \tag{3.2}$$

where H_{10} hops an electron from the top to the bottom layer, and H_{01} brings us back into the ground state subspace of no holes in the top layer. Assume that the density in the bottom layer is such that there is a paramagnetic metal. In this case, the virtual contribution to the energy when there is a single hole in the top layer, by

Nagaoka's result, is minimized when the top layer is a fully polarized ferromagnet. Then for nearly all densities at large Δ, the degenerate groundstate subspace splits in a way that causes the ferromagnetic state to become the true ground state. However, this argument breaks down at the lowest electron densities, since here there are no electrons present at different spatial sites to fill the virtual hole in the top layer. The electron is then effectively localized and the ferromagnetism is lost.

We will now make this argument precise. We expand the Hamiltonian to order $(t/\Delta)^3$, by using the identity

$$\frac{1}{\omega - H} = \frac{1}{\omega} + \frac{1}{\omega} H \frac{1}{\omega - H}. \tag{3.3}$$

The lowest order effect, which occurs at order $(t/\Delta)^2$, is

$$\begin{aligned} H'^{(1)} &= -\frac{t^3}{\Delta^2} \sum_{\langle ij \rangle} \sum_{\sigma\sigma'\sigma''} c^\dagger_{i2\sigma} c_{i1\sigma} c^\dagger_{j2\sigma'} c_{i2\sigma'} c^\dagger_{j1\sigma''} c_{j2\sigma''} \\ &= -\frac{t^3}{\Delta^2} \sum_{\langle ij \rangle} \sum_{\alpha\beta} \Big[\vec{S}_i \cdot \vec{S}_j \, \delta_{\alpha\beta} + \frac{1}{2} (\vec{S}_i + \vec{S}_j) \cdot \vec{\sigma}_{\alpha\beta} \\ &\qquad - \; i (\vec{S}_i \times \vec{S}_j) \cdot \vec{\sigma}_{\alpha\beta} \Big] \mathcal{P} c^\dagger_{j1\alpha} c_{i1\beta} \mathcal{P} \end{aligned} \tag{3.4}$$

This expression suggests an obvious way to decouple the terms at the mean field level, by taking expectation values of operators in the same layer. This leaves us with an effective spin model for the upper layer and a doped electron system in the bottom layer. The antisymmetric form of the third term in Eq. (3.4) implies we can ignore its mean field effect at this order in perturbation theory. The first term then gives the effective interaction in the upper layer as a ferromagnetic Heisenberg interaction with $J_{FM} = -t^3 \langle c^\dagger_j c_i \rangle / \Delta^2 \sim (t^3 n)/\Delta^2$.

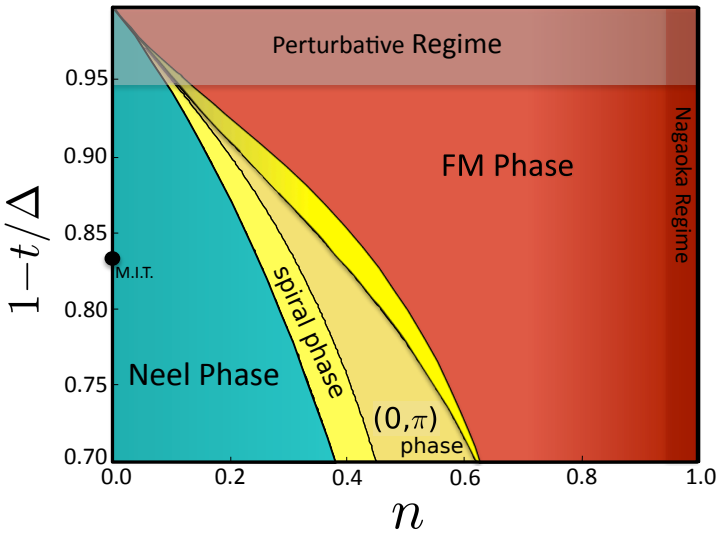

Figure 3.2: We embed the classical phases of the $J_1 - J_2 - J_3$ Heisenberg model into our bilayer Hubbard phase diagram, using the form of J_1, J_2 and J_3 given in the text. These results become rigorous for large Δ/t. The highest densities are ferromagnetic by Nagaoka's theorem.

At zero temperature, the energy can be lowered at the mean-field level if the upper layer forms a fully polarized ferromagnet. The second term of Eq. (3.4) then provides an effective magnetic field in the ordering direction of the upper layer spins. If $n \to 0$ then $J_{FM} \to 0$ also, and we must look at the next order in perturbation theory. At this order, we derive additional antiferromagnetic interactions which compete with the lowest order term. These can be written as

$$\begin{aligned} H'^{(2)} &= \frac{4t^4}{\Delta^3}\langle(1-n)\rangle^2 \sum_{\langle ij\rangle} \vec{S}_i \cdot \vec{S}_j \\ &+ \frac{t^4}{\Delta^3} \sum_{\langle\langle ijk\rangle\rangle} \langle c_i^\dagger c_k\rangle \left[(\vec{S}_i + \vec{S}_j + \vec{S}_k)\cdot(\vec{S}_i + \vec{S}_j + \vec{S}_k)\right] \end{aligned} \tag{3.5}$$

where $\langle\langle ijk\rangle\rangle$ implies the sum is over all connected clusters of 3 sites on the same layer. This therefore describes next and third nearest-neighbor interactions.

Phase Diagram – When (t/Δ) is small, we can treat the upper layer of our bilayer model as a spin system with nearest, next-nearest and third-nearest neighbor interactions. The resulting effective Hamiltonian is equivalent to the so called $J_1 - J_2 - J_3$ Heisenberg model. The parameters, J_1, J_2, and J_3, are related to the original parameters t and Δ via the results of the previous section. J_1 can thus be either ferromagnetic (FM) or antiferromagnetic (AFM), but J_2 and J_3 are always antiferromagnetic. Away from $n \approx 1$ and $\Delta/t \approx \infty$, this effective Hamiltonian is frustrated. While a full quantum solution for this model is still lacking, the classical solution is well understood [29, 132, 133, 134, 135]. We embed this classical solution in the $t - n$ phase diagram in Fig. 2.1.

There are four distinct phases. When Δ is large, J_1 is large and positive and the ground state is a simple ferromagnet. At lower densities, J_1 is large and negative and the system is in a Néel phase. Between these limits, the two contributions to J_1 nearly cancel, and the second- and third- neighbor terms become important. In these cases the ground state is either a striped phase with wave-vector peaked at $(0, \pi)$, or a spiral phase which interpolates between the striped and FM or the striped and Néel phases. We note that, quantum mechanically, the regime of competing exchanges might host another exotic state such as a valence bond solid or quantum spin liquid.

3.3 Instability of Ferromagnetism

We next study the instability of ferromagnetism using a variational method. Since double occupancy is forbidden automatically in the fully polarized or 'half-metallic ferromagnet' (HMF) state due to fermi statistics, its energy can be calculated exactly. We then can prove that this state is *not* the ground state if we find any state with

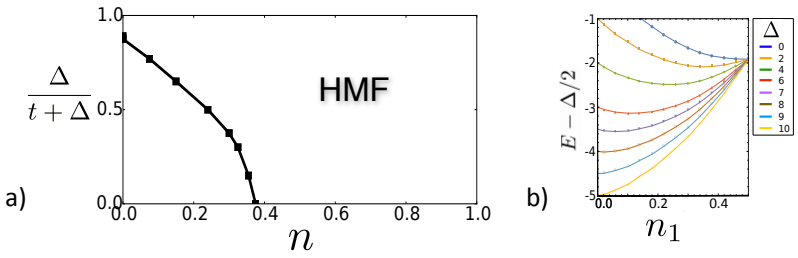

Figure 3.3: Result of (a) the variational calculation and (b) the Gutzwiller approximation. (a) The stability of the fully polarized FM state to the Gutzwiller projected trial state with a single flipped spin. The FM state becomes unstable inside the area bounded by the solid line. (b) Ground state energy with respect to $n_1 = \sum_\sigma \langle n_{i\sigma 1} \rangle$ calculated by Gutzwiller approximation at $n = 0$.

lower variational energy.

The details of the variational calculation are given in the supplementary material [136] where we consider the same trial state as in Ref. [130]. The results are shown in Fig. 2.3(a). The trend is towards increased ferromagnetism for larger Δ, in agreement with the perturbative results. This implies that for large enough hole concentrations, the Nagaoka state is unstable to flipping an electron spin, consistent with the intuitive picture. The instability, however, weakens for larger Δ and we could not find an unstable region for $\Delta \gtrsim 6.5$.

Metal-insulator transition – We next turn our attention to the metal-insulator transition (MIT) at $n = 0$ with increasing Δ. To investigate the MIT, we here study the model in Eq. 3.1 by the Gutzwiller approximation assuming a paramagnetic solution [137, 138, 139, 140]. In this framework, the MIT is characterized by the absence of electrons in the bottom layer. As is shown in Fig. 2.3(b), this occurs at $\Delta \simeq 8t$. This is consistent with our DMRG results, where we find the single particle excitation gap $E_g = E(n+1) - 2E(n) + E(n-1)$ becomes nonzero continuously in the 4 leg ladder at $\Delta = 6t$.

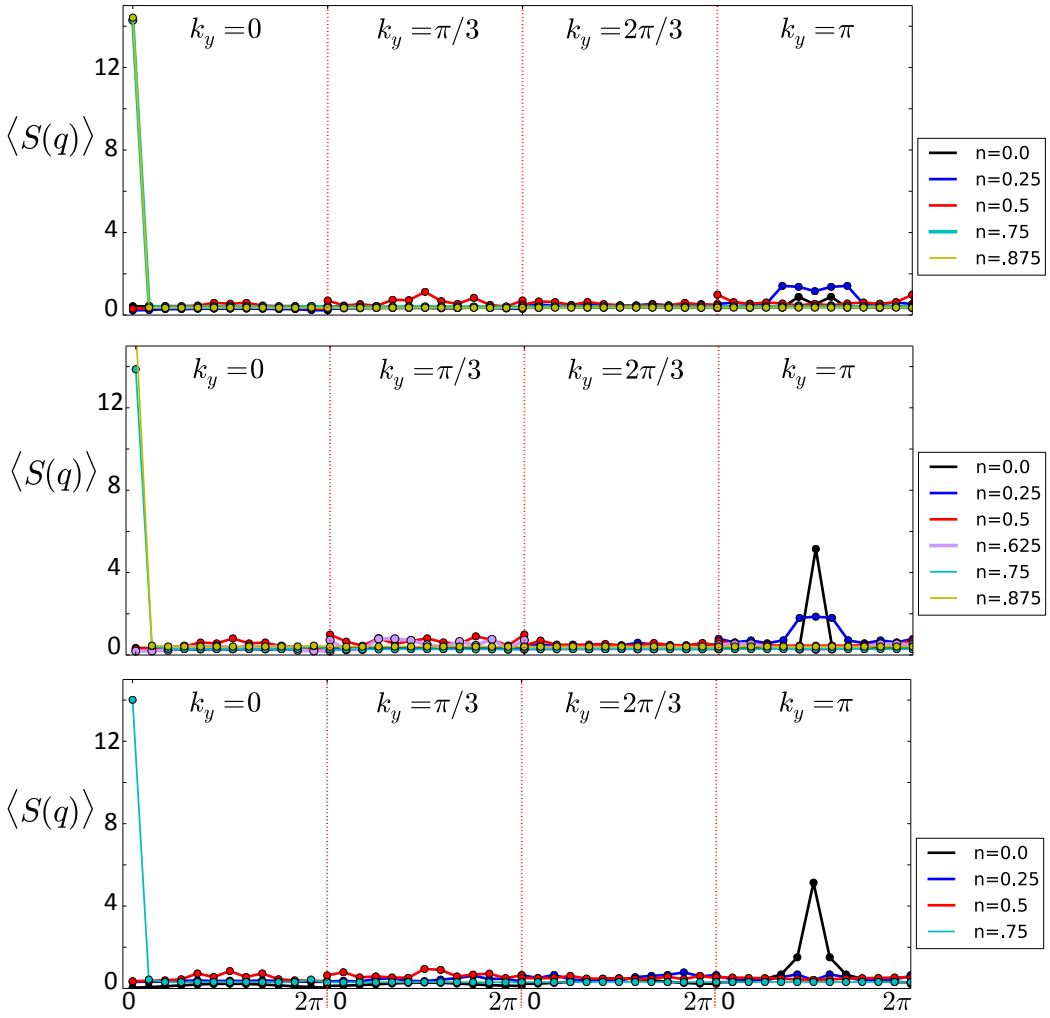

Figure 3.4: The structure factors for the 6x24x2 system for (*from top to bottom*) $\Delta = 4, 6$ and 10. The highest densities are always ferromagnetic. Néel order becomes more stable for smaller Δ, and the intermediate regions show no strong peaks.

3.4 Numerical Results

We will now demonstrate the consistency of our analytic arguments with unbiased numerical results. We performed a series of DMRG calculations on bilayer systems of up to six leg ladders. The total number of sites is then $2\times24\times6$. We keep 4000 to 6000 states and the truncation error is of the order of 10^{-6} in the ferromagnetic phase, but increases to 10^{-4} in the paramagnetic phase.

Due to the difficulty of the simulations, we limit our search over phase space to values of $\Delta/t = 4, 6$ and 10 and the fillings $n = 0, 0.25, 0.5, 0.75$ and 0.875. We focus mainly on the spin-spin structure factor $S(q) = \sum_j e^{i\vec{q}\cdot\vec{x}_{ij}}\langle\vec{S}_i \cdot \vec{S}_j\rangle$. These results are summarized in Fig. 2.2.

For $n \geq 0.75$ and all $\Delta \geq 4$, we find very large peaks in the structure factor at wave-vector $(q_x, q_y) = (0, 0)$, consistent with a nearly fully polarized ground state. In all cases, the total spin S satisfies $S \geq 0.90S_{\max}$. In fact, for $\{n = 0.875; \Delta = 4, 6\}$, we find $S \geq 0.98S_{\max}$. Note that this does extend the range of ferromagnetism from the results of Ref. [71], which find the HMF in the single layer model only up to fillings $n = 0.8$.

At the lowest densities $n = 0$ and $n = 0.25$, we find very strong agreement with our predicted results from perturbation theory. At $\{n = 0, \Delta = 6, 10\}$, there are large peaks in the structure factor at the (π, π) wave-vector. This suggests the presence of strong staggered magnetism consistent with a Néel phase. For $n = 0.25$, we find a smaller Néel peak at $\Delta = 6$, which then disappears as Δ is increased to $\Delta = 10$. This is again consistent with our perturbative results which suggest that AFM exchange is stronger for smaller Δ.

From the classical phase diagram of the effective perturbative spin model we

expect striped or spiral order to interpolate between the Néel and FM phases. Our results on 6-leg ladders for $\{n = 0.5; \Delta = 6, 10\}$ and $\{n = 0.25; \Delta = 10\}$ show no strong evidence of magnetic order. We do observe small peaks which may presage spiral or stripe order in larger systems.

We provide further evidence for this magnetic ordering in the supplementary material [136], by calculating the momentum distribution function.

Finally, we would like to stress that although ferromagnetism occurs over a smaller range of densities in the numerical results, our perturbative phase diagram must be exactly correct for sufficiently large Δ. However, it is possible that the range of Δ accessible in our simulations is not large enough to see the full extent of this effect.

3.5 Further Details

3.5.1 Momentum Distribution Function

In this section, we present the momentum distribution function as calculated using DMRG for a 6-leg ladder and $\Delta = 4$. We can estimate the position of the Fermi surface from the apparent discontinuity in the distribution function. We only show the results for $\Delta = 4$. We again exclude $2L_yL_x/4$ sites on each end of the ladder for the purpose of reducing boundary effects.

For the largest two densities, $n = 0.75$ and $n = 0.875$, the volume enclosed by the Fermi surface is $\mathrm{Vol}/(2\pi)^2 = 0.75$ and 0.875 respectively. This Luttinger volume is consistent with a polarized Fermi gas, whereby the upper band is completely filled and every electron fills a different momentum state in the lower band. The discontinuity gives the quasiparticle residue. We see that this value is slightly less than that of a noninteracting polarized Fermi gas, signaling the fact that the ground state here is

nearly fully polarized with a few flipped spins (i.e. $S > 0.90 S_{max}$).

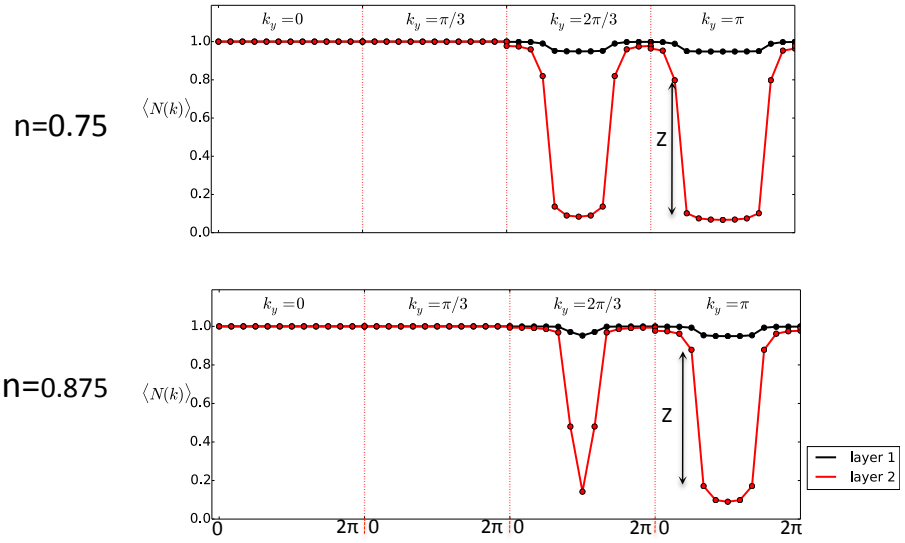

Figure 3.5: The momentum distribution function of the 6-leg bilayer model, for $\Delta = 4$ and high electron densities. The Luttinger volume is consistent with a polarized state. We show only the k_y cuts that are not related by inversion symmetry.

In Fig. 3.6 shows the same calculation for $n = 0.25$ and $n = 0.5$. The top layer is filled very uniformly, with all momentum states occupied. The Fermi surface then encloses a volume equal to half that of the number of electrons in the bottom layer. This is consistent with the small Fermi volume of an unpolarized Fermi liquid. For $n = 0.25$ the structure factor indicates the presence of Néel order, which implies there is a doubling of the unit cell. This allows the upper layer electrons to form a completely filled band so that only the lower layer electrons contribute to the Luttinger volume. For $n = 0.5$, we find the same Luttinger volume as the $n = 0.25$ case. Here, however, the structure factor showed no evidence of magnetic order. The fact that only the lower layer electrons contribute to the Fermi volume, however, rules out the possibility of a trivial paramagnetic metal. If the absence of magnetic order

survived to the thermodynamic limit, this would be the FL^* phase, which describes a quantum paramagnetic metal with a 'small' Fermi volume. We also see that the quasiparticle residue is much smaller in this regime, indicating that the ground state here is a strongly interacting state.

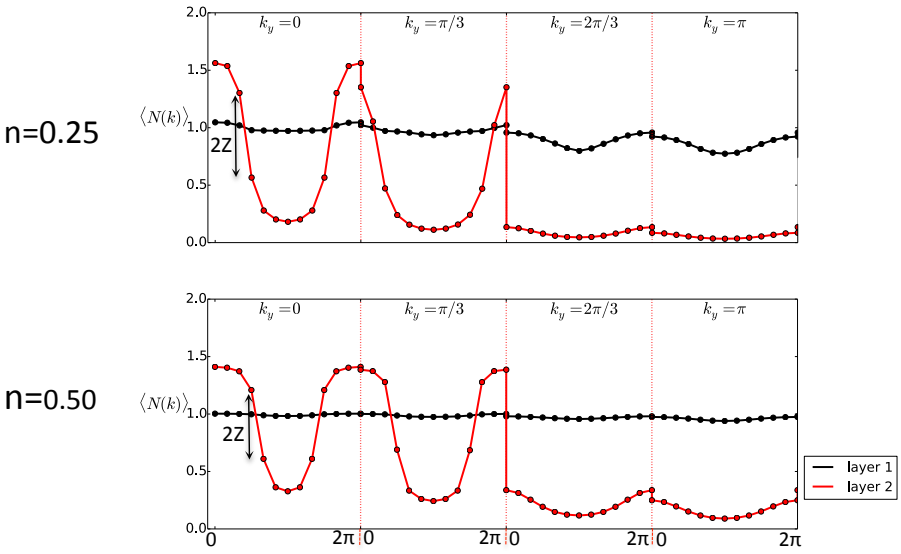

Figure 3.6: The momentum distribution function for $n = 0.25$ and $n = 0.5$. With the smaller Luttinger volume, the discontinuity now gives twice the quasiparticle residue.

Finally, we look at the case when $n = 0$. For this filling, there exists a metal insulator transition at a critical Δ_c. When $\Delta = 4$, we are on the metallic side of this transition. From Fig. 3.7, we see no apparent discontinuities in the momentum distribution. This could indicate the existence of a non-Fermi liquid ground state in this parameter range. Note that although we are on the metallic side of the MIT, the structure factor shows a small (π, π) peak. This type of spin-density wavetransition coupled to a Fermi surface has been studied extensively in the literature and is strongly suspected to show non-Fermi liquid behavior.

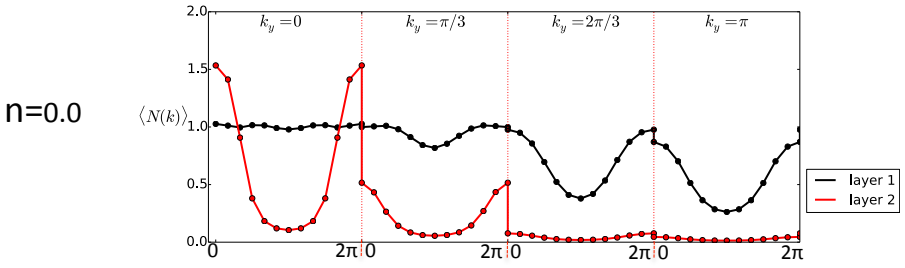

.

Figure 3.7: When $n = 0$, and at $\Delta = 4$, there appear to be no sharp discontinuities.

3.5.2 Variational Results

We have already shown the instability of the fully-polarized ferromagnetic state by comparing the energy to a trial state. Here, we present details of the method we used.

In the variational calculation, we consider a trial state

$$|\psi\rangle = \mathcal{P}\psi_\downarrow^\dagger |FM'\rangle \tag{3.6}$$

$$\psi_\downarrow = \sum_{i\alpha} \xi_{i\alpha} c_{i\alpha\downarrow}^\dagger \tag{3.7}$$

where $|FM'\rangle = c_{\vec{k}_F} |FM\rangle$ is the fully polarized metal with one less electron than $|\psi\rangle$, and $\mathcal{P}$ is the Gutzwiller projection operator which forbids double occupancy of any site, and $\xi_{i\alpha}$ are variational parameters.

With some calculation, we obtain

$$\varepsilon_\downarrow = \frac{\langle\psi| H - E_{\rm FM} |\psi\rangle}{\langle\psi|\psi\rangle} = \sum_k \hat{\xi}_k h_k \hat{\xi}_k, \tag{3.8}$$

where $E_{\rm FM}$ is the ground state energy for the fully-polarized state and $\hat{\xi}_k = (\xi_{k1}, \xi_{k2})$ with $\xi_{k\alpha} = \sum_i \xi_{i\alpha} \exp(i\vec{k}\cdot\vec{r}_i)$, $\alpha = 1, 2$. Additionally, $h_{\mathbf{k}}$ is a 2×2 effective Hamiltonian

whose explicit form is

$$h_{\mathbf{k}} = \begin{pmatrix} -\tilde{t}_0\epsilon_{\mathbf{k}} - T_0 & -\tilde{t}' \\ -\tilde{t}' & \tilde{t}_1\epsilon_{\mathbf{k}} + \tilde{\Delta} - T_1 \end{pmatrix}, \tag{3.9}$$

with

$$\tilde{t}_a = \frac{t}{R}\langle(1-n_{ia\uparrow})(1-n_{ja\downarrow})\rangle \tag{3.10}$$

$$\tilde{t}' = \frac{t'}{R}\langle(1-n_{i1\uparrow})(1-n_{j2\downarrow})\rangle \tag{3.11}$$

$$\tilde{\Delta} = \frac{\Delta}{R} \tag{3.12}$$

$$T_a = \frac{1}{R}\sum_{j,b} t_{ia,jb}\langle c^{\dagger}_{ia\uparrow}c_{jb\uparrow}\rangle \tag{3.13}$$

and where $R^2 = \langle\psi|\,\psi\rangle$. The optimal variational parameters are then just given via the solution of this single particle problem, and $\epsilon_{\downarrow}$ is given by the smallest eigenvalue of $h_{\mathbf{k}}$.

3.5.3 Details of the DMRG Calculation

In our DMRG set up, we first combine the two layer system into an effective one layer system. The new rung index is $R_x^{new} = 2 * (R_x - 1) + \tau$ where R_x is the rung index of each layer, and $\tau = 1, 2$ is the layer index. The DMRG study for the effective one layer system follows the standard DMRG for a cylinder. The two layer system is reflected in the Hamiltonian of the effective one layer system (which has a doubled unit cell along x, besides the open boundary conditions we used). The convergence crucially depends on which state we obtain in the different parameter regimes. For the ferromagnetic ground state, we are able to go to a large total S_z subspace, which has

a substantially reduced Hilbert space dimension. For other phases (the paramagnetic phase in particular), DMRG indeed has a large truncation error and the results are not converged for such a bilayer system (which is not the focus of our study).

3.6 Conclusions

In closing we note that a more faithful representation of the oxide interface would include additional complications such as multiple t_{2g} electron orbitals and super-exchange interaction J. For R=Gd,Sm, which are strongly distorted from the cubic structure, the intrinsic J is so weak that the kinetic mechanism described here is dominant or at least competitive with J, and orbital splittings are large. In general, however, these effects may work to stabilize certain types of magnetic order [141]. For example, directional hopping of the t_{2g} orbitals may act to favor ferromagnetism for smaller values of Δ. Our model avoids these complications by considering a simple limit where only the filling n and band offset Δ are free parameters, yet nevertheless provides a picture of the physics. We suggest that scattering experiments to directly probe the magnetic order in the vicinity of these interfaces would be the most direct test of our theoretical predictions.

Chapter 4

Many-Body Effects in Topological Kondo Insulators

The discovery of topological insulators in "inverted" semiconductors with strong spin orbit coupling led to an explosion of interest in topology in condensed matter systems. The combination of topology and strong correlations of electrons is a subject of major current activity, and systems in which both are at play suspected to host a variety of unique phenomena.[142] "Heavy fermion" and related materials with heavy lanthanide elements are natural places to seek such phenomena, as the electrons on these atoms experience strong spin-orbit coupling (SOC) – which is a driving force for non-trivial topology in many systems – and are strongly correlated. Theory recently suggested a concrete role for topology in these systems in the form of Topological Kondo Insulators (TKIs) [79, 80]. A TKI is a Kondo lattice system involving rare earth ions which at low energies hybridize with lighter conduction electrons forming a topological insulator. SmB_6 is strongly suspected to be such a TKI [143, 144, 126] .

While SmB_6 and indeed any Kondo lattice system is indisputably a strongly corre-

lated electronic system, the *low energy* description of a TKI in terms of effective bands seems indistinguishable from that of an uncorrelated topological insulator. This is disappointing in view of the hope for new phenomena in correlated strong SOC systems. The aim of this article is to consider the possibility of competing states, and seek out new effects arising from electronic correlations in a system which may host a TKI. We do this in the context of a model motivated by the recent proposal of realizing a TKI in graphene doped with heavy adatoms. In this model, described in detail in Sec. 4.1, we obtain a zero temperature phase diagram which embeds the topological insulator physics into the classic Doniach phase diagram [75] for Kondo lattice systems, with its magnetically ordered and Kondo screened phases. The magnetic ordering quantum phase transition is discussed in this context. We also consider the characteristic behavior of the boundary of the TKI, and show that this model is prone to *surface magnetic ordering*, even within the TKI state. Such spontaneous and intrinsic time-reversal breaking at the surface of a TKI could be the desired hallmark of correlations in the TKI state.

4.1 The Model

We study a tight-binding model of graphene, with a localized d-orbital electron site at the center of each face on the honeycomb lattice. Such a model was studied extensively in [145, 146, 147, 148], via a combination of first-principle calculations on a tight binding model and density functional calculations. There it was shown that the strong onsite spin-orbit term for the localized d-electrons, when hybridized with the conduction electrons, c, conspire to create a band insulator with a nontrivial topology. This topological phase on graphene is reminiscent of the original proposal

of topological order in graphene by Kane and Mele in 2005 [83, 84]. Our goal is to study explicitly the effect of interactions on such a model.

In [145], the DFT calculations show that the most important angular momentum states of the d electron are those with L^z quantum number $m = \pm 1$. These arise from the d_{xz} and d_{yz} adatom states, and so we restrict our model to states with these angular momenta. We include a spin-orbit coupling term for the d-electrons, but not for the conduction electrons where the small magnetic moments are expected to lead to a negligibly small amount of spin-orbit coupling. The chemical potential of both the c and d electrons is set so that there are two c and two d electrons per unit cell. This is a necessary condition if the hybridization is to lead to a band insulator.

The complication comes when we include an interaction term between the local d moments and the nearby conduction electrons. In order to write down this interaction, need to know the spin state formed by the composite two-body state sitting at each d-site. We assume that within the $m = \pm 1$ subspace, a Hund's rule type coupling makes it energetically unfavorable for both d-electrons to have the same angular momentum quantum number. We therefore ignore the possibility of the d-electrons forming spin-2 states, $|+\uparrow, +\downarrow\rangle$ and $|-\uparrow, -\downarrow\rangle$, when writing the form of the interaction. The remaining states are

$$\begin{aligned}
\vec{S}_{\rm tot} = 0 \quad &: \quad |+\uparrow, -\downarrow\rangle - |+\downarrow, -\uparrow\rangle \\
\vec{S}_{\rm tot} = 1 \quad &: \quad |+\uparrow, -\uparrow\rangle \\
&\qquad\quad |+\uparrow, -\downarrow\rangle + |+\downarrow, -\uparrow\rangle \\
&\qquad\quad |+\downarrow, -\downarrow\rangle \, .
\end{aligned}$$

Within this subspace the Kondo interaction is a spin-spin interaction which occurs

between the $\vec{S}_{\rm tot} = 1$ states, while the S.O. coupling term favors the $|+\downarrow, -\uparrow\rangle$ state, which is a linear combination of the singlet and triplet $S^z = 0$ states.

We define the operator $C_{i,p,\sigma}$, which is a linear combination of $c_{i\sigma}$ operators which carry angular momentum $p = \pm 1$.

$$\begin{aligned} C_{R,p,\sigma} &= \frac{1}{\sqrt{6}} \sum_{j=1}^{6} e^{-i(\pi/3)p(j-1)} c_{R+e_j,\sigma} \\ &= \sum_k \left(V_p(k) c_{A,k,\sigma} + V^*_{-p}(k) c_{B,k,\sigma} \right) \end{aligned} \tag{4.1}$$

where A and B denote the two sublattices of the honeycomb lattice, and e_j are the nearest-neighbor lattice vectors connecting the c and d sites.

We can now construct a spin-1 operator for both the c and d electrons from two spin-$\frac{1}{2}$ operators as follows,

$$\vec{S}_1 = \frac{1}{2} \sum_{m=\pm 1} d^\dagger_{m,\alpha} \vec{\sigma}_{\alpha\beta} d_{m,\beta} \tag{4.2}$$

$$s_1 = \frac{1}{2} \sum_{m=\pm 1} C^\dagger_{m,\alpha} \vec{\sigma}_{\alpha\beta} C_{m,\beta}, \tag{4.3}$$

where $\vec{\sigma}$ is the usual spin-1/2 Pauli vector. The Kondo interaction is then an anti-ferromagnetic spin-spin interaction between the spin-1 particle on the d-sites and the effective spin-1 formed by a linear combination of the conduction electrons near this d-site. The 4 fermion Kondo interaction is therefore

$$H_K = J \sum_i \vec{S}_{1,i} \cdot \vec{s}_{1,i}. \tag{4.4}$$

We also include an RKKY spin-spin interaction in our model. This is an interaction term between the d-electron states on different sites which is mediated through

conduction electrons. Performing second order perturbation theory in the Kondo interaction, the d-spin on one site interacts antiferromagetically with the conduction electrons near that site which in turn act antiferromagetically with a neighboring d-site. We assume this creates an effective ferromagnetic interaction between the two d-sites and parameterize this term with the variable J_m. Although in principle the RKKY interaction is included in Eq. (4.4), it is difficult to derive both the Kondo and RKKY effects together[149, 150]. Therefore, in our model we include as a separate parameter the RKKY interaction

$$H_{RKKY} = J_m \sum_{\langle ij \rangle} \vec{S}_{1,i} \cdot \vec{S}_{1,j}. \tag{4.5}$$

Therefore, the simplest interacting model that we believe captures the essential many-body physics of the TKI system is

$$\begin{aligned} H &= \sum_{k,\sigma} \epsilon_k c_k^\dagger c_k + \lambda \sum_{i,p,\sigma} (d_{ip\sigma}^\dagger d_{ip\sigma} - 2) + \mu \sum_{i,\sigma} (c_{i\sigma}^\dagger c_{i\sigma} - 2) \\ &\quad + \Lambda \sum_i (d_{+\alpha}^\dagger \sigma_{\alpha\beta}^z d_{+\beta} - d_{-\alpha}^\dagger \sigma_{\alpha\beta}^z d_{-\beta}) \\ &\quad + J \sum_i \vec{S}_{1,i} \cdot \vec{s}_{1,i} + J_m \sum_{\langle ij \rangle} \vec{S}_{1,i} \cdot \vec{S}_{1,j} \end{aligned} \tag{4.6}$$

The goal of this chapter is to examine at the mean field level the effects of the two interaction terms.

4.2 MFT and the Bulk Phase Diagram

4.2.1 Outline

In this section we will describe the general phases which exist in our model. This allows us to embed the TKI phase within the standard phase diagram for the Kondo lattice [151]. We show that there is in general a first order phase transition from a phase with no Kondo order (where the d-spins order magnetically) to a TKI phase at some nonzero value of the Kondo exchange J. Furthermore, this phase can be destroyed by RKKY type spin-spin interactions which are present in the fully interacting theory and so we include as a separate term in our mean-field Hamiltonian. If the system orders magnetically, time-reversal symmetry is broken and any distinction between the topological phase and a trivial insulator loses meaning. A similar MF phase diagram was calculated in Ref.'s [152],[153] for 3D TKIs, which did not consider the role of RKKY interactions.

4.2.2 Methods

We would like the study our fully interacting model at the mean field level. This means we should decouple our Kondo and RKKY interaction terms into the appropriate channels. This amounts to an assumption, which must be checked self-consistently, about the type of order in the interacting groundstate. To this end, we assume that the Kondo interaction,

$$\vec{S}_i \cdot \vec{s}_i = \sum_{m,m'} \vec{\sigma}_{\alpha\beta} \cdot \vec{\sigma}_{\gamma\delta} C^\dagger_{m,\alpha} C_{m,\beta} d^\dagger_{m',\gamma} d_{m',\delta} \tag{4.7}$$

induces a nonzero expectation value for the operator $\langle C^{\dagger}_{i,p,\sigma} d_{i,p,\sigma}\rangle$, and the RKKY interaction causes a nonzero expectation value for the magnetic order parameters $\langle \vec{S}_i \rangle$.

We can now perform the standard mean-field analysis by decoupling the interactions into the channels

$$\begin{aligned} J\, C^{\dagger}_{\alpha} d_{\alpha} d^{\dagger}_{\beta} C_{\beta} \;&\rightarrow\; J(\phi_{\alpha} d^{\dagger}_{\beta} C_{\beta} + \phi^{*}_{\beta} C^{\dagger}_{\alpha} d_{\alpha}) - J\phi_{\alpha}\phi^{*}_{\beta}. \\ J_m(S^x S^x + S^y S^y) \;&\rightarrow\; 2J_m \langle S^x \rangle S^x - J_m \langle S^x \rangle^2 \end{aligned} \tag{4.8}$$

Where α and β denote the two types spin-orbit coupled single particle states.

Notice that the interaction in Eq. (4.4) contains terms like $C^{\dagger}_{+} d_{-} C_{+} d^{\dagger}_{-}$, but these terms vanish after the above substitution since the resulting c-d hopping process does not conserve angular momentum. Also, we assumed that the spin-spin interaction favors magnetic order in the XY plane. We will justify this assumption in the next section.

We are therefore left with a non-interacting Hamiltonian for which the parameters ϕ_{+}, ϕ_{-} and $\langle S^x \rangle$ must be determined self-consistently. We use the parameters μ and λ in Eq.(4.6) to enforce the conditions that there are 2 electrons per d-site and one electron per graphene site, ensuring that the system is a band insulator when there is a full gap at the Fermi energy.

Performing these substitutions, the MF Hamiltonian becomes

$$
\begin{aligned}
H &= \sum_{k,\sigma} \epsilon_k c_k^\dagger c_k + \lambda \sum_{i,p,\sigma} (d_{ip\sigma}^\dagger d_{ip\sigma} - 2) + \mu \sum_{i,\sigma} (c_{i\sigma}^\dagger c_{i\sigma} - 1) \\
&\quad + \Lambda \sum_i (d_{+\alpha}^\dagger \sigma_{\alpha\beta}^z d_{+\beta} - d_{-\alpha}^\dagger \sigma_{\alpha\beta}^z d_{-\beta}) \\
&\quad - J \sum_i \sum_{p,\sigma} (\phi_+ + \phi_-)(C_{ip\sigma}^\dagger d_{ip\sigma} + \text{h.c.}) \\
&\quad - 2J_m \sum_i \langle S^x \rangle (d_{+\uparrow}^\dagger d_{+\downarrow} + d_{-\uparrow}^\dagger d_{-\downarrow} + \text{h.c.}) \\
&\quad + J(\phi_+ + \phi_-)^2 + J_m \langle S^x \rangle^2
\end{aligned} \tag{4.9}
$$

We then diagonalize the mean-field Hamiltonian and write the bare electron operators in terms of the free excitations of the system

$$
\begin{aligned}
d_{k,\alpha\sigma}^\dagger &= \sum_n \alpha_{k,n}^{(\alpha\sigma)} a_{k,n}^\dagger \\
c_{k,\alpha\sigma}^\dagger &= \sum_n \beta_{k,n}^{(\alpha\sigma)} a_{k,n}^\dagger,
\end{aligned} \tag{4.10}
$$

which are linear combinations of c and d electrons. Since H is diagonal in the $a_n^\dagger$ operators, knowledge of the coefficients α_n and β_n allow us to numerically determine the values of $\langle C_\pm^\dagger d_\pm \rangle$, $\langle S \rangle$, $\langle d_i^\dagger d_i \rangle$ and $\langle c_i^\dagger c_i \rangle$. By averaging over all occupied states of the mean-field model we can then find the parameters of H where the mean field constraints are satisfied.

In general, for each order parameter, $\langle \hat{X} \rangle$ there are two self-consistent solutions. These are $\langle \hat{X} \rangle = 0$ and $\langle \hat{X} \rangle = x \neq 0$. The solution with a nonzero order parameter breaks a symmetry of the interacting Hamiltonian and is therefore a distinct phase from the case where $\langle \hat{X} \rangle = 0$. Furthermore, notice that the mean field Hamiltonian

$H = H^0(J_X x)$ is only a function of the product J_X and x. Therefore, for any value of x there will always be a value of J_X such that $\langle X \rangle = x$. At this J_X there are two solutions to the mean-field conditions, $x = \langle X \rangle \neq 0$ and $x = 0$.

The mean field solution is equivalent to the lowest energy noninteracting variational state $|x\rangle$. $E_{var} = \langle x| \mathcal{H} |x\rangle$. E_{var} is a local minimum for the eigenstate $|x\rangle$ of H^{MF} when the self consistency equation $x = \langle X \rangle$ is satisfied. In this case $\langle x| \mathcal{H} |x\rangle = \langle x| H^{MF} |x\rangle$. This argument allows us to compare the energies of the different self consistent solutions. Since these energy of solutions equals the variational energy, the solution with the lowest energy must be the best mean field approximation to the true groundstate.

If the order-disorder transition is continuous, then every solution with nonzero x must be of lower energy than the disordered solution where $x = 0$. However, near a first order transition, there will exist solutions with small $\langle X \rangle$ that are of higher energy than the disordered state $\langle X \rangle = 0$. This gives us an easy way to distinguish between the two types of phase transitions in our calculation.

Note that model (4.9) does not conserve particle hole symmetry, whereas the fully interacting model (4.6) does, so that in order to ensure there are the same number of conduction electrons we need to adjust μ so that each site on the graphene lattice is filled to $n_c = 2$.

4.2.3 Phases

There are three distinct phases in model (4.9), which occur when **a)** $\langle C^\dagger d \rangle = 0$, **b)** $\langle C^\dagger d \rangle \neq 0$ and $\langle S \rangle = 0$ or **c)** $\langle C^\dagger d \rangle \neq 0$ and $\langle S \rangle \neq 0$.

The first case occurs when $\langle C_+^\dagger d_+ \rangle = \langle C_-^\dagger d_- \rangle = 0$ and there is no Kondo screening of the d-electrons. This is the "Fully Polarized" or Magnetic phase. This phase may be

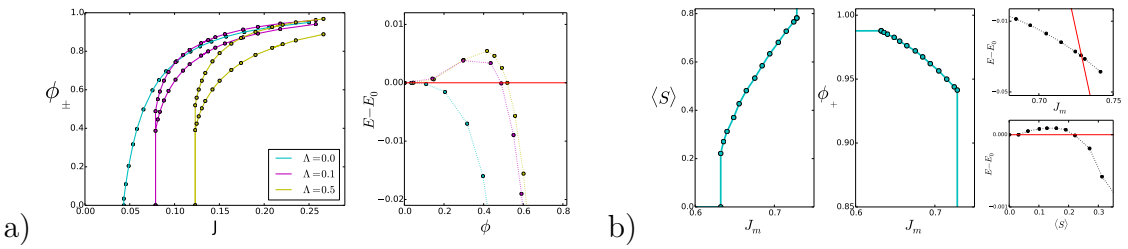

Figure 4.1: **a)** The Kondo order parameter for three values of Λ, ranging from $\Lambda = 0$ to $\Lambda = 0.5$ *(left)* and the corresponding energy gain compared to the $\phi = 0$ solution *(right)* . When $\Lambda = 0$ the transition is continuous but becomes first order when $\Lambda \neq 0$. **b)** The magnetic *(left)* and Kondo *(middle)* order parameters for fixed $J = 0.3$, $\Lambda = 0.5$. The onset of magnetic order with increasing J_m shows the transition from the Kondo phase into the mixed phase. Further increasing J_m to the point where the Kondo order parameter drops to zero this signals the transition into the fully polarized phase. The energy crossover of this mixed phase with the fully magnetic *(top-right)* and TKI *(bottom-right)* phases show that both these transitions are first order.

considered uninteresting as there is no interplay between the c and d electrons, which know nothing about each other at the mean field level. The conduction electrons are thus completely noninteracting and form a semimetal exactly like graphene with a pair of gapless Dirac cones in the band structure. The d-electrons still contain the spin-orbit term and interact through the spin-spin interaction J_m. In principle the spins could order in any number of phases depending on the exact form of the Heisenberg interaction, however the most likely result is that they order magnetically.

4.2.4 Phase Diagram and Transitions

In this section we give the results of our mean-field calculation for the bulk system.

Kondo Order– We start with the simplest case, where we set $J_m = 0$ so that spin-spin interactions do not compete with the tendency for Kondo order. However, even

this simplest case shows interesting physics. First studied by Withoff and Fradkin in Ref. [154], who showed that the effect of a vanishing density of states in the band structure creates a critical point J_c below which the Kondo effect does not take place. Careful renormalization group calculations on the spin-$\frac{1}{2}$ pseudogap Kondo model [155] have since shown that, in the case of graphene, there are significant corrections to the large-N result near such a critical point and that these results depend on the presence or absence of particle-hole symmetry in the model [156, 157, 155].

Our mean field calculation, however, is similar to other large-N studies of the pseudogap Kondo problem [158]. Here the large-N mean field approach is used in order to accurately describe the physics within the Kondo phase, at the cost of not being able to accurately describe the critical point of this phase transition. In the following we will describe the complete solution of the mean-field calculation, including all phase transitions. We should keep in mind, however, that the quantitative details of any continuous transition are valid only as $N \to \infty$ and are not expected to hold beyond the mean field level.

When $\Lambda = 0$, all d-electron sites are equivalent and there is only a single order parameter $\langle C_+^\dagger d_+ \rangle = \langle C_-^\dagger d_- \rangle = \phi$. In Ref. [154] it was shown that the effect of a non-constant density of states leads to a critical $J_c = \frac{1}{\rho_0 D}$, which signals the onset of Kondo order in this model.

We will see how this works in the mean field calculation of our graphene model. Consider the Lagrangian form of Eq. (4.9),

$$\mathcal{L} = \int d\omega dk \left[v_\alpha^\dagger (\mathcal{H}^{\mathrm{MF}}_{\alpha\beta}(k) - i\omega\delta_{\alpha\beta}) v_\beta + I_\alpha v_\alpha + v_\alpha^\dagger \bar{I}_\alpha \right]. \tag{4.11}$$

Integrating out the fermions, $\vec{v} = (c_A, c_B, d_+, d_-)$, produces the generating function,

$$\mathcal{Z} = \exp\left[\int \frac{d\omega}{2\pi} dk \;\; \bar{I}_\alpha \Big(\mathcal{H}^{\rm MF}_{\alpha\beta}(k) - i\omega\delta_{\alpha\beta}\Big)^{-1} I_\beta\right]. \tag{4.12}$$

The desired correlation functions can then be derived from the generating function using the expression

$$\langle v^\dagger_\alpha v_\beta\rangle = \int dk d\omega \;(\mathcal{G}_{\alpha\beta}(k, i\omega)) = \left.\frac{\delta^2\mathcal{Z}}{\delta\bar{I}_\alpha \delta I_\beta}\right|_{I=0} \tag{4.13}$$

This is analytically tractable for small values of $\phi_\pm$, where we can easily take the inverse in Eq. (4.12) and throw out all terms of $\mathcal{O}(\phi^3)$ or greater. This gives

$$\begin{aligned}
\langle C^\dagger_+ d_+\rangle &= \int dk d\omega \frac{J(\phi_+ + \phi_-)(V_+ e^{i\theta} - V^*_-)}{(\lambda + \Lambda - i\omega)(-|f(k)| - i\omega)} \\
\langle C^\dagger_- d_-\rangle &= \int dk d\omega \frac{J(\phi_+ + \phi_-)(V_- e^{i\theta} - V^*_+)}{(\lambda - \Lambda - i\omega)(-|f(k)| - i\omega)} \\
\langle d^\dagger_\pm d_\pm\rangle &= \\
&\int dk \int d\omega \frac{(|f| - i\omega)(-|f| - i\omega)}{(\lambda \pm \Lambda - i\omega)(|f| - i\omega)(-|f| - i\omega) + b_1\phi^2(-|f| - i\omega) + b_2\phi^2(|f| - i\omega)}
\end{aligned} \tag{4.14}$$

where we have written the graphene dispersion as $f(k) = |f(k)|e^{i\theta(k)}$. We perform the ω integral by contour integration and exchange the momentum integral for an integral over energy, $\int k dk = \int_0^D \rho_0 \epsilon d\epsilon$, where D is the bandwidth and ρ_0 is the density of states near the Fermi energy.

The conditions $\langle C^\dagger_+ d_+\rangle = \phi_+$, $\langle C^\dagger_- d_-\rangle = \phi_-$ and $\langle d^\dagger d\rangle = 2$ lead to the three

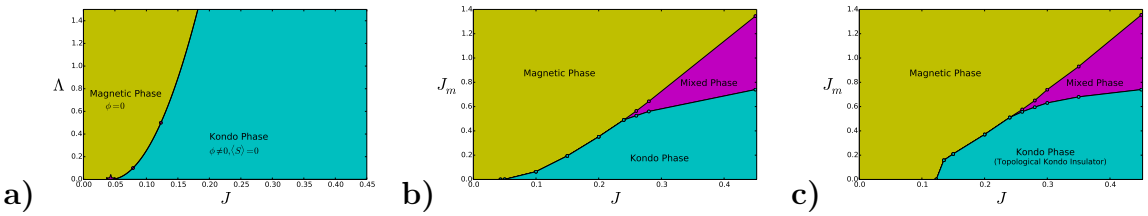

Figure 4.2: Cuts showing the 3D phase diagram. **a)** The $J-\Lambda$ plane when $J_m = 0$. **b)** The $J - J_m$ plane when $\Lambda = 0$. **c)** The $J - J_m$ plane when $\Lambda = 0.5$. See text for the description of the three phases.

equations

$$\begin{aligned}
(\lambda-\Lambda)\log\left[\frac{\lambda-\Lambda}{D+\lambda-\Lambda}\right] &\sim -D + \frac{1}{\rho_0 J(1+\phi_+/\phi_-)} \\
(\lambda+\Lambda)\log\left[\frac{\lambda+\Lambda}{D+\lambda+\Lambda}\right] &\sim -D + \frac{1}{\rho_0 J(1+\phi_-/\phi_+)} \\
\phi^2 &\sim \lambda-\Lambda
\end{aligned} \tag{4.15}$$

where we ignored the constant factor from the k dependence of $V_\pm$ and θ, and the third relation comes from looking at the shift in the residue $i\omega$ due to small but nonzero values of λ and ϕ.

When $\Lambda = 0$, then $\phi_+/\phi_- = 1$. In this case there only exists a solution for Λ when $J > \frac{1}{\rho_0 D}$. Near $J_c = \frac{1}{\rho_0 D}$, Eq's (4.15) give the solution $\lambda = J - J_c$. Therefore, $\phi = \langle C^\dagger d\rangle = \sqrt{J-J_c}$, and there is a second order transition at $J = J_c$.

When there is a nonzero spin-orbit coupling $\Lambda \neq 0$, the ratio $\phi_+/\phi_- \neq 1$, changing the solution to the first two equations in (4.15). Therefore, the value of the critical J for one of these equations is increased while the other decreases. Since both equations must be satisfied the overall effect of Λ is to push the transition back to larger values of $J_c(\Lambda) > J_c(0)$.

We verify these results is Fig. 4.1, through the method detailed earlier. We see

that our results agree with the general argument just presented. In particular, we see that when $\Lambda = 0$, ϕ decreases continuously to zero implying that there is a second order transition at a finite J_c between the phase with no Kondo order and the Kondo phase.

We also consider case where $\Lambda \neq 0$, where we show the numerical data for $\Lambda/t = 0.1$ and 0.5. As expected, we now see a splitting between the ϕ_+ and ϕ_- order parameters. We also see that the phase transition becomes first order. In fact we can always find a self-consistent solution for any value of the order parameters down to $\phi_\pm = 0$, but as shown in Fig. 4.1, these solutions are of higher energy than the disordered phase. This is easy to understand, as a finite Λ lowers the variational energy of the fully polarized phase more than it lowers the energy of the Kondo phase. This is because d-electron-like bands in the Kondo phase are necessarily linear combinations of both d_+ and d_- electrons, while in the fully polarized phase every d-site is filled with d_- electrons. This causes an energy crossing between the two possible phases, which occurs away from the critical point. This pushes the fully polarized phase into Kondo regime as you increase Λ, and causes a first order transition. Fig. 4.2 a) shows the phase diagram in the $J - \Lambda$ plane for $J_m = 0$. The transition at $\Lambda = 0$ is continuous with the critical point described above, while for $\Lambda \neq 0$, the transition is driven first order.

4.2.5 Magnetic Order

Next, we ask what happens when we include the spin-spin interactions between the d-electrons. In this case, there is an interplay between three competing forces, the spin-orbit coupling, the Kondo interaction and the magnetic interaction. Despite this competition, there exists a phase in which both Kondo and magnetic orders coexist.

This is characterized by a nonzero value of both $\langle C^\dagger d\rangle$ and $\langle S\rangle$. Here we will look at the stability of the Kondo phase to both the fully polarized phase and this mixed order phase.

First consider the fully interacting Hamiltonian. Deep within the Kondo phase, the mean field solution to $H^{MF}(\langle C^\dagger d\rangle \neq 0)$ is a saddle point of the action. When $\Lambda \neq 0$, there is a band gap separating the highest occupied band from the lowest unoccupied band so that there are no gapless excitations. We can then treat the spin-spin interaction as a perturbation around this solution, but it will obviously have no effect if the interaction strength is smaller than the gap. At the mean field level, the energies of some occupied states will shift down while an equal number of states will have their energy shifted up. Since all states are a finite energy below the Fermi level due to the band gap, all these states will remain occupied and to lowest order in perturbation theory there will be no effect.

The situation is slightly less obvious when $\Lambda = 0$ and the band structure is gapless. In the Kondo phase the bands touch at the Fermi level only at the Γ point in the Brillouin zone. This gapless band touching is guaranteed by the fact that $V_\pm(\vec{k} = 0) = 0$. In this case, a perturbation on the $J_m = 0$ MF solution will raise the energy of some states near $\vec{k} = 0$ above ϵ_F. The change in energy due to this shift is given by $\sim J\langle S\rangle$, while the number of states is limited to $\sim J\langle S\rangle N(\epsilon_F)$. Meanwhile, from $\mathcal{H}^{MF}$, such a perturbation has a constant energy cost of $J_m\langle S\rangle^2$. To first order, the total change in energy would be

$$\Delta E \sim -c_1(J_m\langle S\rangle)^2 N(\epsilon_F) + J_m(\langle S\rangle)^2. \tag{4.16}$$

Since $N(\epsilon_F) \to 0$, it seems likely that even in the presence of gapless states near the

Γ point, a perturbation in J_m will have a very small effect on the Kondo phase. We verify both these claims by explicit calculation.

Fig. 4.1 b) shows this behavior for a cut in the phase diagram along $J = \text{const}$ and $\Lambda = \text{const}$. For J_m small, there is no magnetic order and the Kondo phase is stable. If the gap to single spin excitations is smaller than the energy cost of destroying the Kondo phase, then the mixed phase is stable for some regime of J_m. The numerical calculation shows the spin order parameter $\langle S \rangle$ turning on for some finite J_m and coexisting with the Kondo order parameter ϕ. As the spin-order increases there is a corresponding drop in the Kondo order parameter. At some points in phase space, for small J, the energy of the fully polarized phase is always lower than the energy of the mixed phase. In this case, there is a direct transition from the Kondo phase to the magnetic phase. The energy crossings in Fig. 4.1 b) show that the transitions both into the mixed phase and into the fully polarized phase are first order.

4.2.6 3D Phase Diagram

Fig. 4.2 shows 2D cuts of the phase diagram at $J_m = 0$ and at two different values of Λ. Taken together these gives us the full 3D mean field phase diagram of our interacting model.

When $J_m = 0$, there is no competing magnetic interaction. At $\Lambda = 0$ there is a second order transition into the Kondo phase at $J = J_c$. As discussed, this critical point is a result of the vanishing density of states near ϵ_F. In the non-Kondo phase the d-electrons have no order but are unstable to any infinitesimal interaction. For $\Lambda \neq 0$, the d-levels are split and a full gap opens in the Kondo band structure which gives the phase a nontrivial topology. Here, the transition between the polarized phase and the Kondo phase is driven first order.

We also show cuts in the $J - J_m$ plane along $\Lambda = 0$ and $\Lambda = 0.5$. The main difference between these is that when $\Lambda \neq 0$, Kondo phase is destroyed suddenly at small J. Further, when $\Lambda \neq 0$ the Kondo phase has a full band gap with a nontrivial topology, while the Kondo phase for $\Lambda = 0$ is a semimetal. The similarity of the two cuts is due to the stability of the Kondo phase against J_m in both cases. At the points in phase space where there is nonzero magnetization, J_m is generally large enough that the effect of Λ only slightly moves the boundaries.

Now, if the spins ordered magnetically in the z-direction, the S.O. term favors the state $|+\downarrow, -\uparrow\rangle$, while the J_m term favors the state $|+\uparrow, -\uparrow\rangle$. These states are completely orthogonal, therefore the spins will order in one of these two states depending on which interaction is stronger. If $\Lambda > J_m$, the first state will be chosen and the energy per site is $E_\Lambda = -\Lambda$. On the other hand if $J_m > \Lambda$, the spins will align in the $S^z = +1$ state and the energy per spin will be $E_Z = -J_m$. On the other hand, if the spin order in the XY plane, the spins order depending on the Hamiltonian

$$H_d = \vec{v}^\dagger \begin{bmatrix} \Lambda & J_m S^x & 0 & 0 \\ J_m S^x & -\Lambda & 0 & 0 \\ 0 & 0 & -\Lambda & J_m S^x \\ 0 & 0 & J_m S^x & \Lambda \end{bmatrix} \vec{v}$$
$$\text{where } \vec{v} = (\ d_{+\uparrow} d_{+\downarrow} d_{-\uparrow} d_{-\downarrow}\ ). \tag{4.17}$$

The energy of the groundstate with $n_d = 2$ is $E_{XY} = -\sqrt{\Lambda^2 + (J_m S^x)}^2$, where the self-consistent value of $S^x = \langle S^x \rangle$ depends on the ratio J_m/Λ. Clearly, by the variational principle, $E_{XY} \leq E_Z$ and $E_{XY} \leq E_\Lambda$ for all Λ and J_m. So ordering in the XY plane allows the spins to partially satisfy both the S.O. and $RKKY$ terms in the

Hamiltonian, so that we can safely assume that the spins order this way. Therefore, in the fully polarized phase the c and d electrons behave independently, with the d electrons ordering magnetically according to the Hamiltonian in (4.17)

4.3 Edge states of the TKI phase

Perhaps the most dramatic consequence of symmetry protected topological states is the necessary existence of nontrivial edge states in systems with a boundary. In two dimensions the allowed edge states are either A) gapless or B) spontaneously break the symmetry, while the system remains gapped with unbroken symmetry within the bulk [159]. In three dimensions a third allowed possibility is a surface with topological order [160, 161, 162]. It would be very interesting if such a surface state could be achieved with a topological Kondo insulator, however in our 2D system we must restrict ourselves to the first two possibilities. It has been shown that on the surface of 3D TKIs, fluctuations around the mean-field state can lead to strongly interacting surface theories [163]. We take a similar approach below for 2D TKIs where we first discuss the mean-field solution and then go beyond MFT to look at the true low energy theory of our edge states.

4.3.1 Mean Field Analysis

We now show that at the mean field level, when the system is studied on a finite strip, so that the noninteracting TKI phase contains gapless edge states, the edges are always unstable to magnetic perturbations at the Fermi level. In this way, the TKI is a simple way to realize a time-reversal invariant insulator with spontaneous breaking of the TR symmetry on the edges.

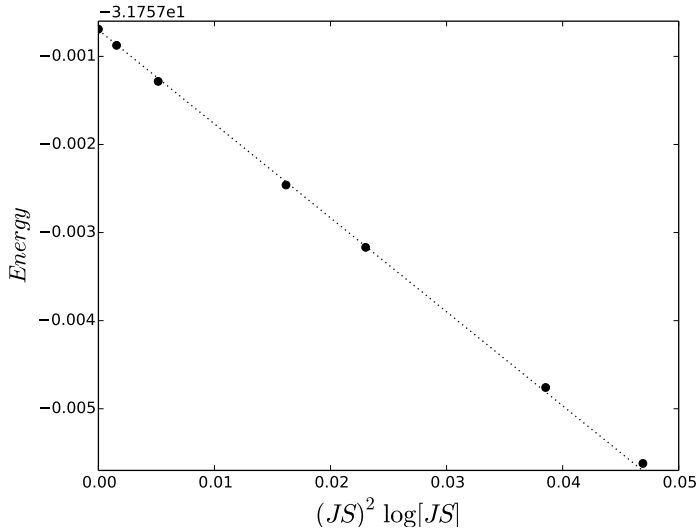

Figure 4.3: The energy gained by opening a gap at the Fermi level near $k = \pi$ is logarithmic in JS in the mean-field calculation.

In the bulk system, deep within the Kondo regime, the effect of an infinitesimal RKKY interaction is negligible due to the presence of a gap to any spin-1 excitations.

Our argument for the MF edge theory is similar to the Peierls argument [164, 165, 166] whereby in one dimension, if we ignore the dynamics of the phonons, logarithmically more energy can always be gained by the electrons ordering. The mean field $\langle S \rangle$ plays the role of the static phonon fields, and the periodic lattice distortion is instead replaced by a coupling between right and left moving electron fields. The effect of the magnetic interaction is to open a gap at the Fermi level, replacing the edge spectrum $\epsilon_k \sim v_k k$ with $\epsilon_k \sim \sqrt{(v_k k)^2 + \Delta^2}$ where $\Delta = J_m \langle S \rangle$. Following the standard argument, one dimensional gapped systems contain a singularity in the density of states, and a proper estimate for the change in energy due to the magnetic ordering is

$$\delta E \sim \int_0^\Lambda dk(\sqrt{(v_k k)^2 + \Delta^2} - v_k k) = \frac{1}{4}\Delta^2 \log[4e\Lambda^2/\Delta^2]. \tag{4.18}$$

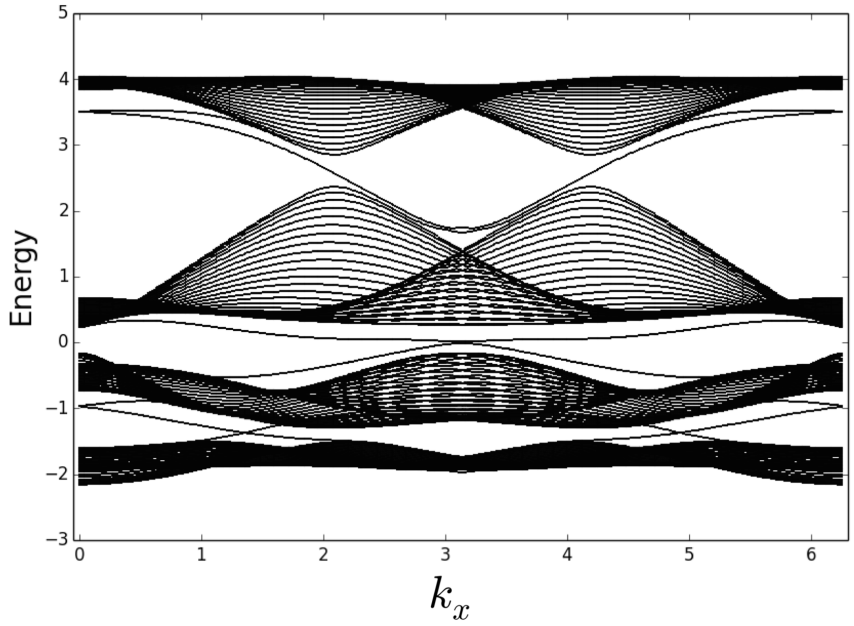

Figure 4.4: The single-particle band structure on a finite strip shows in gap edge states and a gap opening in the edge spectrum for small J_m.

We verify this argument with an explicit mean-field calculation in the same vein as in section 4.2.4 for the bulk phase diagram. We perform the mean-field calculation in the same way as for the bulk system. The Hamiltonian now has an $8N_y$ site basis, where N_y is the number of unit cells of our finite strip in the y direction. We use different order parameters for sites on the edge and in the bulk and find the self-consistent values of these order parameters. For the bulk order parameter we average the order over all sites that are not on the edge. In Fig.4.5, we have tuned J and Λ to a point deep within the Kondo phase. We saw in the previous section that this phase is extremely robust against the formation of magnetic order. An important point is that in order to satisfy the conditions $\langle d^\dagger d\rangle = \langle c^\dagger c\rangle = 2$ on every site, the edge states need to intersect the Fermi level, ϵ_F, at exactly $k = \pi$. This is the time-reversal invariant momentum at which, due to Kramer's theorem, the two edge states intersect. In the

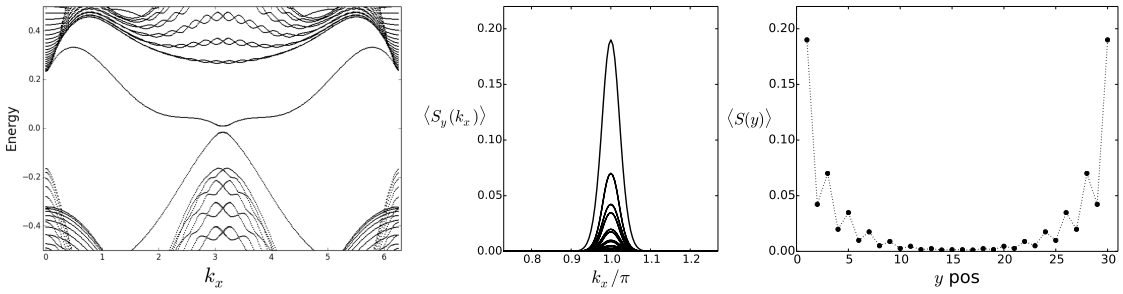

Figure 4.5: *(Left)* The band structure near the zero energy edge states. *(Center)* Measuring the symmetry breaking shows that the magnetic order is localized near $k_x = \pi$, and at the edges of the strip $y = 0, L_y$ *(right).* ($y = 0$ and $y = L_y/2$ gives the largest and smallest peaks respectively.)

mean field, the spin-spin interaction term couples fermions of opposite spin at the same momentum. At $k = \pi$, these two fermions modes are degenerate with energy $\epsilon = \epsilon_F$. The spin interaction breaks this degeneracy, sending one state above ϵ_F and one below ϵ_F. Consider the Hamiltonian describing of the edge states near k_F,

$$H_{\text{edge}} = \sum_{-\Lambda<k-\pi<\Lambda} \begin{pmatrix} c^\dagger_{k\uparrow} c^\dagger_{k\downarrow} \end{pmatrix} \begin{bmatrix} \epsilon_k & J_m \\ J_m & -\epsilon_k \end{bmatrix} \begin{pmatrix} c_{k\uparrow} \\ c_{k\downarrow} \end{pmatrix}. \tag{4.19}$$

The eigenvalues of H are $\epsilon_\pm = \sqrt{\epsilon_k^2 + J_m^2}$. When $\epsilon_k \ll J_m$, the corresponding eigenstates are given by $v_\pm = c_{k\uparrow} \pm c_{k\downarrow} + \mathcal{O}(\frac{\epsilon}{J})$. Meanwhile, for $J \ll \epsilon_k$, to first order the eigenstates are just the original states $v_+ = c_{k\uparrow} + \frac{J}{2\epsilon_k} c_{k\downarrow}$ and $v_- = c_{k\downarrow} - \frac{J}{2\epsilon_k} c_{k\uparrow}$. In the first case, the conduction electrons are almost completely polarized in the XY plane, while in the second case the eigenstates have very little magnetic order. Therefore, it is only in the regime where $\epsilon_k \ll J_m$, that a small J_m creates a significant magnetization. But since the edge states are gapless there will always be some finite region where this condition is true, and it is these small number of states which contribute to the spontaneous breaking of TR symmetry on the edge.

In Fig. 4.3, we verify that the energy of a self-consistent solution of the MF Hamiltonian as a function of the input parameter JS is

$$\Delta E \sim (J_m S)^2 |\log(J_m S/\tilde{\Delta})| - J_m S^2 \tag{4.20}$$

where Δ is an arbitrary cutoff. Therefore, for any value of J_m, there is an S for which the energy gain is positive, making this TR broken state favorable. Since the self-consistent point $S = \langle S \rangle$ is the variational minimum, it must therefore also have a positive gain in energy. Fig. 4.5 shows that the symmetry breaking is localized to momenta near the TRIM $k = \pi$ and is localized in space to the edge of the strip. Meanwhile, Fig.4.4 shows the band structure of the finite strip. In particular, they show the opening of a gap at the Fermi level due to a small nonzero J_m.

4.3.2 Luttinger Liquid Physics

The Peierls argument and mean-field calculations in the previous section are only valid in the limit of a static spin field (similar to how the lattice Peierls argument is only valid for static phonons). For a one-dimensional system, however, we can solve the low-energy theory exactly using bosonization techniques. In gapless 1D system, the low-energy excitations are bosonic degrees of freedom which are localized near the Fermi points. For a non-interacting topological insulator it is well known that each edge contains a time-reversed pair of chiral fermion modes [83], for example a right-moving spin up mode and a left-moving spin-down mode. Taken together these comprise a single bosonic degree of freedom, so that the problem maps onto a spinless fermion problem. In the absence of interactions, which may couple the right and left moving modes, the bosonic action for the edge of our TKI is just the action of a free

bosonic particle

$$S = v_k \int dx d\tau \left[K(\partial_x \phi)^2 + \frac{1}{K}(\partial_\tau \phi)^2 \right]. \tag{4.21}$$

In our case, the neutrality condition

$$\frac{1}{N}\sum_k \langle d^\dagger d \rangle = \frac{1}{N}\sum_k \langle c^\dagger c \rangle = 2 \tag{4.22}$$

ensures that the edge states cross the Fermi level at exactly $k = \pi$. Near this Fermi level, the right and left moving modes can be bosonized to give a single free bosonic degree of freedom which describes the low-energy dynamics of the system. This allows us to give a rather simple interpretation of the mean-field result in terms of the allowed interaction between the low-energy modes of our theory. We will further see how the mean field result fails to properly capture the fluctuations of the 1D edge modes.

At the Fermi point we have a single right moving spin up mode and a left moving spin down mode. The spin-spin interaction, J_m, couples these modes together. We can expand the fermion creation and annihilation operators in terms of bosonic operators. The most relevant terms in this expansion are

$$\psi^\dagger_{R/L} \sim e^{i(\theta \pm \phi)}. \tag{4.23}$$

At the mean field level, the spin-spin interaction is $J_m \langle S \rangle S^x$, where $S^x = (d^\dagger_{+\uparrow} d_{+\downarrow} + d^\dagger_{-\uparrow} d_{-\downarrow} + \text{h.c.})$. ψ_R is a linear combination of all spin up c and d operators, and likewise for ψ_L and spin down operators. Therefore, writing this interaction in terms of $\psi_{R/L}$

produces a number of terms. The most relevant allowed terms is,

$$g_{\rm MF}\left(\psi_R^\dagger\psi_L+\psi_L^\dagger\psi_R\right)\sim\cos(2\theta), \tag{4.24}$$

where $g_{\rm MF}\sim J_m\langle S\rangle$. The scaling dimension of such an operator is well known from the form of the free bosonic correlation function to be

$$\dim[\cos(p\theta)]=\frac{p^2}{4K}\ ,\ \dim[\cos(p\phi)]=\frac{p^2K}{4}. \tag{4.25}$$

Therefore the operator $\cos(2\theta)$ is a highly relevant perturbation at the noninteracting point $K=1$. This implies that for the mean-field model, an infinitesimal perturbation J_m will flow under RG to strong coupling. The resulting model is a sine-Gordon model, in which the θ field is pinned at strong coupling, breaking TR symmetry.

However, this type of naive analysis ignores the fluctuations of the spin order parameter $\langle S\rangle$, which can drastically affect the physics. In particular, we can write down all allowed interactions involving a single right and a single left moving mode. These interactions are

$$H_{\rm int}^{(1)} = g_1\psi_R^\dagger\psi_R\psi_L^\dagger\psi_L \tag{4.26}$$

$$H_{\rm int}^{(2)} = g_2\psi_R^\dagger\psi_R^\dagger\psi_L\psi_L \tag{4.27}$$

where the umklapp operator g_2, can only exist in systems with a single fermion species if there is point splitting $g_2\sim\psi_R^\dagger(x)\psi_R^\dagger(x+a)\psi_L^\dagger(x)\psi_L(x+a)$. This introduces a derivative upon taking the continuum limit, making this operator less relevant.

The most relevant bosonized expressions contained in Eq.'s (4.26) and (4.27) are

$$H_{\text{int}}^{(1)} \sim g_1 \left[(\partial_x \phi)^2 - (\partial_x \theta)^2\right] \tag{4.28}$$

$$H_{\text{int}}^{(2)} \sim g_2 \cos(4\theta). \tag{4.29}$$

The g_1 term can be absorbed into the action, Eq. (4.21), by renormalizing the value of the Luttinger parameter K. The g_2 term, however, will attempt to pin the field θ, thus opening a gap in the energy spectrum at the Fermi level. This process is relevant if the scaling dimension for the g_2 operator is less than 2. In that case, the cosine operator will flow to strong coupling and pin the θ field. By Eq. (4.25), the scaling dimension of the g_2 operator is $\dim[g_2] = 4/K$. This implies that at the noninteracting point $K = 1$, the cosine term is irrelevant and the action of the edge states remains gapless. It is only when the g_1 term pushes the value of K past $K = 2$ that the cosine operator becomes relevant. At this point there is a Kosterlitz-Thouless transition into a phase where the θ field is pinned. The θ field in this case acts like the S^x spin operator since, by the bosonization rules above

$$S^x \sim \psi_\uparrow^\dagger \psi_\downarrow + \psi_\downarrow^\dagger \psi_\uparrow = \psi_R^\dagger \psi_L + \psi_L^\dagger \psi_R = \cos(2\theta). \tag{4.30}$$

Pinning θ at $\theta = 0$, implies that $\langle S^x \rangle \neq 0$, and so time reversal symmetry is broken on the edge.

The stability of edge states in the spin-quantum Hall effect has been studied previously, focusing on the effect of a screened Coulomb interaction [167, 168]. The results in those works similarly find that a single Kramer's pair of edge modes are stable at weak coupling, but may be driven into a gapped phase by sufficiently strong

interactions. In our problem, the analogous interactions are included naturally in the form of the RKKY interaction term.

This result leaves two possibilities for the full phase diagram in the presence of edge states. The first case is that the strength of RKKY interactions, J_m, required to gap the edge modes for a given value of J is less than that required to drive the edge into a magnetic phase. In this case, time-reversal symmetry will be broken spontaneously on the edge of the system while being preserved within the bulk, and the edge properties of the TKI in this phase will differ dramatically from that of the uncorrelated 2D topological insulator of Ref's [146],[83].

The second possibility is that for all J, the required J_m to drive the edge to a gapped state is greater or equal to that required to drive the bulk into the magnetic or mixed phases. In this case, the low energy theory of the TKI is qualitatively similar at weak coupling to the noninteracting TKI phase of Ref. [146]. However, even in this case, the low-energy edge theory, while gapless, is still governed by the action in Eq. (4.21) and controlled by the Luttinger parameters v_F and K and thus will show quantitative differences from the noninteracting theory.

We may also ask, in what case is the mean-field analysis of the previous section valid. If we generalize our model to one with N_f flavors of fermions on each lattice site we enter a regime where the large-N_f and slave-boson approaches to the Kondo problem become justified [76, 152]. In the limit $N_f \to \infty$, the mean-field result becomes exact as fluctuations, even on the edge, are strongly suppressed. Within the Luttinger liquid framework, we now need to study a system with N_f time-reversed pairs of gapless modes on each edge. In the topologically nontrivial phase, N_f must be odd. It is mentioned in Ref. [167] that the $N_f = 3$ case is less stable to interactions than the $N_f = 1$ case. This is due to the enlarged number of allowed interactions

which appear when we include terms which couple different modes together. We therefore speculate that as $N_f \to \infty$, the huge number of allowed interactions in the low-energy picture will always gap out all edge modes in order to agree with the high-energy mean field picture. The large-N_f theory should always fall under the first case discussed above where TR symmetry is broken on the edge but preserved within the bulk.

Chapter 5

Concluding Remarks

I would like to conclude this dissertation by summarizing the main results. We focused on three main models which have relevance to experimental materials and show emergent quantum behavior.

In chapter 2, we studied a very general spin-orbit coupled model on the triangular lattice. This model is believed to be a good description of the material $YbMgGaO_4$. In this material strong spin-orbit coupling effects lead to interactions among effective spin-$\frac{1}{2}$ moments which are highly anisotropic in real space. Experiments on $YbMgGaO_4$ find enticing evidence of a spinon Fermi surface spin liquid state, both from thermodynamic measurements and inelastic neutron scattering experiments. The goal of our work was to provide a comprehensive commentary on the possibility of $U(1)$ spin liquid physics in a very general spin-orbit coupled model on the triangular lattice. We did this by looking at a set of variational wavefunctions which allow us to study both the spin liquid and magnetic phases within a single unified framework. Using the variational Monte Carlo technique we can study these wavefunctions numerically and find quantitatively accurate results about the ground

state physics of our model. By doing so, we were able to paint a complete picture of the ground state phase diagram for this model. We found that with only first- and second-neighbor interactions, a spin liquid ground state can in fact be stabilized, which agrees with previous work studying the isotropic $J_1 - J_2$ Heisenberg model on a triangular lattice. However, both XXZ anisotropy and the $J_{\pm\pm}$ spin-orbit interactions work to limit the spin liquid phase to a very small region of the parameter space. We then further found that adding a small third-neighbor interaction quite dramatically increases the extent and stability of the spin liquid phase in this model.

In respect to $YbMgGaO_4$, our results support the idea that the experimental parameters of the material likely place its ground state outside the spin liquid phase. Furthermore, the spin liquid we are able to stabilize in our variational calculation is always the Dirac spin liquid, not the spinon metal state which appears consistent with the experiments. It seems likely that the very strong disorder present in the material is obscuring the true nature of the low energy physics in the experiments. However, all hope is not lost. In our work, we developed a numerical method to incorporate many-body spin-orbit effects into the variational wavefunction. To accomplish this, we had to find a way to incorporate perturbative corrections into the wavefunction in a way which is extensive in system size. These effects do seem to favor the spinon metal state over the Dirac spin liquid state, and so leave the door open that such a spinon Fermi surface spin liquid may exist in a related material, possibly assisted by other factors such as disorder or a small ring-exchange interaction. We also identified some unique effects which should be present if such a spin-orbit coupled spinon metal does exist. We showed that the spin-orbit interactions could explain the existence of broad peaks at the M points in the spin structure factor and predicted that measurements of the spin-polarized structure factors would show polarization-dependent peaks reflecting

the anisotropic interactions. We also showed that such a wavefunction may have a rather large thermal Hall conductivity. This thermal Hall conductivity is the result of a topological contribution to the emergent spinon quasiparticle conductivity and so is a rather unique phenomenon for a spin system. Furthermore, it is interesting that such a spinon conductivity can be induced simply by a Zeeman coupling of the effective spins to the external magnetic field.

In chapter 3, we studied a very simple bilayer Hubbard model with the extreme limit where $U = \infty$. When doped away from half-filling, the only term present in such a model is the projected hopping of fermions on the lattice with the strict condition that two fermions can never occupy the same site. Amazingly, we were able to find quite rich physics in this model and relate this to the behavior seen in GTO/STO oxide heterostructures. In particular, a chemical potential offset between the two layers can be tuned so that the density of electrons in one layer is kept close to half filling and the system models a localized 2D layer of spins coupled to a second 2D layer of itinerant fermions. We showed that virtual hopping of an electron from the insulating layer to the metallic layer leads to an effect whereby kinetic ferromagnetism emerges in the ground state wavefunction. By controlling the electron doping and chemical potential offset, a rich variety of magnetic order can be shown to exist in the ground state phase diagram. The advantage of studying our model is that its simplicity allows for a complete solution of the physics. We solved for the magnetism quite rigorously in the perturbative regime, and used a combination of analytic approximations and exact unbiased numerical calculations to solve for the behavior in the intermediate coupling regime. As a result we were able to demonstrate for the first time an example whereby itinerant magnetism emerges solely due to the presence the Mott insulator/band insulator interface.

In chapter 4, we discussed the role of interactions in the physics of 2D topological Kondo insulators. To this end, we wrote down a realistic theory for a system of graphene doped with localized spin-1 magnetic moments which interact with the nearby conduction electrons. We performed mean-field calculations on this model and found that the bulk phase diagram separated into three distinct regions, a topological Kondo insulator, a magnetic insulator with no Kondo order and a phase with both Kondo and magnetic order. We then studied the effects of the Kondo interaction on the gapless edge states in the topological phase. We found that there exists a critical number of gapless edge modes, above which the interactions lead to a spontaneous breaking of time-reversal symmetry on the edges.

Appendix A

Variational Monte Carlo

A.1 Generalities of VMC

The ability to construct interacting spin liquid wavefunctions by Gutzwiller projecting noninteracting fermionic wavefunctions has immense practical benefits. We can study these projected fermionic wavefunctions numerically using the variational Monte Carlo technique (VMC). In this appendix we review the basic theory which underlies the VMC algorithm. A more detailed account can be found in Ref. [169]. As the name suggests, this is a variational technique where one constructs a class of trial wavefunctions which are used as an ansatz for the ground state wavefunction of a particular Hamiltonian H. The goal is then to tune parameters in order to find the wavefunction with the lowest possible energy. That is, we would like to find the wavefunction that minimizes the function

$$E_{var} = \frac{\langle \Psi_{var} | \, H \, | \Psi_{var} \rangle}{\langle \Psi_{var} | \, \Psi_{var} \rangle}. \tag{A.1}$$

where for a local Hilbert space with quantum variables $\{\alpha_i\}$ our variational wavefunction can be written as

$$|\Psi_{var}\rangle = \sum_{\{\alpha_i\}} \Psi_{\{\alpha_i\}} \big|\{\alpha_i\}\big\rangle. \tag{A.2}$$

The coefficients $\Psi_{\{\alpha_i\}}$ are set by our variational ansatz, and therefore we can in principle calculate the value of any observable $\mathcal{O}$ by directly performing the sum over basis states

$$\begin{aligned} \langle \mathcal{O} \rangle &= \frac{\langle \Psi_{var} | \, \mathcal{O} \, | \Psi_{var} \rangle}{\langle \Psi_{var} | \, \Psi_{var} \rangle} \\ &= \frac{\sum_{\{\alpha_i\}} \sum_{\{\beta_i\}} \Psi^*_{\{\beta_i\}} \Psi_{\{\alpha_i\}} \langle \{\beta_i\} | \, \mathcal{O} \, | \{\alpha_i\} \rangle}{\sum_{\{\alpha_i\}} |\Psi_{\{\alpha_i\}}|^2} \\ &= \frac{\sum_{\{\alpha_i\}} \Psi^*_{\{\alpha_i \to \mathcal{O}\alpha_i\}} \Psi_{\{\alpha_i\}}}{\sum_{\{\alpha_i\}} |\Psi_{\{\alpha_i\}}|^2}. \end{aligned} \tag{A.3}$$

However, for any modestly sized system, there are far too many terms in this sum to evaluate exactly. Instead, the approach we take is to use Monte Carlo methods to evaluate the sum in Eq. A.3 numerically. As in all Monte Carlo methods, we randomly sample the phase space

$$\langle \mathcal{O} \rangle = \sum_{\{\alpha_i\}} \mathcal{P}(\{\alpha_i\}) f(\{\alpha_i\}) \approx \frac{1}{N} \sum_{i=1}^{N} f(\{\tilde{\alpha}_i\}) \tag{A.4}$$

where we first rewrite the sum in Eq. A.3 as a product of a probability distribution $\mathcal{P}(\{\alpha_i\})$ and a function $f(\{\alpha_i\})$. We then approximate this expectation value with a sum over N random variables $\{\tilde{\alpha}_i\}$ which are randomly distributed according to $\mathcal{P}(\{\tilde{\alpha}_i\})$.

If we randomly select configurations $\{\alpha_i\}$, so that $\mathcal{P}(\{\alpha_i\}) = \mathcal{D}^{-N}$ where $\mathcal{D}$ is

the dimension of the local Hilbert space on site i, then we would have $f(\{\alpha_i\}) = \Psi_{\{\mathcal{O}\alpha_i\}}\Psi_{\{\alpha_i\}}/\sum_{\{\alpha_i\}}|\Psi_{\{\alpha_i\}}|^2$. The problem is that in most cases the function $f(\{\alpha_i\})$ is sharply peaked around certain points in phase space so that most of the terms in the sum contribute very little to the expectation value. It is then not possible with a uniform probability distribution to sample enough terms that we reach a good approximation for the total sum in a reasonable amount of time.

The way around this is to use a technique known as importance sampling. Within the importance sampling scheme, configurations are sampled according to a probability distribution which is large in the same regions of the configuration space where the function $f(\{\alpha\})$ is sizable. For most cases which we care about, this means that configurations $\{\alpha_i\}$ are sampled according to the probability distribution $\mathcal{P}(\{\alpha_i\}) = |\Psi_{\{\alpha_i\}}|^2/\sum_{\{\alpha_i\}}|\Psi_{\{\alpha_i\}}|^2$.

The next step is then to generate random numbers according to this probability distribution. This is accomplished using Markov chains. Starting from a random configuration x_n, a new configuration x_{n+1} is generated according to some function $F(x_n, \xi_n)$ which depends only on the current configuration plus some random variable ξ_n,

$$x_{n+1} = F(x_n, \xi_n). \tag{A.5}$$

The so called 'Master equation' associated with the Markov chain tells us how the probability distribution $\mathcal{P}(\{\alpha\})$ evolves under the function F. We write this as

$$\mathcal{P}_{n+1}(x') = \sum_x \omega(x'|x)\mathcal{P}_n(x) \tag{A.6}$$

where $\omega(x|x')$ is the conditional probability or transition rate between the two con-

figuration. Given this, we can show that as long as a few conditions are satisfied, the probability distribution $\mathcal{P}_{n\to\infty}$ approaches an equilibrium probability distribution. Furthermore, by choosing the correct transition rate between configurations, we can make it so that this probability distribution is the same as our target probability distribution.

A sufficient condition to guarantee that P_n is an equilibrium probability distribution is that it satisfies the *detailed balance* condition

$$\omega(x'|x)\mathcal{P}_{eq}(x) = \omega(x|x')\mathcal{P}_{eq}(x'). \tag{A.7}$$

Furthermore, if the Markov process is *ergodic*, meaning that it is possible to visit all other states with nonzero probability in a finite number of steps, then it can be shown that the equilibrium probability distribution is unique.

These two conditions, of detailed balance and ergodicity, can be guaranteed using the so called *Metropolis algorithm*. In this algorithm, we propose single site updates to the configuration and accept these updates with probability

$$\omega(x'|x) = \min\left\{1, \frac{\mathcal{P}_{eq}(x')}{\mathcal{P}_{eq}(x)}\right\} \tag{A.8}$$

A.2 Studying Fermion Wave Functions

In order to apply the Monte Carlo algorithm to quantum wavefunctions, we would like to sample eigenstates in a local basis so that $P_{eq}(x)$ is the same as the probability distribution of the ground state wavefunction. Specifically, if we write the wavefunc-

tion like

$$|\Psi\rangle = \sum_i a_i \, |\{x^{(i)}\}\rangle \, , \tag{A.9}$$

then we would like to sample the configuration $|\{x^{(i)}\}\rangle$ with probability $|a_i^2|$.

To study fermionic systems, generally one starts from a free-fermion wavefunction

$$|\psi\rangle = \prod_k c_k^\dagger \, |0\rangle \tag{A.10}$$

where

$$c_k = \sum_{i=1}^{N} \sum_\alpha A_{k,i}^{(\alpha)} c_{i,\alpha}^\dagger \tag{A.11}$$

and $c_{i\alpha}^\dagger$ creates an electron on site i with quantum numbers α. Variational parameters can then be applied to this ansatz to transform it to an interacting wavefunction.

The most common examples is applying a Gutzwiller projection operator

$$\begin{aligned} |\Psi\rangle &= \mathcal{P} \, |\psi\rangle \\ &= \prod_i (1 - \gamma \, \hat{n}_{i\uparrow} \hat{n}_{i\downarrow}) \, |\psi\rangle \\ &= \prod_i (1 - \gamma \, \hat{n}_{i\uparrow} \hat{n}_{i\downarrow}) \prod_{k\sigma} c_{k,\sigma}^\dagger \, |0\rangle \, . \end{aligned} \tag{A.12}$$

where γ is a variational parameter. The effect of $\mathcal{P}$ is to reduce the probability amplitude of configurations with doubly occupied sites. When $\gamma = 1$, it is completely forbidden to have a doubly occupied site. If our lattice model contains one fermion per site, then this total projection transforms our free-fermion wavefunction to a spin-1/2 wavefunction.

As another example, consider the case where we add correlations between nearby electrons (in addition to the 'single body' correlations induced by the fermion minus sign). This can be achieved by using the so called 'Jastrow factors'. In this case we apply the operator $\mathcal{J}$ to the free-fermion wavefunction

$$\mathcal{J} = \exp\left[\sum_{ij} v_{ij}\hat{n}_i\hat{n}_j\right]|\psi\rangle = \mathcal{J}\,|\psi\rangle \tag{A.13}$$

where the terms v_{ij} are variational parameters.

In both of the above cases, one needs to write the free-fermion wavefunction in real-space in order to apply the operators $\mathcal{P}_G$ and $\mathcal{J}$. Consider the case of free spinful fermions on a lattice. For electron systems, a good variational ansatz is generally a free-fermion wavefunction.

This free-fermion wavefunction can be written in a local basis as a single Slater determinant

$$\begin{aligned} |\psi\rangle &= \sum_{\{x\}}\sum_{\{y\}} \det(A)\,|\{x_1, x_2, \ldots, x_n\}\rangle \\ &= \sum_{\{x\}}\sum_{\{y\}} \begin{vmatrix} A_{x_1,1} & A_{x_1,2} & \ldots & A_{x_1,N} \\ A_{x_2,1} & A_{x_2,2} & \ldots & A_{x_2,N} \\ \vdots & \vdots & \ddots & \vdots \\ A_{x_N,1} & A_{x_N,2} & \ldots & A_{x_N,N} \end{vmatrix} |\{x_1, x_2, \ldots, x_n\}\rangle\,. \end{aligned} \tag{A.14}$$

where N_e is the number of electrons and $|\{x_n\}\rangle = \prod_i c^\dagger_{x_i}|0\rangle$ is the basis state where electrons are localized at the lattice positions given by the set $\{x_n\}$. We can absorb the internal degree of freedom $\alpha \in \{\alpha_1, \ldots \alpha_m\}$ into the position label x_i by letting n range from 1 to mN. The probability amplitude of any given configuration $\{x_n\}$ is

therefore $|\det(A_{x_i,j})|^2$.

The VMC algorithm in this case then starts from a random initial configuration $|\{x^{(0)}\}\rangle$, and proposes updates by moving a single electron from site x_i to x_j. The transition rate of this process is given by the ratio of the two probability amplitudes

$$\omega(x^{(n)}|x^{(n+1)}) = \frac{|\det[A^{(n)})]|^2}{|\det[A^{(n+1)}]|^2}. \tag{A.15}$$

Once we are sure we are sampling configurations with the equilibrium probability distribution, we can calculate observables of our wavefunction.

For diagonal operators $\mathcal{O}_{i,i}$, the expectation value can be written as:

$$\langle \mathcal{O}_{diag} \rangle = \frac{\sum_n |\det[A^{(n)}]|^2 \langle \{x^{(n)}\}| \mathcal{O}_{diag} |\{x^{(n)}\}\rangle}{\sum_n |\det[A^{(n)}]|^2 \langle \{x^{(n)}\}| \{x^{(n)}\}\rangle} \tag{A.16}$$

We sample the basis states according to the probability distribution

$$\mathcal{P}_{eq}(x^{(n)}) = \frac{|\det[A^{(n)}]|^2}{\sum_n |\det[A^{(n)}]|^2}. \tag{A.17}$$

Therefore, according to Eq. A.4, within our VMC simulation we can estimate the observable $\langle \mathcal{O}_{diag} \rangle$ by averaging over N samples of our configuration

$$\langle O_{diag} \rangle \approx \frac{1}{N} \sum_n \langle x^{(n)}| \mathcal{O}_{diag} |x^{(n)}\rangle = \frac{1}{N} \sum_n \mathcal{O}_{x^{(n)},x^{(n)}}, \tag{A.18}$$

where $\mathcal{O}_{m,n} = \langle x^{(m)}| \mathcal{O} |x^{(n)}\rangle$.

Using the same sampling scheme, we can also calculate the expectation value of observables which are off-diagonal operators in our local basis. An off-diagonal operator will in general send the state $|x\rangle$ to the new state $|x'\rangle$. Therefore, to calculate

the expectation value of such an off-diagonal operator $\mathcal{O}_{off}$ we need to calculate the expectation value

$$\begin{aligned}\langle \mathcal{O}_{off} \rangle &= \frac{\sum_n \sum_m \det[A^{(m)}]^* \det[A^{(n)}] \langle \{x^{(m)}\} | \mathcal{O}_{off} | \{x^{(n)}\} \rangle}{\sum_n |\det[A^{(n)}]|^2 \langle \{x^{(n)}\} | \{x^{(n)}\} \rangle} \\ &= \mathcal{P}(x^{(n)}) \sum_m \frac{\det[A^{(m)}]^*}{\det[A^{(n)}]^*} \mathcal{O}_{m,n}. \end{aligned} \tag{A.19}$$

In general we can write the off-diagonal operator as a sum over creation/annihilation operators in our local basis

$$\mathcal{O} = \sum_{I_1,\ldots,I_n} \sum_{J_1,\ldots,J_n} \mathcal{O}_{I_1,\ldots,I_n;J_1,\ldots,J_n} d^\dagger_{I_1} d_{J_1} \ldots d^\dagger_{I_n} d_{J_n}, \tag{A.20}$$

so that the operator $\mathcal{O}$ sends the state $|x^{(i)}\rangle$ to at most n other states $|x^{(j)}\rangle$.

In order to work with the interacting Gutzwiller or Jastrow wavefunctions described above, we only need to modify the probability amplitudes. However, this is simple once we write the wavefunction in real space, as the basis states $|\{x\}\rangle$ are eigenstates of both the $\mathcal{P}_G$ and $\mathcal{J}$. Therefore, applying these operators to $|\psi\rangle$ amounts to calculating the eigenvalues of the operators $\mathcal{O}|\{x\}\rangle = c_x |\{x\}\rangle$ and modifying the amplitudes above as $\det[A^{(x)}] \to c_x \det[A^{(x)}]$.

Fast Computation of the Determinant

In general, when studying a lattice with N sites, one needs to perform $\mathcal{O}(N)$ Monte Carlo configuration updates between sampling two independent configurations. Measuring the expectation value of an operator which is extensive in system size, such as the Hamiltonian, also takes $\mathcal{O}(N)$ steps. However, calculating the determinant

$\det[A]$ for an $N \times N$ matrix A takes time $\mathcal{O}(N^3)$. Therefore, when performing variational Monte Carlo on fermionic wavefunctions, calculating the determinant is by far the slowest part of the algorithm.

Luckily, one does not need to calculate the full determinant at each step whenever $A^{(n)} \to A^{(n+1)}$. Instead, there exists a trick for finding $\det[A^{(n+1)}]$ using only $A^{(n)}$ and $\det[A^{(n)}]$, as long as $\{x^{(n+1)}\}$ can be created from $\{x^{(n)}\}$ by hopping only a few electrons.

The **matrix determinant lemma** states that for a matrix $\mathbf{A}$ and vectors $\mathbf{u}$ and $\mathbf{v}$, the determinant of the matrix $\mathbf{A} + \mathbf{u}\mathbf{v}^\mathbf{T}$ is given by the expression

$$\det(\mathbf{A} + \mathbf{u}\mathbf{v}^\mathbf{T}) = (\mathbf{1} + \mathbf{v}^\mathbf{T}\mathbf{A}^{-\mathbf{1}}\mathbf{U}) \det(\mathbf{A}). \tag{A.21}$$

The vectors $\mathbf{u}$ and $\mathbf{v}$ can be chosen so that $\mathbf{B} = \mathbf{A} + \mathbf{u}\mathbf{v}^\mathbf{T}$ is made by replacing a single row or column of $\mathbf{A}$. This is exactly what one needs to update the Slater determinant after hopping a single electron between two sites. Therefore, if one knows $\det(\mathbf{A})$ and $\mathbf{A}^{-\mathbf{1}}$, one can calculate the updated Slater determinant in $\mathcal{O}(N^2)$ operations.

However, calculating the matrix inverse $\mathbf{A}^{-\mathbf{1}}$ in general takes $\mathcal{O}(N^3)$ operations. Fortunately, the **Sherman-Morrison formula** tells us how to calculate $\mathbf{B}^{-\mathbf{1}}$ from $\mathbf{A}^{-\mathbf{1}}$ again using only $\mathcal{O}(N^2)$ operations. The formula is

$$(\mathbf{A} + \mathbf{u}\mathbf{v}^\mathbf{T})^{-\mathbf{1}} = \mathbf{A}^{-\mathbf{1}} - \frac{\mathbf{A}^{-\mathbf{1}}\mathbf{u}\mathbf{v}^\mathbf{T}\mathbf{A}^{-\mathbf{1}}}{\mathbf{1} + \mathbf{v}^\mathbf{T}\mathbf{A}^{-\mathbf{1}}\mathbf{u}}. \tag{A.22}$$

Since the calculation of the determinant is the bottleneck of the VMC algorithm when working with fermionic wavefunctions, this method of calculating the determinant gives an overall $\mathcal{O}(N)$ speedup, and is therefore a necessary component in any practical VMC implementation.

A.3 An Implementation of the VMC Algorithm

We now have all the tools to sample a fermionic wavefunction numerically using VMC.

1. Choose a starting configuration of electrons $|\{x^{(0)}\}\rangle$. Fill in the Slater matrix $\mathbf{A}$ using the coefficients of the single particle orbitals $A_{x_i,k}$. Create a vector $\mathbf{a}$ to keep track of which row of $\mathbf{A}$ refers to which occupied sites x_i.

2. Make sure that the initial configuration $\{x^{(0)}\}$ is not singular. That is, ensure that $\langle x\,|\Psi\rangle \neq 0$. Calculate the inverse matrix $\mathbf{A^{-1}}$. The value of the determinant $\det A$ is not needed, as we only ever need to make use of the ratio of two Slater determinants.

3. Propose a new configuration $|x'\rangle$ by moving one or a few electrons. Refer to our vector $\mathbf{a}$ to update the proper row of the matrix $\mathbf{A}$. Calculate the ratio of determinants of the old and new matrices $\mathbf{A}$.

4. Accept or reject the proposed configuration according to the Metropolis condition, using the ratio of probability amplitudes given by the ratio of determinants multiplied by a factor which comes from the Gutzwiller projector $\mathcal{P}_G$ and/or the Jastrow factor $\mathcal{J}$. If the update is accepted, calculate the new inverse matrix $\mathbf{A^{-1}}$.

5. Every T updates, measure the observables using the techniques described above. Choose T so that two configurations connected by T steps are uncorrelated. In general $T \sim \mathcal{O}\big(N\big)$

A.4 More Advanced Techniques

We have so far described a tractable method of working with many body fermionic wavefunctions. The final step of VMC is then to choose the variational parameters so as to minimize the variational energy. If the trial wavefunction contains only a few variational parameters (i.e. one or two), the best method for finding the parameters which give the lowest variational energies may be to map out the energy over the entire phase space of variational parameters. This quickly becomes infeasible as the number of variational parameters increases. Instead, more sophisticated methods for optimizing a large number of variational parameters must be used. Most of the popular methods make use of some form of stochastic gradient descent.

Calculating Energy Derivatives in VMC

The naive approach to gradient descent, directly calculating the discrete energy gradient by running the VMC algorithm for $\{\alpha\}$ and $\{\alpha + \delta\alpha\}$, turns out to be much too slow to be of practical use. Instead, the proper approach is to calculate some estimator of the gradient of the energy with respect to the individual variational parameters. This gradient can then be measured directly in the VMC simulation.

This turns out to be fairly straightforward when optimizing over variational parameters of diagonal operators. Consider, for example, variational parameters of the form of $\mathcal{J}$.

$$\begin{aligned} |\Psi\rangle &= \mathcal{J}\,|\psi\rangle \\ &= \exp\left[\sum_k \alpha_k \hat{\mathcal{O}}_k\right]|\psi\rangle \\ \Rightarrow \frac{\partial\,|\Psi\rangle}{\partial\alpha_k} &= \left(\hat{\mathcal{O}}_k\right)\mathcal{J}\,|\psi\rangle = \hat{\mathcal{O}}_k\,|\Psi\rangle\,. \end{aligned} \tag{A.23}$$

Then we have

$$\begin{aligned} \frac{\partial}{\partial\alpha_k}\langle H\rangle &= \frac{1}{\langle\Psi|\,\Psi\rangle}\left(\frac{\partial\,\langle\Psi|}{\partial\alpha_k}H\,|\Psi\rangle + \langle\Psi|\,H\frac{\partial\,|\Psi\rangle}{\partial\alpha_k}\right) \\ &\quad -\frac{1}{\langle\Psi|\,\Psi|\rangle^2}\left(\frac{\partial\,\langle\Psi|}{\partial\alpha_k}\,|\Psi\rangle + \langle\Psi|\,\frac{\partial\,|\Psi\rangle}{\partial\alpha_k}\right) \\ &= \langle\mathcal{O}_k H\rangle + \langle H\mathcal{O}_k\rangle - 2\langle H\rangle\langle\mathcal{O}_k\rangle \\ &= 2\,\mathrm{Re}\left[\langle\mathcal{O}_k H\rangle - \langle\mathcal{O}_k\rangle\langle H\rangle\right]. \end{aligned} \tag{A.24}$$

Derivatives of the free-fermion ansatz can also be calculated in the following way. Consider the effect of perturbing the free-fermion Hamiltonian by letting $\mathcal{H}_{mf} \to \mathcal{H}_{mf} + \alpha\mathcal{V}$ where $\mathcal{V} = \sum_{ij} V_{ij} c_i^\dagger c_j$. To lowest order in perturbation theory, the change in the non-interacting wavefunction is

$$|\psi(\alpha)\rangle = |\psi\rangle - \frac{\alpha}{\mathcal{H}_{mf} - E_0}(\mathcal{V} - \langle\mathcal{V}\rangle_0)\,|\psi\rangle + \mathcal{O}\big(\alpha^2\big). \tag{A.25}$$

We can express $\mathcal{V}$ in terms of the fermion operators which diagonalize $\mathcal{H}_{mf}$. That is $c_k = \sum_i A_{i,k} c_i^\dagger$ diagonalizes $\mathcal{H}_{mf}$, and we can write $\mathcal{V} = \sum_{k,k'} \tilde{\lambda}_{k,k'} c_k^\dagger c_{k'}$. We can

then rewrite $|\psi(\alpha)\rangle$ as

$$|\psi(\alpha)\rangle = |\psi\rangle - \alpha \sum_{k \neq k'} \frac{\lambda_{kk'}}{\epsilon_k - \epsilon_{k'}} c_k^\dagger c_{k'} |\psi\rangle . \tag{A.26}$$

Therefore, to linear order in α, we can write

$$\begin{aligned} |\Psi(\alpha)\rangle &= e^{\alpha \hat{\mathcal{O}}} |\psi\rangle \\ \text{with} \qquad \hat{\mathcal{O}} &= \frac{-\lambda_{kk'}}{\epsilon_k - \epsilon_{k'}} c_k^\dagger c_{k'}. \end{aligned} \tag{A.27}$$

Once the free-fermion wavefunction is written in this exponentiated form, we can calculate energy derivatives in the same way as above.

Performing Gradient Descent

We can now perform gradient descent by updating our variational parameters $\alpha_k \to \alpha_k + \delta\alpha_k$, where

$$\delta\alpha_k = \Delta f_k \tag{A.28}$$

$$f_k = -\frac{\partial E}{\partial \alpha_k}, \tag{A.29}$$

so that $\Delta E = -\sum_k f_k \delta\alpha_k + \mathcal{O}(\delta\alpha_k^2)$.

We can define a metric in the space of variational wavefunctions by defining

$$\delta s^2 = \sum_k \delta\alpha_k^2. \tag{A.30}$$

It is then reasonable to optimize the change in variational energy subject to the

constraint that the total change in the wavefunction as measured by δs^2 is a small constant. We can do this by optimizing the quadratic form

$$\Delta E + \mu \delta s^2 = \sum_k (-f_k \delta\alpha_k + \mu \delta\alpha_k^2) \tag{A.31}$$

which is minimized by choosing

$$\delta\alpha_k = \frac{f_k}{2\mu}. \tag{A.32}$$

Therefore by choosing α_k, the change in energy is given by $\Delta E = -\frac{1}{2\mu}\sum_k f_k^2 < 0$.

The Stochastic Reconfiguration Algorithm

Changes to different variational parameters affect the wavefunction in different ways. A small change in one parameter may have a large effect on the wavefunction, while a similar change in another parameter may barely affect our simulation. On top of this, the changes caused by all the variational parameters are correlated with each other in complicated ways. We can define the metric δs^2 to measure the change in the variational wavefunction as a function of the variational parameters in a way which takes these facts into account by defining

$$\delta s^2 \;=\; ||\,|\psi(\alpha+\delta\alpha)\rangle - |\psi(\alpha)\rangle\,||. \tag{A.33}$$

The normalized wavefunction $|\psi(\alpha+\delta\alpha)\rangle$ to linear order in $\delta\alpha_k$ can be written as

$$\begin{aligned} |\psi(\alpha+\delta\alpha)\rangle &= 1+\sum_k (\mathcal{O}_k - \langle\mathcal{O}_k\rangle)\,|\psi\rangle \\ &= 1+\sum_k \delta\alpha_k \bar{\mathcal{O}}_k\,|\psi\rangle\,. \end{aligned} \tag{A.34}$$

With a little algebra we can write the metric as

$$\delta s^2 = \sum_{k,k'} \langle\psi|\,(1+\delta\alpha_k\bar{\mathcal{O}}_k)(1+\delta\alpha_{k'}\bar{\mathcal{O}}_{k'})\,|\psi\rangle \tag{A.35}$$

$$\begin{aligned} &= \sum_{k,k'} 2\mathrm{Re}[\langle\bar{\mathcal{O}}_k\bar{\mathcal{O}}_{k'}\rangle]\delta\alpha_k\delta\alpha_{k'} \\ &= \sum_{k,k'} S_{k,k'}\delta\alpha_k\delta\alpha_{k'}. \end{aligned} \tag{A.36}$$

This metric measures distance in the space of variational wavefunctions in a way which takes into account the correlations between the different variational parameters. With this new metric, we can solve for the optimal values of $\delta\alpha_k$ which minimizes the energy subject to the constraint that we only change the wavefunction by an amount governed by δs^2.

Minimizing $\Delta E + \mu\delta_s^2$ now gives

$$\delta\alpha_k = \frac{1}{2\mu}\mathbf{S}^{-1}_{k,k'}\cdot\mathbf{f_k}. \tag{A.37}$$

This method can be generalized by including second order derivatives of the energy. This is similar to implementations of Newton's method in higher dimensions which is based on the inversion of the Hessian matrix. Calculating the Hessian for an arbitrary operator can be computationally expensive. Instead, we can use an approximation where we expand the wavefunction only to linear order in $\delta\alpha_k$. We then

calculate the Hessian within this approximation. The algorithm proceeds by finding the paramter updates $\delta\alpha$ which solve the generalized eigenvalue equation

$$\sum_{k'=0} H_{k,k'}\delta\alpha_{k'} = \lambda \sum_{k'=0} S_{k,k'}\delta\alpha_{k'} \tag{A.38}$$

where

$$H_{k,k'} = \langle \bar{\mathcal{O}}_k H \bar{\mathcal{O}}_{k'} \rangle \tag{A.39}$$

and where $\mathcal{O}_0 = \mathbb{I}$ is the identity matrix and $\delta\alpha_0^2 = 1 - \sum_{k=1}^{M} \delta\alpha_k^2$ gives the overlap of the new wavefunction with the original wavefunction $|\psi(\alpha)\rangle$.

Choosing the eigenvector with largest $\delta\alpha_0$ is often useful to give a smooth convergence to the lowest energy state. Using this second order gradient descent method can greatly speed up the optimization procedure. This then allows for the use of up to hundreds of variational parameters within the VMC algorithm.

Bibliography

[1] J. Iaconis, C. Liu, G. B. Halász, and L. Balents, *Spin Liquid versus Spin Orbit Coupling on the Triangular Lattice*, *SciPost Phys.* **4** (2018) 003.

[2] J. Iaconis, H. Ishizuka, D. N. Sheng, and L. Balents, *Kinetic magnetism at the interface between mott and band insulators*, *Phys. Rev. B* **93** (Apr, 2016) 155144.

[3] J. Iaconis and L. Balents, *Many-body effects in topological kondo insulators*, *Phys. Rev. B* **91** (Jun, 2015) 245127.

[4] R. Shankar, *Renormalization-group approach to interacting fermions*, *Rev. Mod. Phys.* **66** (Jan, 1994) 129–192.

[5] J. Polchinski, *Effective Field Theory and the Fermi Surface*, *ArXiv e-prints* (Oct., 1992) [hep-th/9210046].

[6] L. Landau and E. Lifshitz, *Statistical Physics*. No. v. 5. Elsevier Science, 2013.

[7] V. Ginzburg and L. Landau, *On the theory of superconductivity*, *J. Exp. Theor. Phys.* **20**.

[8] X. Wen, *Quantum Field Theory of Many-Body Systems: From the Origin of Sound to an Origin of Light and Electrons*. Oxford Graduate Texts. OUP Oxford, 2004.

[9] M. Levin and X.-G. Wen, *Colloquium: Photons and electrons as emergent phenomena*, *Rev. Mod. Phys.* **77** (Sep, 2005) 871–879.

[10] R. B. Laughlin, *The cup of the hand*, *Science* **303** (2004), no. 5663 1475–1477.

[11] G. Volovik, *The Universe in a Helium Droplet*. International Series of Monographs on Physics. OUP Oxford, 2009.

[12] X.-G. Wen, *Quantum orders and symmetric spin liquids*, *Phys. Rev. B* **65** (Apr, 2002) 165113.

[13] L. Balents, *Spin liquids in frustrated magnets*, *Nature* **464** (March, 2010) 199–208.

[14] L. Savary and L. Balents, *Quantum spin liquids: a review*, *Rep. Prog. Phys.* **80** (2017), no. 1 016502.

[15] X.-G. Wen, *Quantum order: a quantum entanglement of many particles*, *Physics Letters A* **300** (2002), no. 2 175 – 181.

[16] M. Levin and X.-G. Wen, *Detecting topological order in a ground state wave function*, *Phys. Rev. Lett.* **96** (Mar, 2006) 110405.

[17] A. Kitaev and J. Preskill, *Topological entanglement entropy*, *Phys. Rev. Lett.* **96** (Mar, 2006) 110404.

[18] C. Mudry and E. Fradkin, *Separation of spin and charge quantum numbers in strongly correlated systems*, *Phys. Rev. B* **49** (Feb, 1994) 5200–5219.

[19] X. G. Wen, *Mean-field theory of spin-liquid states with finite energy gap and topological orders*, *Phys. Rev. B* **44** (Aug, 1991) 2664–2672.

[20] M. Levin and T. Senthil, *Deconfined quantum criticality and néel order via dimer disorder*, *Phys. Rev. B* **70** (Dec, 2004) 220403.

[21] T. Senthil and M. P. A. Fisher, *Z_2 gauge theory of electron fractionalization in strongly correlated systems*, *Phys. Rev. B* **62** (Sep, 2000) 7850–7881.

[22] T. Senthil and M. P. A. Fisher, *Fractionalization in the cuprates: Detecting the topological order*, *Phys. Rev. Lett.* **86** (Jan, 2001) 292–295.

[23] J. B. Kogut, *An introduction to lattice gauge theory and spin systems*, *Rev. Mod. Phys.* **51** (Oct, 1979) 659–713.

[24] Y. Zhou, K. Kanoda, and T.-K. Ng, *Quantum spin liquid states*, *Rev. Mod. Phys.* **89** (Apr, 2017) 025003.

[25] S. Elitzur, *Impossibility of spontaneously breaking local symmetries*, *Phys. Rev. D* **12** (Dec, 1975) 3978–3982.

[26] A. Polyakov, *Quark confinement and topology of gauge theories*, *Nuclear Physics B* **120** (1977), no. 3 429 – 458.

[27] A. Kitaev, *Fault-tolerant quantum computation by anyons*, *Annals of Physics* **303** (2003), no. 1 2 – 30.

[28] M. B. Hastings and X.-G. Wen, *Quasiadiabatic continuation of quantum states: The stability of topological ground-state degeneracy and emergent gauge invariance*, *Phys. Rev. B* **72** (Jul, 2005) 045141.

[29] N. Read and S. Sachdev, *Large- N expansion for frustrated quantum antiferromagnets*, *Phys. Rev. Lett.* **66** (Apr, 1991) 1773–1776.

[30] A. E. Ruckenstein, P. J. Hirschfeld, and J. Appel, *Mean-field theory of high-T_c superconductivity: The superexchange mechanism*, *Phys. Rev. B* **36** (Jul, 1987) 857–860.

[31] G. Baskaran, Z. Zou, and P. Anderson, *The resonating valence bond state and high-tc superconductivity a mean field theory*, *Solid State Communications* **63** (1987), no. 11 973 – 976.

[32] E. Dagotto, E. Fradkin, and A. Moreo, *Su(2) gauge invariance and order parameters in strongly coupled electronic systems*, *Phys. Rev. B* **38** (Aug, 1988) 2926–2929.

[33] I. Affleck, Z. Zou, T. Hsu, and P. W. Anderson, *Su(2) gauge symmetry of the large-u limit of the hubbard model*, *Phys. Rev. B* **38** (Jul, 1988) 745–747.

[34] G. Baskaran and P. W. Anderson, *Gauge theory of high-temperature superconductors and strongly correlated fermi systems*, *Phys. Rev. B* **37** (Jan, 1988) 580–583.

[35] Y. Ran, M. Hermele, P. A. Lee, and X.-G. Wen, *Projected-wave-function study of the spin-1/2 heisenberg model on the kagomé lattice*, *Phys. Rev. Lett.* **98** (Mar, 2007) 117205.

[36] N. Nagaosa and P. A. Lee, *Normal-state properties of the uniform resonating-valence-bond state*, *Phys. Rev. Lett.* **64** (May, 1990) 2450–2453.

[37] P. A. Lee and N. Nagaosa, *Gauge theory of the normal state of high-t_c superconductors*, *Phys. Rev. B* **46** (Sep, 1992) 5621–5639.

[38] J. Polchinski, *Low-energy dynamics of the spinon-gauge system*, *Nuclear Physics B* **422** (1994), no. 3 617 – 633.

[39] J. Reuther, S.-P. Lee, and J. Alicea, *Classification of spin liquids on the square lattice with strong spin-orbit coupling*, *Phys. Rev. B* **90** (Nov, 2014) 174417.

[40] B. Huang, Y. B. Kim, and Y.-M. Lu, *Interplay of nonsymmorphic symmetry and spin-orbit coupling in hyperkagome spin liquids: Applications to* $\mathrm{na_4ir_3o_8}$, *Phys. Rev. B* **95** (Feb, 2017) 054404.

[41] Y.-Z. You, I. Kimchi, and A. Vishwanath, *Doping a spin-orbit mott insulator: Topological superconductivity from the kitaev-heisenberg model and possible application to $(na_2/li_2)iro_3$*, *Phys. Rev. B* **86** (Aug, 2012) 085145.

[42] P. Anderson, *Resonating valence bonds: A new kind of insulator?*, *Materials Research Bulletin* **8** (1973), no. 2 153 – 160.

[43] S. R. White and A. L. Chernyshev, *Neél order in square and triangular lattice heisenberg models*, *Phys. Rev. Lett.* **99** (Sep, 2007) 127004.

[44] O. I. Motrunich, *Variational study of triangular lattice spin-1/2 model with ring exchanges and spin liquid state in $\kappa-(\mathrm{ET})_2\mathrm{Cu}_2(\mathrm{CN})_3$*, *Phys. Rev. B* **72** (Jul, 2005) 045105.

[45] D. N. Sheng, O. I. Motrunich, and M. P. A. Fisher, *Spin bose-metal phase in a spin-$\frac{1}{2}$ model with ring exchange on a two-leg triangular strip*, *Phys. Rev. B* **79** (May, 2009) 205112.

[46] Z. Zhu and S. R. White, *Spin liquid phase of the $S = \frac{1}{2}$ $J_1 - J_2$ Heisenberg model on the triangular lattice*, *Phys. Rev. B* **92** (Jul, 2015) 041105.

[47] W.-J. Hu, S.-S. Gong, W. Zhu, and D. N. Sheng, *Competing spin-liquid states in the spin-$\frac{1}{2}$ Heisenberg model on the triangular lattice*, *Phys. Rev. B* **92** (Oct, 2015) 140403.

[48] S. Florens and A. Georges, *Slave-rotor mean-field theories of strongly correlated systems and the mott transition in finite dimensions*, *Phys. Rev. B* **70** (Jul, 2004) 035114.

[49] S.-S. Lee and P. A. Lee, *U(1) gauge theory of the hubbard model: Spin liquid states and possible application to $\kappa-(\mathrm{BEDT-TTF})_2\mathrm{cu}_2(\mathrm{CN})_3$*, *Phys. Rev. Lett.* **95** (Jul, 2005) 036403.

[50] R. V. Mishmash, I. González, R. G. Melko, O. I. Motrunich, and M. P. A. Fisher, *Continuous mott transition between a metal and a quantum spin liquid*, *Phys. Rev. B* **91** (Jun, 2015) 235140.

[51] G. Jackeli and G. Khaliullin, *Mott Insulators in the Strong Spin-Orbit Coupling Limit: From Heisenberg to a Quantum Compass and Kitaev Models*, *Phys. Rev. Lett.* **102** (Jan, 2009) 017205.

[52] A. Kitaev, *Anyons in an exactly solved model and beyond*, *Ann. Phys.* **321** (2006), no. 1 2.

[53] J. c. v. Chaloupka, G. Jackeli, and G. Khaliullin, *Kitaev-heisenberg model on a honeycomb lattice: Possible exotic phases in iridium oxides* $A_2\mathrm{iro}_3$, *Phys. Rev. Lett.* **105** (Jul, 2010) 027204.

[54] K. W. Plumb, J. P. Clancy, L. J. Sandilands, V. V. Shankar, Y. F. Hu, K. S. Burch, H.-Y. Kee, and Y.-J. Kim, $\alpha - \mathrm{rucl}_3$*: A spin-orbit assisted mott insulator on a honeycomb lattice*, *Phys. Rev. B* **90** (Jul, 2014) 041112.

[55] X. Liu, T. Berlijn, W.-G. Yin, W. Ku, A. Tsvelik, Y.-J. Kim, H. Gretarsson, Y. Singh, P. Gegenwart, and J. P. Hill, *Long-range magnetic ordering in* na_2iro_3, *Phys. Rev. B* **83** (Jun, 2011) 220403.

[56] Y. Shen, Y.-D. Li, H. Wo, Y. Li, S. Shen, B. Pan, Q. Wang, H. C. Walker, P. Steffens, M. Boehm, Y. Hao, D. L. Quintero-Castro, L. W. Harriger, M. D. Frontzek, L. Hao, S. Meng, Q. Zhang, G. Chen, and J. Zhao, *Evidence for a spinon Fermi surface in a triangular-lattice quantum-spin-liquid candidate*, *Nature* **540** (12, 2016) 559–562.

[57] J. A. M. Paddison, M. Daum, Z. Dun, G. Ehlers, Y. Liu, M. B. Stone, H. Zhou, and M. Mourigal, *Continuous excitations of the triangular-lattice quantum spin liquid YbMgGaO4*, *Nat. Phys.* **13** (02, 2017) 117–122.

[58] Y. Li, D. Adroja, R. I. Bewley, D. Voneshen, A. A. Tsirlin, P. Gegenwart, and Q. Zhang, *Crystalline electric-field randomness in the triangular lattice spin-liquid* $\mathrm{ybmggao}_4$, *Phys. Rev. Lett.* **118** (Mar, 2017) 107202.

[59] Z. Zhu, P. A. Maksimov, S. R. White, and A. L. Chernyshev, *Disorder-induced mimicry of a spin liquid in* $\mathrm{ybmggao}_4$, *Phys. Rev. Lett.* **119** (Oct, 2017) 157201.

[60] I. Kimchi, A. Nahum, and T. Senthil, *Valence Bonds in Random Quantum Magnets: Theory and Application to YbMgGaO4*, *ArXiv e-prints* (Oct., 2017) [arXiv:1710.0686].

[61] S. Stemmer and A. J. Millis, *Quantum confinement in oxide quantum wells*, *MRS Bulletin* **38** (12, 2013) 1032–1039.

[62] J. Coey, Ariando, and W. Pickett, *Magnetism at the edge: New phenomena at oxide interfaces*, *MRS Bulletin* **38** (2013), no. 12 10401047.

[63] W. A. Harrison, E. A. Kraut, J. R. Waldrop, and R. W. Grant, *Polar heterojunction interfaces*, *Phys. Rev. B* **18** (Oct, 1978) 4402–4410.

[64] A. Ohtomo and H. Y. Hwang, *A high-mobility electron gas at the laalo3/srtio3 heterointerface*, *Nature* **427** (01, 2004) 423–426.

[65] P. Moetakef, T. A. Cain, D. G. Ouellette, J. Y. Zhang, D. O. Klenov, A. Janotti, C. G. Van de Walle, S. Rajan, S. J. Allen, and S. Stemmer, *Electrostatic carrier doping of gdtio3/srtio3 interfaces*, *Applied Physics Letters* **99** (2011), no. 23 –.

[66] T. A. Cain, S. Lee, P. Moetakef, L. Balents, S. Stemmer, and S. James Allen, *Seebeck coefficient of a quantum confined, high-electron-density electron gas in srtio3*, *Applied Physics Letters* **100** (2012), no. 16 –.

[67] G. Conti, A. M. Kaiser, A. X. Gray, S. Nemk, G. K. Plsson, J. Son, P. Moetakef, A. Janotti, L. Bjaalie, C. S. Conlon, D. Eiteneer, A. A. Greer, A. Keqi, A. Rattanachata, A. Y. Saw, A. Bostwick, W. C. Stolte, A. Gloskovskii, W. Drube, S. Ueda, M. Kobata, K. Kobayashi, C. G. Van de Walle, S. Stemmer, C. M. Schneider, and C. S. Fadley, *Band offsets in complex-oxide thin films and heterostructures of srtio3/lanio3 and srtio3/gdtio3 by soft and hard x-ray photoelectron spectroscopy*, *Journal of Applied Physics* **113** (2013), no. 14 –.

[68] P. Moetakef, J. R. Williams, D. G. Ouellette, A. P. Kajdos, D. Goldhaber-Gordon, S. J. Allen, and S. Stemmer, *Carrier-controlled ferromagnetism in* srtio_3, *Phys. Rev. X* **2** (Jun, 2012) 021014.

[69] C. A. Jackson and S. Stemmer, *Interface-induced magnetism in perovskite quantum wells*, *Phys. Rev. B* **88** (Nov, 2013) 180403.

[70] Y. Nagaoka, *Ferromagnetism in a narrow, almost half-filled s band*, *Phys. Rev.* **147** (Jul, 1966) 392–405.

[71] L. Liu, H. Yao, E. Berg, S. R. White, and S. A. Kivelson, *Phases of the infinite u hubbard model on square lattices*, *Phys. Rev. Lett.* **108** (Mar, 2012) 126406.

[72] H. Tasaki, *From nagaoka's ferromagnetism to flat-band ferromagnetism and beyondan introduction to ferromagnetism in the hubbard model*, *Progress of Theoretical Physics* **99** (1998), no. 4 489–548.

[73] P. Coleman, *Heavy Fermions: electrons at the edge of magnetism*, *eprint arXiv:cond-mat/0612006* (Nov., 2006) [cond-mat/0612006].

[74] P. W. Anderson, *A poor man's derivation of scaling laws for the kondo problem*, *Journal of Physics C: Solid State Physics* **3** (1970), no. 12 2436.

[75] S. Doniach, *The kondo lattice and weak antiferromagnetism*, *Physica B+C* **91** (1977), no. 0 231 – 234.

[76] N. Read, D. M. Newns, and S. Doniach, *Stability of the kondo lattice in the large-n limit*, *Phys. Rev. B* **30** (Oct, 1984) 3841–3844.

[77] T. Senthil, S. Sachdev, and M. Vojta, *Fractionalized fermi liquids*, *Phys. Rev. Lett.* **90** (May, 2003) 216403.

[78] T. Senthil, M. Vojta, and S. Sachdev, *Weak magnetism and non-fermi liquids near heavy-fermion critical points*, *Phys. Rev. B* **69** (Jan, 2004) 035111.

[79] M. Dzero, K. Sun, P. Coleman, and V. Galitski, *Theory of topological kondo insulators*, *Phys. Rev. B* **85** (Jan, 2012) 045130.

[80] M. Dzero, K. Sun, V. Galitski, and P. Coleman, *Topological kondo insulators*, *Phys. Rev. Lett.* **104** (Mar, 2010) 106408.

[81] M. Z. Hasan and C. L. Kane, *Colloquium: Topological insulators*, *Rev. Mod. Phys.* **82** (Nov, 2010) 3045–3067.

[82] J. E. Moore, *The birth of topological insulators*, *Nature* **464** (03, 2010) 194 EP –.

[83] C. L. Kane and E. J. Mele, *Quantum spin hall effect in graphene*, *Phys. Rev. Lett.* **95** (Nov, 2005) 226801.

[84] C. L. Kane and E. J. Mele, *Z_2 topological order and the quantum spin hall effect*, *Phys. Rev. Lett.* **95** (Sep, 2005) 146802.

[85] L. Fu and C. L. Kane, *Topological insulators with inversion symmetry*, *Phys. Rev. B* **76** (Jul, 2007) 045302.

[86] F. D. M. Haldane, *Model for a quantum hall effect without landau levels: Condensed-matter realization of the "parity anomaly"*, *Phys. Rev. Lett.* **61** (Oct, 1988) 2015–2018.

[87] J. E. Moore and L. Balents, *Topological invariants of time-reversal-invariant band structures*, *Phys. Rev. B* **75** (Mar, 2007) 121306.

[88] B. A. Bernevig, T. L. Hughes, and S.-C. Zhang, *Quantum spin hall effect and topological phase transition in hgte quantum wells*, *Science* **314** (2006), no. 5806 1757–1761.

[89] L. Fu, C. L. Kane, and E. J. Mele, *Topological insulators in three dimensions*, *Phys. Rev. Lett.* **98** (Mar, 2007) 106803.

[90] M. König, S. Wiedmann, C. Brüne, A. Roth, H. Buhmann, L. W. Molenkamp, X.-L. Qi, and S.-C. Zhang, *Quantum spin hall insulator state in hgte quantum wells*, *Science* **318** (2007), no. 5851 766–770.

[91] H. Zhang, C.-X. Liu, X.-L. Qi, X. Dai, Z. Fang, and S.-C. Zhang, *Topological insulators in bi2se3, bi2te3 and sb2te3 with a single dirac cone on the surface*, *Nature Physics* **5** (05, 2009) 438 EP –.

[92] Y. Xia, D. Qian, D. Hsieh, L. Wray, A. Pal, H. Lin, A. Bansil, D. Grauer, Y. S. Hor, R. J. Cava, and M. Z. Hasan, *Observation of a large-gap topological-insulator class with a single dirac cone on the surface*, *Nature Physics* **5** (05, 2009) 398 EP –.

[93] Y. L. Chen, J. G. Analytis, J.-H. Chu, Z. K. Liu, S.-K. Mo, X. L. Qi, H. J. Zhang, D. H. Lu, X. Dai, Z. Fang, S. C. Zhang, I. R. Fisher, Z. Hussain, and Z.-X. Shen, *Experimental realization of a three-dimensional topological insulator, bi2te3*, *Science* **325** (2009), no. 5937 178–181.

[94] F. D. M. Haldane, *Berry Curvature on the Fermi Surface: Anomalous Hall Effect as a Topological Fermi-Liquid Property*, *Phys. Rev. Lett.* **93** (Nov, 2004) 206602.

[95] W. Witczak-Krempa, G. Chen, Y. B. Kim, and L. Balents, *Correlated Quantum Phenomena in the Strong Spin-Orbit Regime*, *Annu. Rev. Condens. Matter Phys.* **5** (2014), no. 1 57–82.

[96] G. Khaliullin, *Orbital Order and Fluctuations in Mott Insulators*, *Progress of Theoretical Physics Supplement* **160** (2005) 155–202.

[97] Y. Li, H. Liao, Z. Zhang, S. Li, F. Jin, L. Ling, L. Zhang, Y. Zou, L. Pi, Z. Yang, J. Wang, Z. Wu, and Q. Zhang *Sci. Rep.* **5** (2015) 16419.

[98] Y. Li, G. Chen, W. Tong, L. Pi, J. Liu, Z. Yang, X. Wang, and Q. Zhang, *Rare-Earth Triangular Lattice Spin Liquid: A Single-Crystal Study of $YbMgGaO_4$*, *Phys. Rev. Lett.* **115** (Oct, 2015) 167203.

[99] Y. Li, D. Adroja, P. K. Biswas, P. J. Baker, Q. Zhang, J. Liu, A. A. Tsirlin, P. Gegenwart, and Q. Zhang, *Muon Spin Relaxation Evidence for the U(1) Quantum Spin-Liquid Ground State in the Triangular Antiferromagnet $YbMgGaO_4$*, *Phys. Rev. Lett.* **117** (Aug, 2016) 097201.

[100] Y.-D. Li, X. Wang, and G. Chen, *Anisotropic spin model of strong spin-orbit-coupled triangular antiferromagnets*, *Phys. Rev. B* **94** (Jul, 2016) 035107.

[101] C. Liu, R. Yu, and X. Wang, *Semiclassical ground-state phase diagram and multi-Q phase of a spin-orbit-coupled model on triangular lattice*, *Phys. Rev. B* **94** (Nov, 2016) 174424.

[102] Y. D. Li, Y. Shen, Y. Li, J. Zhao, and G. Chen, *The effect of spin-orbit coupling on the effective-spin correlation in YbMgGaO4*, *ArXiv e-prints* (Aug., 2016) [arXiv:1608.0644].

[103] Y. D. Li, Y.-M. Lu, and G. Chen, *The Spinon Fermi Surface U(1) Spin Liquid in a Spin-Orbit-Coupled Triangular Lattice Mott Insulator YbMgGaO4*, *ArXiv e-prints* (Dec., 2016) [arXiv:1612.0344].

[104] Y.-D. Li and G. Chen, *Detecting spin fractionalization in a spinon Fermi surface spin liquid*, *Phys. Rev. B* **96** (Aug, 2017) 075105.

[105] O. I. Motrunich, *Orbital magnetic field effects in spin liquid with spinon Fermi sea: Possible application to* $\kappa-(\mathrm{ET})_2\mathrm{Cu}_2(\mathrm{CN})_3$, *Phys. Rev. B* **73** (Apr, 2006) 155115.

[106] Y. Iqbal, W.-J. Hu, R. Thomale, D. Poilblanc, and F. Becca, *Spin liquid nature in the Heisenberg* $J_1 - J_2$ *triangular antiferromagnet*, *Phys. Rev. B* **93** (Apr, 2016) 144411.

[107] S. Sorella, *Wave function optimization in the variational Monte Carlo method*, *Phys. Rev. B* **71** (Jun, 2005) 241103.

[108] S. Sorella, *Generalized Lanczos algorithm for variational quantum Monte Carlo*, *Phys. Rev. B* **64** (Jun, 2001) 024512.

[109] F. Becca, W.-J. Hu, Y. Iqbal, A. Parola, D. Poilblanc, and S. Sorella, *Lanczos steps to improve variational wave functions*, *Journal of Physics: Conference Series* **640** (2015), no. 1 012039.

[110] P. Kos and M. Punk, *Quantum spin liquid ground states of the Heisenberg-Kitaev model on the triangular lattice*, *Phys. Rev. B* **95** (Jan, 2017) 024421.

[111] S. Hwan Chun, J.-W. Kim, J. Kim, H. Zheng, C. C. Stoumpos, C. D. Malliakas, J. F. Mitchell, K. Mehlawat, Y. Singh, Y. Choi, T. Gog, A. Al-Zein, M. M. Sala, M. Krisch, J. Chaloupka, G. Jackeli, G. Khaliullin, and B. J. Kim, *Direct evidence for dominant bond-directional interactions in a honeycomb lattice iridate Na2IrO3*, *Nat. Phys.* **11** (06, 2015) 462–466.

[112] H. Katsura, N. Nagaosa, and P. A. Lee, *Theory of the Thermal Hall Effect in Quantum Magnets*, *Phys. Rev. Lett.* **104** (Feb, 2010) 066403.

[113] Z. Zhu, P. A. Maksimov, S. R. White, and A. L. Chernyshev, *Disorder-induced Mimicry of a Spin Liquid in YbMgGaO_4*, *ArXiv e-prints* (Mar., 2017) [arXiv:1703.0297].

[114] N. Nagaosa, J. Sinova, S. Onoda, A. MacDonald, and N. Ong, *Anomalous hall effect*, *Rev. Mod. Phys.* **82** (2010), no. 2 1539.

[115] A. M. Turner, F. Wang, and A. Vishwanath, *Kinetic magnetism and orbital order in iron telluride*, *Phys. Rev. B* **80** (Dec, 2009) 224504.

[116] Y.-F. Wang, C.-D. Gong, and Z. D. Wang, *Tuning kinetic magnetism of strongly correlated electrons via a staggered flux*, *Phys. Rev. Lett.* **100** (Jan, 2008) 037202.

[117] W. O. Putikka, M. U. Luchini, and M. Ogata, *Ferromagnetism in the two-dimensional t - J model*, *Phys. Rev. Lett.* **69** (Oct, 1992) 2288–2291.

[118] G. Herranz, M. Basletić, M. Bibes, C. Carrétéro, E. Tafra, E. Jacquet, K. Bouzehouane, C. Deranlot, A. Hamzić, J.-M. Broto, A. Barthélémy, and A. Fert, *High mobility in* $\mathrm{laalo_3/srtio_3}$ *heterostructures: Origin, dimensionality, and perspectives*, *Phys. Rev. Lett.* **98** (May, 2007) 216803.

[119] W. Siemons, G. Koster, H. Yamamoto, W. A. Harrison, G. Lucovsky, T. H. Geballe, D. H. A. Blank, and M. R. Beasley, *Origin of charge density at* $\mathrm{laalo_3}$ *on* $\mathrm{srtio_3}$ *heterointerfaces: Possibility of intrinsic doping*, *Phys. Rev. Lett.* **98** (May, 2007) 196802.

[120] R. Chen, S. Lee, and L. Balents, *Dimer mott insulator in an oxide heterostructure*, *Phys. Rev. B* **87** (Apr, 2013) 161119.

[121] S. Okamoto and A. J. Millis, *Electronic reconstruction at an interface between a mott insulator and a band insulator*, *Nature* **428** (04, 2004) 630–633.

[122] M. Stengel, *First-principles modeling of electrostatically doped perovskite systems*, *Phys. Rev. Lett.* **106** (Mar, 2011) 136803.

[123] P. Delugas, A. Filippetti, V. Fiorentini, D. I. Bilc, D. Fontaine, and P. Ghosez, *Spontaneous 2-dimensional carrier confinement at the n-type* $\mathrm{srtio_3/laalo_3}$ *interface*, *Phys. Rev. Lett.* **106** (Apr, 2011) 166807.

[124] P. Moetakef, D. G. Ouellette, J. R. Williams, S. James Allen, L. Balents, D. Goldhaber-Gordon, and S. Stemmer, *Quantum oscillations from a two-dimensional electron gas at a mott/band insulator interface*, *Applied Physics Letters* **101** (2012), no. 15.

[125] G. Khalsa and A. H. MacDonald, *Theory of the srtio$_3$ surface state two-dimensional electron gas*, *Phys. Rev. B* **86** (Sep, 2012) 125121.

[126] A. F. Santander-Syro, O. Copie, T. Kondo, F. Fortuna, S. Pailhes, R. Weht, X. G. Qiu, F. Bertran, A. Nicolaou, A. Taleb-Ibrahimi, P. Le Fevre, G. Herranz, M. Bibes, N. Reyren, Y. Apertet, P. Lecoeur, A. Barthelemy, and M. J. Rozenberg, *Two-dimensional electron gas with universal subbands at the surface of srtio3*, *Nature* **469** (01, 2011) 189–193.

[127] H. D. Zhou and J. B. Goodenough, *Localized or itinerant tio 3 electrons in rtio 3 perovskites*, *Journal of Physics: Condensed Matter* **17** (2005), no. 46 7395.

[128] G. Kotliar and A. E. Ruckenstein, *New functional integral approach to strongly correlated fermi systems: The gutzwiller approximation as a saddle point*, *Phys. Rev. Lett.* **57** (Sep, 1986) 1362–1365.

[129] F. Becca and S. Sorella, *Nagaoka ferromagnetism in the two-dimensional infinite- U hubbard model*, *Phys. Rev. Lett.* **86** (Apr, 2001) 3396–3399.

[130] B. S. Shastry, H. R. Krishnamurthy, and P. W. Anderson, *Instability of the nagaoka ferromagnetic state of the U=∞ hubbard model*, *Phys. Rev. B* **41** (Feb, 1990) 2375–2379.

[131] M. Brunner and A. Muramatsu, *Quantum monte carlo simulations of infinitely strongly correlated fermions*, *Phys. Rev. B* **58** (Oct, 1998) R10100–R10103.

[132] J. Ferrer, *Spin-liquid phase for the frustrated quantum heisenberg antiferromagnet on a square lattice*, *Phys. Rev. B* **47** (Apr, 1993) 8769–8782.

[133] A. Chubukov, *First-order transition in frustrated quantum antiferromagnets*, *Phys. Rev. B* **44** (Jul, 1991) 392–394.

[134] A. Moreo, E. Dagotto, T. Jolicoeur, and J. Riera, *Incommensurate correlations in the t - J and frustrated spin-1/2 heisenberg models*, *Phys. Rev. B* **42** (Oct, 1990) 6283–6293.

[135] M. P. Gelfand, R. R. P. Singh, and D. A. Huse, *Zero-temperature ordering in two-dimensional frustrated quantum heisenberg antiferromagnets*, *Phys. Rev. B* **40** (Dec, 1989) 10801–10809.

[136] See Supplemental Material at [URL will be inserted by publisher].

[137] M. C. Gutzwiller, *Correlation of electrons in a narrow s band*, *Phys. Rev.* **137** (Mar, 1965) A1726–A1735.

[138] M. C. Gutzwiller, *Effect of correlation on the ferromagnetism of transition metals*, *Phys. Rev. Lett.* **10** (Mar, 1963) 159–162.

[139] T. Ogawa, K. Kanda, and T. Matsubara, *Gutzwiller approximation for antiferromagnetism in hubbard model*, *Progress of Theoretical Physics* **53** (1975), no. 3 614–633.

[140] D. Vollhardt, *Normal* ^{3}He*: an almost localized fermi liquid*, *Rev. Mod. Phys.* **56** (Jan, 1984) 99–120.

[141] S. Banerjee, O. Erten, and M. Randeria, *Ferromagnetic exchange, spin-orbit coupling and spiral magnetism at the laalo3/srtio3 interface*, *Nature Physics* **9** (10, 2013) 626–630.

[142] W. Witczak-Krempa, G. Chen, Y.-B. Kim, and L. Balents, *Correlated quantum phenomena in the strong spin-orbit regime*, *Annual Review of Condensed Matter Physics* **5** (2014), no. 1 57–82.

[143] S. Wolgast, C. Kurdak, K. Sun, J. W. Allen, D.-J. Kim, and Z. Fisk, *Low-temperature surface conduction in the kondo insulator* smb_6, *Phys. Rev. B* **88** (Nov, 2013) 180405.

[144] X. Zhang, N. P. Butch, P. Syers, S. Ziemak, R. L. Greene, and J. Paglione, *Hybridization, inter-ion correlation, and surface states in the kondo insulator* smb_6, *Phys. Rev. X* **3** (Feb, 2013) 011011.

[145] J. Hu, J. Alicea, R. Wu, and M. Franz, *Giant topological insulator gap in graphene with* 5*d adatoms*, *Phys. Rev. Lett.* **109** (Dec, 2012) 266801.

[146] C. Weeks, J. Hu, J. Alicea, M. Franz, and R. Wu, *Engineering a robust quantum spin hall state in graphene via adatom deposition*, *Phys. Rev. X* **1** (Oct, 2011) 021001.

[147] Z. Qiao, S. A. Yang, W. Feng, W.-K. Tse, J. Ding, Y. Yao, J. Wang, and Q. Niu, *Quantum anomalous hall effect in graphene from rashba and exchange effects*, *Phys. Rev. B* **82** (Oct, 2010) 161414.

[148] H. Zhang, C. Lazo, S. Blügel, S. Heinze, and Y. Mokrousov, *Electrically tunable quantum anomalous hall effect in graphene decorated by* 5*d transition-metal adatoms*, *Phys. Rev. Lett.* **108** (Feb, 2012) 056802.

[149] B. Coqblin, C. Lacroix, M. A. Gusmão, and J. R. Iglesias, *Band-filling effects on kondo-lattice properties*, *Phys. Rev. B* **67** (Feb, 2003) 064417.

[150] J. R. Iglesias, C. Lacroix, and B. Coqblin, *Revisited doniach diagram: Influence of short-range antiferromagnetic correlations in the kondo lattice*, *Phys. Rev. B* **56** (Nov, 1997) 11820–11826.

[151] C. Lacroix and M. Cyrot, *Phase diagram of the kondo lattice*, *Phys. Rev. B* **20** (Sep, 1979) 1969–1976.

[152] M.-T. Tran, T. Takimoto, and K.-S. Kim, *Phase diagram for a topological kondo insulating system*, *Phys. Rev. B* **85** (Mar, 2012) 125128.

[153] M. Legner, A. Rüegg, and M. Sigrist, *Topological invariants, surface states, and interaction-driven phase transitions in correlated kondo insulators with cubic symmetry*, *Phys. Rev. B* **89** (Feb, 2014) 085110.

[154] D. Withoff and E. Fradkin, *Phase transitions in gapless fermi systems with magnetic impurities*, *Phys. Rev. Lett.* **64** (Apr, 1990) 1835–1838.

[155] L. Fritz and M. Vojta, *The physics of kondo impurities in graphene*, *Reports on Progress in Physics* **76** (2013), no. 3 032501.

[156] C. Gonzalez-Buxton and K. Ingersent, *Renormalization-group study of anderson and kondo impurities in gapless fermi systems*, *Phys. Rev. B* **57** (Jun, 1998) 14254–14293.

[157] M. Vojta and L. Fritz, *Upper critical dimension in a quantum impurity model:critical theory of the asymmetric pseudogap kondo problem*, *Phys. Rev. B* **70** (Sep, 2004) 094502.

[158] A. Polkovnikov, S. Sachdev, and M. Vojta, *Impurity in a d-wave superconductor: Kondo effect and stm spectra*, *Phys. Rev. Lett.* **86** (Jan, 2001) 296–299.

[159] Y.-M. Lu and A. Vishwanath, *Theory and classification of interacting integer topological phases in two dimensions: A chern-simons approach*, *Phys. Rev. B* **86** (Sep, 2012) 125119.

[160] C. Wang, A. C. Potter, and T. Senthil, *Gapped symmetry preserving surface state for the electron topological insulator*, *Phys. Rev. B* **88** (Sep, 2013) 115137.

[161] M. A. Metlitski, C. L. Kane, and M. P. A. Fisher, *A symmetry-respecting topologically-ordered surface phase of 3d electron topological insulators*, *ArXiv e-prints* (June, 2013) [arXiv:1306.3286].

[162] X. Chen, L. Fidkowski, and A. Vishwanath, *Symmetry enforced non-abelian topological order at the surface of a topological insulator*, *Phys. Rev. B* **89** (Apr, 2014) 165132.

[163] D. K. Efimkin and V. Galitski, *Strongly interacting dirac liquid on the surface of a topological kondo insulator*, *Phys. Rev. B* **90** (Aug, 2014) 081113.

[164] R. Peierls, *Quantum Theory of Solids*. Oxford University Press, 1955.

[165] M. Rice and S. Strassler, *Theory of a quasi-one-dimensional band-conductor*, *Solid State Communications* **13** (1973), no. 1 125 – 128.

[166] T. Giamarchi, *Quantum Physics in One Dimension*. Clarendon Press, 2003.

[167] C. Xu and J. E. Moore, *Stability of the quantum spin hall effect: Effects of interactions, disorder, and F_2 topology*, *Phys. Rev. B* **73** (Jan, 2006) 045322.

[168] C. Wu, B. A. Bernevig, and S.-C. Zhang, *Helical liquid and the edge of quantum spin hall systems*, *Phys. Rev. Lett.* **96** (Mar, 2006) 106401.

[169] F. Becca and S. Sorella, *Quantum Monte Carlo Approaches for Correlated Systems*. Cambridge University Press, 2017.